

Spring 2017

Improvement of fluorescence-based microfluidic DNA analyzers

Collin Tranter
Louisiana Tech University

Follow this and additional works at: <https://digitalcommons.latech.edu/dissertations>

 Part of the [Biology Commons](#), and the [Other Biomedical Engineering and Bioengineering Commons](#)

Recommended Citation

Tranter, Collin, "" (2017). *Dissertation*. 61.
<https://digitalcommons.latech.edu/dissertations/61>

This Dissertation is brought to you for free and open access by the Graduate School at Louisiana Tech Digital Commons. It has been accepted for inclusion in Doctoral Dissertations by an authorized administrator of Louisiana Tech Digital Commons. For more information, please contact digitalcommons@latech.edu.

**IMPROVEMENT OF FLUORESCENCE-BASED
MICROFLUIDIC DNA ANALYZERS**

by

Collin Tranter, B.S.

A Dissertation Presented in Partial Fulfillment
of the Requirements of the Degree
Doctor of Philosophy

COLLEGE OF ENGINEERING AND SCIENCE
LOUISIANA TECH UNIVERSITY

May 2017

ProQuest Number: 10644146

All rights reserved

INFORMATION TO ALL USERS

The quality of this reproduction is dependent upon the quality of the copy submitted.

In the unlikely event that the author did not send a complete manuscript and there are missing pages, these will be noted. Also, if material had to be removed, a note will indicate the deletion.



ProQuest 10644146

Published by ProQuest LLC(2017). Copyright of the Dissertation is held by the Author.

All rights reserved.

This work is protected against unauthorized copying under Title 17, United States Code.
Microform Edition © ProQuest LLC.

ProQuest LLC
789 East Eisenhower Parkway
P.O. Box 1346
Ann Arbor, MI 48106-1346

LOUISIANA TECH UNIVERSITY

THE GRADUATE SCHOOL

April 5, 2017

Date

We hereby recommend that the dissertation prepared under our supervision by

Collin Tranter, B.S.

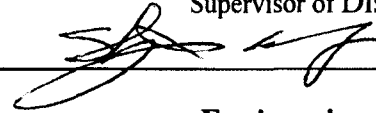
entitled Improvement Of Fluorescence-Based Microfluidic DNA Analyzers

be accepted in partial fulfillment of the requirements for the Degree of

Doctor of Philosophy in Engineering



Supervisor of Dissertation Research

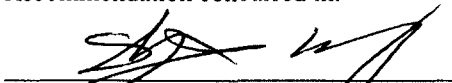


Head of Department

Engineering

Department

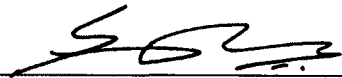
Recommendation concurred in:



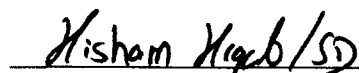



Advisory Committee

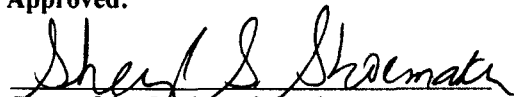
Approved:



Director of Graduate Studies


Dean of the College

Approved:



Dean of the Graduate School

ABSTRACT

A tremendous effort continues in the development of micro-total-analysis-systems; in support of this, many chemical passivation methods have been developed to enhance the biocompatibility of such microfluidic systems. However, the suitability of these passivation techniques to many fluorescence-based assays still remains inconsistent. This part of this work is focused on the performance of a third generation intercalating DNA dye when used within microfluidic devices treated with a select variety of passivating coatings. The results of these tests indicate that passivation coatings which are intended to shed DNA based on electrostatic repulsion will in fact imbibe the fluorescent DNA intercalating dye by the same mechanism. Blocking this charge-based dye adsorption, such as with bovine serum albumen (BSA), has yielded mixed results in the literature. As an alternative, this present work indicates that preloading the bio-passivated microchannel with a small amount of this dye will prevent both the DNA and the DNA dye from being adsorbed from solution onto the channel walls. By characterizing the saturating behavior of this preloaded dye, a protocol is here suggested to optimize dye performance in passivated microfluidics. Furthermore, the intent and achievement of this work has been to design a BSA-free treatment method, thereby eliminating common fluorescent artifacts. The amount of dye preloading required is found to be proportional to the microchannel surface area, and can be predicted by a new material property defined for each chemical coating processes. Theoretical and

experimental results indicate that this is independent of operating temperature, flow rate, and channel aspect ratio. Thus this is a property of the material, and not just a product of the several operational parameters. This property has been measured for four coatings as part of this work.

Improvements in passivation are crucial to the development of lab-on-a-chip devices, important in solving current medical and healthcare problems. Challenging topics include the need for fast pathogen detection (i.e. ebola epidemic, HIV, water-borne diseases typhoid, cholera, dysentery) and the need for personalized medicine (i.e. cancer genomics, drug susceptibility). A novel microfluidic DNA analysis device was developed, incorporating helicase dependent amplification (HDA) and sequence-specific fluorescence based detection. These are incorporated into a glass/polymer platform that is hand operated and powered by a laptop computer. Thermal modeling sets operation at less than 3 Watts and fabrication consistency testing ensures samples volumes of 17 μ L. The heating element and optical components are powered via 3 USB ports. The heating element consists of a thin film heater and thermistor controlled in a feedback loop with Matlab and Arduino interfacing. Using fuzzy logic control, the temperature of the PCR chamber has been controlled by varying the heater voltage. On-chip amplification has been verified using a commercial LightScanner32 device and HDA detection and DNA melting analysis were performed on-chip.

APPROVAL FOR SCHOLARLY DISSEMINATION

The author grants to the Prescott Memorial Library of Louisiana Tech University the right to reproduce, by appropriate methods, upon request, any or all portions of this Dissertation. It is understood that "proper request" consists of the agreement, on the part of the requesting party, that said reproduction is for his personal use and that subsequent reproduction will not occur without written approval of the author of this Dissertation. Further, any portions of the Dissertation used in books, papers, and other works must be appropriately referenced to this Dissertation.

Finally, the author of this Dissertation reserves the right to publish freely, in the literature, at any time, any or all portions of this Dissertation.

Author Colin Grant

Date 5/2/2017

DEDICATION

I would like to dedicate this work to my family – my three children Liam, Lilian, and Henry – and especially to my wife, Sarah. For your support and love.

TABLE OF CONTENTS

ABSTRACT	iii
DEDICATION.....	vi
LIST OF TABLES.....	x
LIST OF FIGURES	xi
ACKNOWLEDGMENTS	xiii
CHAPTER 1 INTRODUCTION.....	1
1.1 Grand Challenges of Engineering.....	1
1.2 DNA Analysis.....	2
1.2.1 History	2
1.2.2 Modern Focus	3
CHAPTER 2 BACKGROUND.....	5
2.1 DNA Amplification	5
2.2 Nucleic Acid Detection.....	6
2.2.1 Quantitative Polymerase Chain Reaction	7
2.2.2 Melting Curve Analysis	7
2.2.3 Effect of Dye Concentration on Melting Temperature.....	8
2.2.4 Isothermal Amplification.....	11
2.3 Microfluidics.....	13
2.3.1 Heat Transfer in Microfluidics	13
2.3.2 Fabrication Technique – Xurography	15
2.3.3 Passivation of Microfluidic Devices.....	15

CHAPTER 3 PASSIVATION OF GLASS MICROFLUIDICS FOR FLUORESCENCE-BASED ASSAYS.....	19
3.1 Introduction.....	19
3.2 Methods	20
3.2.1 Microfluidic Chip Fabrication	20
3.2.2 Optical and Heating System	23
3.2.3 Experimental Conditions	24
3.3 Results and Discussion	25
3.3.1 Identifying and Exploring Reagent Depletion.....	25
3.3.2 Derivation of Dye Saturation Model	28
3.3.3 Effect of Passivation Coating on Dye Depletion.....	31
3.3.4 Effect of Experimental Parameters on N_{sat}	34
3.3.5 Pretreatment.....	37
3.3.6 Conclusions.....	42
CHAPTER 4 MICROFLUIDIC HELICASE-DEPENDENT AMPLIFICATION FOR μ TAS APPLICATION.....	43
4.1 Introduction.....	43
4.2 Isothermal DNA Amplification	43
4.2.1 Helicase-Dependent Amplification	43
4.2.2 Reduction of Incubation Time	49
4.2.3 Asymmetric Helicase-Dependent Amplification.....	51
CHAPTER 5 DESIGN OF A PORTABLE DNA ANALYZER.....	59
5.1 Introduction.....	59
5.2 Fabrication	60
5.2.1 Composite Device Fabrication	61
5.2.2 Fabrication Consistency Testing.....	64

5.2.2.1	Thickness Measurement	64
5.2.2.2	Sample Volume Uptake.....	67
5.3	Thermal Management.....	69
5.3.1	Heating Element Design	69
5.3.2	Thermal Modeling	72
5.4	Optical System.....	77
5.5	On-Chip Testing	80
5.5.1	On-Chip Amplification.....	80
5.6	Summary.....	87
CHAPTER 6 CONCLUSIONS AND FUTURE WORK.....		88
6.1	Conclusions	88
6.1.1	Accomplishments	88
6.1.2	Impact	88
6.2	Future Work.....	89
APPENDIX A NUCLEIC ACID SEQUENCES FOR DNA ANALYSIS DEVICE DEVELOPMENT		91
A.1	Phi X 174 Sequence.....	91
A.2	Synthetic Melting Duplex Sequences.....	95
APPENDIX B μ TAS HDA SYSTEM CONTROL DOCUMENTS.....		96
B.1	Circuit Diagram for Heating Control and LED Illumination Systems	96
B.2	μ TAS Control Codes	97
BIBLIOGRAPHY.....		104

LIST OF TABLES

Table 2-1: Table outlining research in diagnostic isothermal nucleic acid amplification, sorted by amplification type.	12
Table 3-1: Empirical values of N_{sat} calculated for each of the four coatings.	33
Table 3-2: Specific experimental conditions used for parametric tests. A-H correspond to experiments described in Figure 3-8. Tests (A-G) were conducted in channels fabricated with 100 μm thick tape and test (H) was conducted in a channel fabricated with a 320 μm thick tape-PDMS layer.	37
Table 4-1: Sample compositions for asymmetric HDA.....	52

LIST OF FIGURES

Figure 2-1: DNA melting temperature as a function of intercalating dye concentration and oligonucleotide concentration. High resolution melting analysis was performed in a LightScanner32 system.....	10
Figure 3-1: Four different passivation coatings were evaluated with respect to biological and fluorescence compatibility: (A) DDMS, (B) Long-chain fluorosilane, (C) Aquaphobe CM, (D) and Aquaphobe CF.....	21
Figure 3-2: Double sided Kapton tape is patterned and sandwiched between two treated glass slides. The resulting channel is composed primarily of treated glass surfaces, through which fluorescent signal is observed, and of inert, thermostable polymer tape, which accounts for a small portion of the surface area.....	22
Figure 3-3: Experimental setup for fluorescence analysis in microfluidic channels. Microfluidic chip (A) rests on a heater block (B), while imaged via CCD camera (C), and illuminated by LED excitation source (D). Sample is flowed into the device via syringe pump (E). Device temperature is managed by PID controller (F) and verified via IR camera (G).	24
Figure 4-1: The effect of LC Green Plus+ on helicase-dependent amplification. Melting curve analysis results of products amplified in the presence and absence of 1 X concentration LC Green Plus.....	46
Figure 4-2: Increased enzyme concentration overcomes HDA inhibition by LC Green Plus. Real-time HDA (top) and MCA (middle and bottom) were performed on samples containing 1 X LC Green and either 1 X or 2 X HDA enzyme mix.	48
Figure 4-3: Increased enzyme concentration allows for decreased HDA incubation time. HDA mixtures containing enzyme concentrations of 2 X to 5 X were incubated for 30 min and MCA was performed.....	50
Figure 4-4: Asymmetric HDA amplification (top) and melting curves (middle and bottom) for multiple primer ratios. Each curve was an average of multiple trials (N = 4 for each sample type, except F2:1 where N = 3).	53
Figure 4-5: Gel electrophoresis imaging for asymmetric HDA. PCR marker (lane 1) is used to compare lengths of samples in lanes 3 through 7.....	55

Figure 4-6: Melting curve analysis used to detect ssDNA product of asymmetric helicase-dependent amplification. A primer based probe was added to the symmetric HDA control and asymmetric HDA amplicon, resulting in increased probe-to-target signal ratio in the asymmetric sample.	57
Figure 5-1: Diagram of the DNA analysis lab-on-a-chip system. The glass/polymer microfluidic device (A) is heated via USB power and interfaces via Arduino (B) with a laptop (D). Fluorescent signal is acquired with a USB spectrometer (D). Thermal and optical control and processing are managed simultaneously.	60
Figure 5-2: Pattern of microfluidic channels and reservoirs. A 100 μm thick polyimide double-adhesive tape was cut via xurography and used to mold a PDMS layer.	62
Figure 5-3: Fabrication workflow (A) for microfluidic HDA chip - (1) Pattern tape via xurography (2) Cure PDMS over mold (3) Remove patterned tape and mask molded PDMS (4) Exposed PDMS and glass slide to oxygen plasma (5) Remove mask and bond PDMS to glass. Molded PDMS (B) is masked to form a flat valve channel. The finished chip (C).	63
Figure 5-4: The thicknesses of 10 identically fabricated PDMS/glass composite devices were measured at points 1-7. The measurements include both PDMS and glass layers.	65
Figure 5-5: Device thickness across 10 similarly fabricated PDMS/glass composite microfluidic devices.	66
Figure 5-6: Height measurements at each location (shown in Figure 5-5), normalized for average height of each device.	67
Figure 5-7: Sample uptake volume using thumb actuated pumping in PDMS/glass composite microfluidic chips.	68
Figure 5-8: The glass/PDMS composite device with mounted thin film heater, thermistor, and insulating foam.	70
Figure 5-9: Simplified model of glass/PDMS microfluidic device, used for thermal modeling.	73
Figure 5-10: Modelled effect of heater contact resistance on the device temperature. Based on the best case and worst case scenarios described above, the temperature due to a 67°C heat source can be seen in the three zones: 1) the glass slide, 2) the reservoir, 3) the PDMS.	74
Figure 5-11: Modelled time response of reservoir temperature to an input time-variable heater temperature.	75
Figure B-1: Circuit Diagram for Heating Control and LED Illumination Systems	96

ACKNOWLEDGMENTS

I would like to thank all those involved in my research at Louisiana Tech University: my advisor, Dr. Niel Crews, for his ongoing support and mentorship; my lab-mates, present and past – Ilija Pjescic, Manasa Paidipalli, James Haywood, Brian Cox, Barrett Routon, Shyan Davani, Varun Koppa, Suvhashis Thapta, Gergana Nestorova, Nabamita Pal, Siyovush Abdurakhimov, and Thomas Holland; my committee members – Shengian Wang, Yuri Lvov, Mary Caldorera-Moore, and Sven Eklund for their constructive input; Institute for Micromanufacturing staff members – Davis Bailey, Debbie Wood, Alfred Gunasekaran, and Philip Chapman.

This work was funded in part by the Louisiana Space Consortium, and includes findings from work supported by the National Science Foundation under Grant No.1151148, and by the National Aeronautics and Space Administration under Contract NNX13AN05A issued through NASA EPSCoR.

CHAPTER 1

INTRODUCTION

1.1 Grand Challenges of Engineering

The advancement of multiple fields of science and engineering have allowed the development of lab-on-a-chip devices, capable of performing biological, chemical, and other laboratory functions on a miniaturized device. The development of these type of devices are important in solving current medical and healthcare problems, such as the need for fast pathogen detection (i.e. ebola epidemic, HIV, water borne diseases typhoid, cholera, dysentery) and the need for personalized medicine (i.e. cancer genomics, drug susceptibility). Some of the key developments that enable these more portable and efficient technologies are materials and fabrication, surface passivation, and improved sample handling. One important technique used in nearly any type of genetic testing is nucleic acid amplification. The goals of this work are to investigate and improve passivation in fluorescent-analysis based microfluidic devices and to develop a lab-on-a-chip device for sequence specific amplification and fluorescent detection. It incorporates helicase dependent amplification, fluorescent detection, hand operated sample manipulation, and complete USB power.

1.2 DNA Analysis

1.2.1 History

The field of genetics - beginning as far back as the mid-1800s with Gregor Mendel, Friedrich Mescher, and Thomas Hunt Morgan - saw advancements in heredity and the identification of nucleic acids. Into the twentieth century, genetics had expanded into studying chromosomes and their functions (Barbara McClintock) as well as x-ray induced mutation (Hermann Joseph Muller), the role of genes (Edward Tatum, George Beadle, and Joshua Lederberg), and identification and study of DNA (Oswald Avery, Evelyn Witkin). The 1950s saw an explosion of research in the structure of DNA (Erwin Chargaff, Rosalind Franklin, Maurice Wilkins, Alfred Hershey and Martha Chase, Linus Pauling) leading to the discovery of the double helix structure of DNA (James Watson and Francis Crick), followed quickly by a development in understanding of flow of information within the cell (Francis Crick), the action of RNA (Paul Zamecnik, Matthew Meselson and Franklin Stahl, Sydney Brenner), and the isolation of DNA polymerase – the enzyme responsible for replicating DNA (Arthur Kornberg). In the 1960s, researchers revealed details about the genetic code and protein expression (Marshall Nirenberg, Francois Jacob and Jacques Monod, Roy Britten), followed in the 1970s with the discoveries of reverse transcriptase – the enzyme that transcribes DNA from RNA (David Baltimore and Howard Temin), recombinant DNA (Stanley Norman Cohen and Herbert Boyer), RNA splicing (Richard Roberts and Phillip Sharp), chromatin structure (Roger Kornberg), and DNA sequencing (Frederick Sanger). In the next decade, these advances in understanding led to being able to identify specific genes and their functions, i.e. ones responsible for regulation of the cell cycle (Leland Hartwell) and those in embryonic

development (Christiane Nusslein-Volhard and Eric Francis Wieschaus). The 1980s also saw the development of a technique directly important to this research, polymerase chain reaction (PCR) (Alec Jeffreys). The foundations for DNA fingerprinting/profiling were also laid (Alec Jeffreys) [1].

All of these biological foundations have changed the way we understand medicine, healthcare, and overall how we interact with the living world around us. Advancements in material science and fabrication techniques have combined with biological knowledge in the field of microfluidics, particularly bio-microfluidics. The last few decades have seen leaps and bounds in what kind are possible and at what scale biological and chemical testing can be done [2-5].

1.2.2 Modern Focus

Nucleic acid amplification is an important tool for many applications including pathogen detection, medical diagnostics, forensic identification, and genetics. The most common and oldest technique, PCR has been developed over the last several decades, with emphasis on improved speed and reduced size. Microfluidic PCR is a development dating back to the early 2000s [6] that opens the doors to many applications that require a portable device, both smaller and low power. These biological lab-on-a-chip devices aim to incorporate multiple functions, such as sample preparation, amplification, and detection into one device. This has been the focus of much research and numerous approaches have been taken.

The objective of this work is to improve microfluidic DNA analysis devices, enabling and furthering capabilities in diagnostics and research. Part of this work is an investigation into compatibility of biological passivation methods used in biological

microfluidics and fluorescent sensing techniques. A portable DNA analysis device was also developed, demonstrating the combination of isothermal DNA amplification and fluorescent sensing techniques in a microfluidic device.

CHAPTER 2

BACKGROUND

2.1 DNA Amplification

Polymerase chain reaction (PCR) is fundamental technique, used across many disciplines and fields. It is a means of amplifying a biological signal by facilitating the activity of the enzyme, DNA polymerase, in a controlled and focused way. A DNA sequence of interest is selected from a sample genome (i.e. template) and replicated, producing millions of copies of double stranded DNA (dsDNA) fragments, i.e. PCR product or amplicon. These fragments can be analyzed by a variety of methods, most commonly by fluorescent dyes.

The region of interest is targeted by specifically designed, short nucleic acid sequences, called primers. They are designed to bind (i.e. hybridize) to complementary regions of the sample genome that bound the targeted region. Polymerase, under the right conditions will attach to the template/primer complex and begin incorporating complementary nucleotide bases, extending the primer in the 5'-3' direction, and copying the DNA by producing a complementary strand. This occurs on each of the two DNA strands, producing two segments of double stranded DNA from one. This occurs over and over, doubling the number target regions produced with each iteration (logarithmic amplification). Eventually the reaction slows and ceases due to multiple factors, including depletion of reactants (primers, nucleotides), accumulation of reaction

inhibiting byproducts (pyrophosphatase), and polymerase binding competition between primers and amplified product [7].

This process requires thermal management, activating the polymerase enzyme at specific temperature ranges (dependent on the strain of enzyme) and specific temperature ranges to control the separation of DNA strands primer annealing. Traditionally, three distinct temperatures or temperature ranges are defined and employed in PCR: 1) denaturing or melting, where the DNA strands are completely separated at high temperature (usually around 95°C), 2) annealing, when the temperature of the system is quickly lowered, allowing the primers to attach to the complementary regions on the denatured single-stranded DNA (ssDNA) (occurring around 58 – 66°C), and 3) extension, where the temperature is increased to increase polymerase activity and copy the targeted sequence (around 72 – 75°C for traditional techniques). PCR systems usually achieve this through thermal cycling, heating and cooling the sample between these target regions [8].

2.2 Nucleic Acid Detection

A variety of methods for detecting nucleic acids, including, but not limited to, fluorescent intercalating DNA dyes, fluorescent or chemiluminescent tagged probes, and electro-chemical detection. These vary from being real-time detection methods, post amplification detection, or can be employed as either. Intercalating DNA dyes are fluorophores that bind to double stranded DNA, between the nucleotide bases, via hydrogen bonding. They produce a stronger fluorescent response when intercalated with double stranded DNA, and a much weaker response otherwise. The fluorescent signal of most dyes decrease, following a logarithmic decay, as temperature increases, whether

isolated or in the presence of DNA. This family of dyes has been employed in real-time detection techniques (quantitative PCR, or qPCR) [9, 10] as well as post amplification detection (melting curve analysis) [11].

2.2.1 Quantitative Polymerase Chain Reaction

qPCR is accomplished by measuring the fluorescent signal of a sample as PCR is being conducted, usually during the same temperature phase each cycle. As DNA concentration increases, fluorescent signal increases, producing an amplification curve. The baseline signal (due to the innate behavior of the fluorescent dye) is constant for the first several cycles, and as DNA concentration raises to a detectable limit (during the exponential phase of the reaction), the fluorescent signal increases linearly. The slope of this increase is indicative of the efficiency of the reaction, and the point or cycle number at which the signal transitioned into the exponential phase is called the crossing point (C_p). The crossing point indicates the relative concentration of the template DNA, or specifically the number of copies. As the reaction slows and ceases, the linear increase in signal decreases in slope and levels off to a plateau. This plateau height, in relation to the initial background signal, is indicative of the final concentration of nucleic acid.

2.2.2 Melting Curve Analysis

Melting analysis is a post amplification technique, used to identify the amplified sequence, and potentially reveal details about change in its composition (i.e. mutation scanning [12], genotyping [11, 13, 14] or DNA damage detection [15, 16]). Similar to how dsDNA denaturation is induced in PCR cycling, an amplified target sequence is slowly heated and the fluorescent signal of the sample is recorded. dsDNA separates in a very predictable and repeatable way, dependent on the sequence and nucleotide

composition. As the DNA strands separate, the signal decreases, providing a DNA melting curve. The features of this curve are specific to the dsDNA sequence, serving as an identifiable melting signature. For visibility and ease of use, the derivative of this signal is often analyzed, yielding peaks at the specific temperatures of melting. Short sequences (on the order of 100bp or less) often melt at a single temperature, producing a single peak at this temperature. Longer sequences with multiple regions of varied sequence composition partially denature at one temperature (causing a decrease in signal) and completely denature at a higher temperature (causing an additional decrease). Longer sequences often produce multiple peaks at specific temperatures; this is often beneficial in positively identifying target sequences. Under extremely controlled thermal and optical conditions, slight changes in curve conformation can be detected, indicating small differences in sequence (i.e. single nucleotide polymorphisms) [17, 18]

2.2.3 Effect of Dye Concentration on Melting Temperature

A study was performed to investigate the effects of an intercalating DNA dye on DNA melting temperature. This work serves as a precursor and internal reference for later work in characterizing and developing DNA analysis systems, and is thus reported as 'background' information. It has been noted in literature [19] that intercalating dyes being in the presence of DNA stabilize the double stranded structure. By introducing a charged, planar molecule between the bases, the phosphate backbones and the nucleotides are bound not only by the existing hydrogen bonds (two in the case of adenine-thymine bonds and three in the case of cytosine-guanine bonds) but also by weak electrostatic interactions between the intercalating molecule and the phosphate backbones. While many intercalating dyes only occupy one tenth or less of the possible

intercalation locations, third generation dyes or 'saturating' dyes, designed for high resolution melting curve analysis and mutation scanning, occupy a much higher proportion of the available intercalation locations. This has been noted by the producer of LC Green Plus (BioFire Defense, UT, USA) that this dye can increase the melting temperature of a PCR product by 1-3°C.

This effect was investigated for application to my work, testing the effect of LC Green Plus on the melting temperature of a 50 base pair (50bp), synthetic DNA sequence. In developing microfluidic DNA analysis devices and characterizing passivation of microfluidic devices for fluorescent assays, varying concentrations of isolated DNA and intercalating dye are used, and it is important to establish some baseline values for some ΔT_m associated with intercalating dye use. Melting analysis was performed using a LightScanner32 system (BioFire) with a variety of dye concentrations, ranging from 0.25 X to 4 X LC Green, in samples containing 0.5 μM , 1 μM , and 2 μM oligonucleotides. Figure 2-1 shows the melting temperatures as a function of dye concentration and oligonucleotide concentration. Triplicate samples of each dye concentration were used for the 1 μM oligonucleotide samples and duplicate samples of each dye concentration were used for the 0.5 and 2 μM oligonucleotide samples.

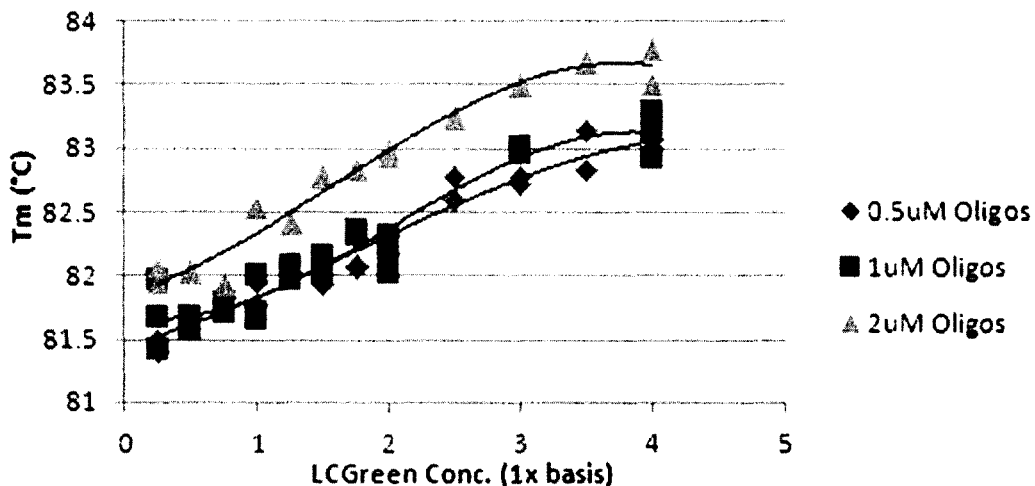


Figure 2-1: DNA melting temperature as a function of intercalating dye concentration and oligonucleotide concentration. High resolution melting analysis was performed in a LightScanner32 system.

This 50 base pair sequence was designed to exhibit a single peak melt profile around 81.9°C; a melting temperature of 81.7°C under standard conditions (1 X LC Green, 1 μ M oligonucleotide concentrations) was detected. As could be expected, decreasing dye concentration slightly lowers T_m (by approximately 0.3°C at 0.25 X) and increasing dye concentration increases T_m (by approximately 2.5°C at 4 X LC Green). This trend vaguely follows a cubic trend, indicating a plateau in this increase around approximately 4 X LC Green. The increase in T_m with increase in oligonucleotide concentration indicates some limitation of thermal controls in the LightScanner32 system. Such a limitation should also be considered and expected when designing microfluidic or μ TAS DNA analysis devices, particularly when utilizing highly concentrated nucleic acid samples (typical PCR product concentrations are below the 1 μ M standard oligonucleotide concentration used here). Sequences longer than 50bp or of higher G-C content may show a greater difference in T_m , with the overall increased

energy of melting (due to either more bases per DNA strand or the higher hydrogen bond density) being further increased by the stabilizing effect of the intercalating dye. Further research into these effects would be of interest to researchers developing intercalating dyes or specialized fluorescent based DNA melting assays.

2.2.4 Isothermal Amplification

Other techniques and modifications to PCR exist, in which multiple temperatures are not relied upon to achieve these goals. Numerous isothermal techniques have been developed, in which other enzymes, proteins, probes, and other modifications are used to replace the need thermal energy in the separation and management of the DNA strands [20-22]. This allows for simplified systems and reduced thermal management, overall reducing size and, often, process time.

Several research groups have developed assays and μ TAS devices that facilitate isothermal nucleic acid amplification, utilizing either off chip or integrated detection [23]. Fluorescent markers [24-27], fluorescent intercalating dyes [28, 29], and electrochemical sensing [30-32] have all shown promise. Table 2-1 outlines research by several groups, separated by isothermal amplification technique employed.

Table 2-1: Table outlining research in diagnostic isothermal nucleic acid amplification, sorted by amplification type.

Isothermal amplification technique	Research group	Detection method
Recombinase polymerase amplification (RPA)	Santiago-Felipe (2014)	Fluorescent (on a disk)
HDA	Kivlehan (2011)	Electrochemical (Redox probe intercalates with DNA, decreasing conc. in sol.)
	Mahalanabis (2010)	Separate thermocycler device and gel Bioanalyzer
Reverse-transcription helicase dependent amplification (RT-HDA)	Tang (2010)	Colorimetric (BEST cassette)
Loop-mediated amplification (LAMP)	Lee (2007)	Optical (turbidity of solution from Mg pyrophosphate production)
	Nagatani (2011)	Electrochemical (Methylene Blue binds to electrode in tube)
	Jiang (2012)	Electrochemical (MB/redox probe)
Nucleic acid-based sequence amplification	Lucchi (2010)	Fluorescent (tube reader)
	Kebe (2011), Lilian (2010), Halfon (2010)	Fluorescent (hybridize with molecular beacon)

One isothermal technique in particular, helicase-dependent amplification [21], relies on an enzyme, helicase, rather than thermal energy, to unwind and separate the DNA double helix. This allows for denaturing, primer hybridization, and extension to

occur in the same temperature region. This technique is utilized in this work, in the development of a portable DNA analysis device.

2.3 Microfluidics

Incorporating DNA amplification and detection methods into microfluidic platforms provides many operational advantages and broadens the potential applications of such devices. Reducing the sample sizes to microliter volumes, not only reduces the amount of test material to be acquired (for example: less invasive sampling from patients, or more reliable testing in researching biological microenvironments), but also has positive effects on the thermal and power requirements of the device. In the case of PCR or isothermal DNA amplification, heating a smaller sample mass requires less energy, which in turn reduces power requirements, which in turn reduces overall sample size. This trend very much lends itself to portable systems, capable of addressing pressing issues such as healthcare and food safety in remote places, as well as biological research for spaceflight application. Beyond portability, reduced sample size and power requirements can lead to faster operating times.

2.3.1 Heat Transfer in Microfluidics

Microfluidic PCR devices have taken many approaches but have some common traits based on the requirements of the PCR reaction. Materials used in microfluidics can include material as varied as silicon, glass, elastomers, hydrogels, and paper [33]. Because PCR requires cycling between three precise high temperatures, silicon and glass are often used as substrates for their high thermal conductivity. Polymers such as PDMS and PMMA are employed for their varied and low cost fabrication options and often their elastic properties are employed in novel ways to control liquid samples [34, 35]. All

materials have advantages and disadvantages in heat transfer, biocompatibility, fabrication costs, and material properties effecting sensing and sample transport.

Material selection is important, not only for biological tailoring and passivation, but also thermal management. Effective heating, temperature control, and insulation can be ensured by material selection and device geometry design, assessed by thermal modelling. Heat transfer in microfluidics is primarily conduction based, with popular heat sources including thin film heaters, heating/cooling blocks, embedded resistance wires, flexible printed circuits, and hot or cold fluid streams. Heat transfer in conduction based systems is dictated by Fourier's law, which in its differential form states:

$$q = -k\nabla T \quad \text{Eq. 2-1}$$

where q is the heat flux through a unit area per unit time (W/m^2), k is the conductivity of the material ($\text{W}/\text{m}\cdot\text{K}$), and ∇T is the temperature gradient across the material.

Convective heat transfer often plays a role in heated microsystems as well, with either forced or natural convection being used to cool heated devices. Convective heat transfer is most basically defined as:

$$Q = hA(T_a - T_b) \quad \text{Eq. 2-2}$$

where Q is heat transferred per time (W), A is the area of the area of heat transfer (m^2), h is the experimentally determined heat transfer coefficient ($\text{W}/\text{m}^2\text{K}$), T_a is the temperature (K) of the object, and T_b is the temperature (K) of the fluid, or in the case of natural convection, the temperature of the ambient environment.

These simple equations, and their integral forms, are employed in modeling heat transfer in microfluidic devices, either in simple analytical solutions or computer aided

modeling. Finite element analysis employing these fundamental concepts was used to assess the thermal performance of the proposed device.

2.3.2 Fabrication Technique – Xurography

Xurography is a fabrication technique used in microfluidics and sensor development [13, 36-39], where microstructures are cut into various films using a cutting plotter. The technique has become crucial to rapid prototyping and research applications, due to its low cost and fast turn-around time. Initial publications on the topic reported positive features as small as 35 μm and negative features as small as 18 μm cut into films ranging from 25 μm to 1000 μm [40]. These patterned films can be used as masks or molds in additive or subtractive manufacturing techniques, such as electroplating, etching, molding, or channel formation. Specifically in molding and channel formation, varying thickness films or multiple layers of films can be used to control feature sizes beyond the two dimensional pattern cut into the film. For example a film can be patterned multiple times and stacked to varying heights, before pouring and curing a liquid polymer over the pattern. The molded polymer can be bonded to another substrate to create enclosed features of varying depths [41, 42]. Composite devices can be fabricated by joining a molded material with a different material substrate, such as a molded polymer with glass.

2.3.3 Passivation of Microfluidic Devices

Surface passivation is an important tool in biological microfluidics for the prevention of unwanted interaction of samples with the surfaces contacted by the fluid. These surfaces are generally of the same material or substrate from which the entire device is fabricated. Passivation is more important for microscale geometries than for

conventional macroscale devices because of their increased surface area to volume ratio (SVR), which can cause surface chemistry effects become more prevalent. Such unwanted interactions can inhibit biological processes or obstruct the detection of analytes. Common methods to passivate substrates for use in biochemical microfluidic devices can be categorized as either static and/or dynamic [6]. Static methods consist of pretreatments in which a passivating or blocking agent is applied to the interior of a microchannel before the biological samples are introduced. Examples of this are covalently-bonded silane coatings or immobilized blocking agents such as proteins or surfactants, each providing many avenues for customization [43, 44]. Popular blocking agents include bovine serum albumen (BSA), poly(N-vinyl-2-pyrrolidone) (PVP), and polyethylene glycol (PEG). Silane and silicone treatments to microfluidic devices provide permanent, reusable surfaces that are chemically tailored for specific biological applications, for example using dichlorodimethylsilane (DDMS) to passivate a device for droplet based PCR [45] or treating a surface with a fluorosilane to allow dielectrophoretic capture of cells without permanent cell adhesion [46]. In contrast to static passivation, dynamic methods involve adding components to the sample mixture itself that will protect reagents and/or competitively adhere to the channel walls as the fluid passes through the microfluidic device. Dynamic methods provide ease of use but can suffer from low reproducibility and/or build-up of deposits with prolonged use [43].

While passivation coatings improve biochemical stability [45], some irregularities persist when implementing fluorescence analyses within high-SVR microfluidics. For example, in their exhaustive review of the field [47], Zhang *et al.*, summarize that BSA passivation is incompatible with fluorescence-based detection techniques due to low

reproducibility and interaction between BSA and the fluorescent dye/probes. In addition to poor compatibility with fluorescence and BSA, Pjescic *et al.*, [48] report a severe loss of intercalating dye during microfluidic DNA analysis. A similar dye depletion effect has been described by Guckenberger *et al.* [49] This causes loss of signal from biological samples and causes some degree of fluorescent background noise. Minimization of these effects is of particular interest.

Second generation intercalating DNA dyes - of which SYBR Green is by far the most popular for PCR applications - can inhibit enzyme activity when used in high concentration. In response, a third generation of intercalating dyes have been created (which include LC Green, SYTO9, EvaGreen, and others) which allow for full saturation of the DNA molecule without reducing PCR efficiency. These saturation dyes can provide extreme fluorescence resolution of the DNA denaturation process, and have catalyzed the research field of high resolution DNA melting analysis (HRMA) [11].

For DNA analysis microfluidics such as those that incorporate polymerase chain reaction (PCR) and associated fluorescent-based analysis techniques, quantitative polymerase chain reaction (qPCR) or melting curve analysis (MCA), combination passivation approaches have shown merit. Using both pretreatments and dynamic passivation methods allows for an inert environment and competitive binding to ensure any remaining charged surfaces are passivated. For example, Wang *et al.* combined hexamethyldisilazane (HMDS) pretreatment in conjunction with BSA or Tween 20 in reaction solution [50] and Matsubara *et al.* combined a static BSA pretreatment and dynamic PVP passivation chemistry [51]. When silicon substrates are used, passivation

has also been achieved by growing SiO₂ on the surface and using BSA in PCR solution [52].

The compatibility of substrates and additives in fluorescence-based microfluidic detection devices is vital to a wide range of lab-on-a-chip processes including DNA analysis [44], protein analysis [53], and cell manipulation [46]. In such devices, glass or clear polymers are often chosen for their optical qualities, the former also being selected for use in high temperature/heated devices because of its favorable thermal properties [43, 44]. This article will focus on glass-based microfluidics in particular.

The compatibility of these passivation methods with fluorescent markers is especially important for devices that require high resolution fluorescent imaging and differentiation of signals either spatially or based on intensity. Examples of these highly accurate yet sensitive processes include spatial DNA melting analysis [54], spatially resolved fluorescence mapping [55], and detection of any analyte at considerably low concentrations such as a growth factor for point-of-care testing [56]. The research findings presented in this article identify the kinetic behavior of the adsorption process that occurs in passivated glass microfluidics. Based on these results, an experimental methodology is presented that will provide maximum performance for fluorescence-based microfluidic assays, in particular for high-temperature applications in the areas of PCR [48, 57, 58], cell lysis [59, 60], fluorescence *in situ* hybridization (FISH) [61, 62], laser induced fluorescence (LIF) [63] or proteomics [64, 65].

CHAPTER 3

PASSIVATION OF GLASS MICROFLUIDICS FOR FLUORESCENCE-BASED ASSAYS

3.1 Introduction

The first objective of the work presented here was to characterize the interaction of the intercalating dye with some common static passivation methods for glass microfluidics. With a quantitative understanding of this behavior, the second objective was to develop a pretreatment technique that is applicable to stationary as well as continuous-flow microfluidics, at temperatures from room temperature up to 100°C. For the characterization studies, continuous-flow microdevices were used with four different surface passivating coatings: two silanes and two silicones. Analysis of reagent depletion was performed by flowing a buffered DNA-dye solution through the channels. This analysis was done (A) continuously, by collecting fluorescent images of the channel during sample flow, and (B) at an end-point condition, by collecting and examining the mixture at the microchannel outlet. Once the depleting reagents were identified, a pretreatment mixture was designed that would preload the channel walls with those same reagents, and thereby reduce or eliminate depletion during sample flow. The performance of this pretreatment strategy was confirmed by MCA.

3.2 Methods

3.2.1 Microfluidic Chip Fabrication

Microfluidic devices were fabricated by sandwiching a patterned, double-sided tape between microscope slides treated with different passivating agents. The glass microscope slides (FisherFinest, Fisher Scientific, PA, USA) were cleaned with detergent (Alconox Inc., NY, USA) and deionized water and dried with compressed air. Four coatings, pictured in Figure 3-1, were examined here, all of which were obtained from Gelest (PA, USA) in >99 % purity liquid concentrations:

1. Dichlorodimethylsilane (DDMS), which is a low atomic weight, methyl terminated silane;
2. (Tridecafluoro-1,1,2,2-tetrahydrooctyl)triethoxysilane, which is a long chain fluorine-terminated silane. In this article, it will be referred to as simply “fluorosilane”;
3. Aquaphobe CM, a methyl-terminated silicone; and
4. Aquaphobe CF, a fluorine-terminated silicone.

polyimide double-adhesive tape (PPTDE 1, Kaptontape.com, CA, USA) with a knife plotter (CE 6000, Graphtec, USA). The patterned tape was then sandwiched between the coated microscope glass slides and evenly pressed with a small vice to form channels, as seen in Figure 3-2. The channel sidewalls are formed by the tape (polyimide and silicone adhesive) and the top and bottom are the treated glass. The channels formed in this way have a rectangular cross-section, with a height equal to the thickness of the tape, which is nominally 100 μm . After assembly the channel heights were measured to be between 80 μm and 120 μm . To fabricate devices with deeper channels, two layers of patterned tape were used (~ 200 μm total height), or two layers of tape sandwiching a thin polydimethylsiloxane (PDMS) film (~ 320 μm total height) were used in the assembly. Microchannel widths between 0.5 mm and 1.5 mm were fabricated, and the channel path was either serpentine (as shown in Figure 3-2) or straight between the inlet and outlet. Since the channels are generally much wider than tall, the glass accounts for the

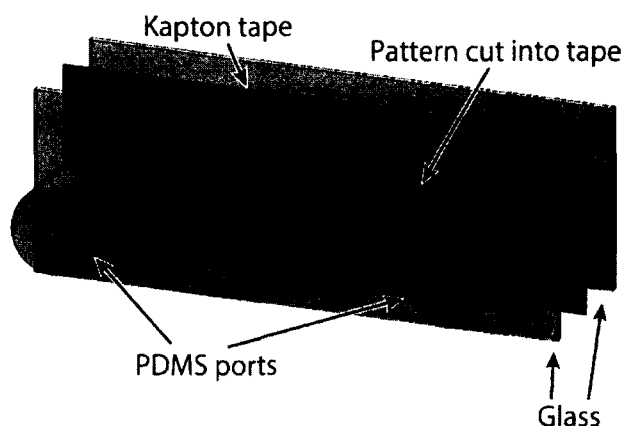


Figure 3-2: Double sided Kapton tape is patterned and sandwiched between two treated glass slides. The resulting channel is composed primarily of treated glass surfaces, through which fluorescent signal is observed, and of inert, thermostable polymer tape, which accounts for a small portion of the surface area.

overwhelming majority of the surface area; therefore, the minor effect of the tape sidewalls on the device performance is not included in this characterization study.

Polydimethylsiloxane (PDMS) ports were attached to the glass by ionizing both surfaces and pressing them together, forming a permanent bond [66]. For this, the mating surfaces were activated with an oxygen plasma generated from an ambient air line into a plasma cleaner (PDC-001, Harrick Plasma, NY, USA).

3.2.2 Optical and Heating System

For all tests, the device was imaged every 3 seconds using an uncooled 1.4 MP monochrome CCD camera (PL-B957U, Pixelink, ON, Canada) fitted with a 50 mm macro lens (Canon, Tokyo, Japan) while illuminated with a diffused LED light source (HPLS-Dragon, LightSpeed Technologies, CA, USA) to excite the dye in the sample. The camera was fitted with a low pass wavelength filter (HQ485LP, Chroma, VT, USA) and the LED with a band-pass wavelength filter (HQ450/50x, Chroma, VT, USA), limiting the LED source to a 50 nm band-pass (425–475 nm) and blocking wavelengths below 480 nm from entering the camera. The excitation light source was located approximately 10cm away from the microfluidic device to provide a mostly uniform spatial illumination across the analysis microchannel. The field of view of the imaging camera was approximately 30 mm x 30 mm. The camera was positioned such that it would image the central region of the microfluidic channel where the excitation light was the most uniform, leaving at least 10 mm of channel length upstream out of the field of view. The device was held on a heater system that was designed in-house and previously reported [48]. Briefly, a heating platform with two heating elements was controlled by a closed-loop temperature controller to elevate the temperature of the device for investigation of

fluorescent behavior at elevated temperatures. An infrared (IR) camera (A320, FLIR, OR, USA) was used for non-contact measurement of the device at the precise channel locations. Experiments were performed from room temperature up to 100°C. This experimental setup can be seen in Figure 3-3.

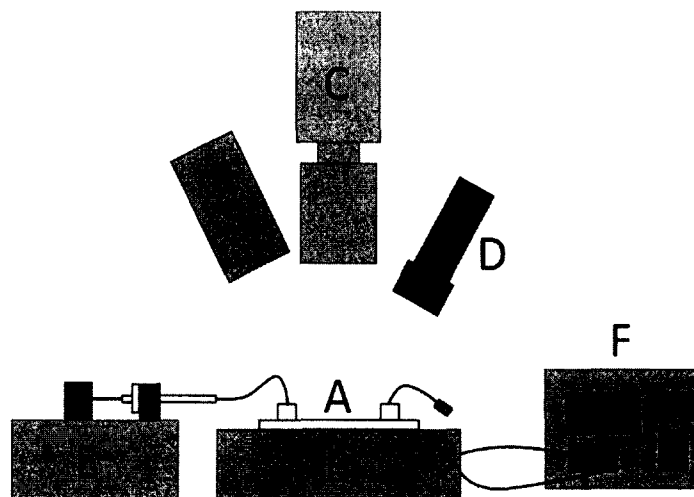


Figure 3-3: Experimental setup for fluorescence analysis in microfluidic channels. Microfluidic chip (A) rests on a heater block (B), while imaged via CCD camera (C), and illuminated by LED excitation source (D). Sample is flowed into the device via syringe pump (E). Device temperature is managed by PID controller (F) and verified via IR camera (G).

3.2.3 Experimental Conditions

Separate microchannels were passivated with each of the four different coatings and evaluated: DDMS, fluorosilane, Aquaphobe CM and Aquaphobe CF. A fluorescent solution was flowed steadily through the channel, and images of the channel were taken at two-second intervals. The solution was comprised of 10 % volume concentration LC Green Plus dye (BioFire Diagnostics, UT, USA), 1 μ M of a 50bp synthetic double-stranded DNA sequence (Integrated DNA Technologies, IA, USA), 50 mM Triz buffer, and 3 mM $MgCl_2$. The sequence of this double-stranded synthetic DNA can be found in

Appendix C. (Note: Once it was determined that the dye, not the DNA, was being adsorbed onto the surface, experiments were continued with this solution less the oligonucleotides.)

The manufacturer would not disclose the molar concentration of the dye, indicating that such details remain proprietary. The stock solution was only defined as being at a “10 X concentration”. Therefore, the final concentration of the dye in the solution described here can only be given as 1 X/ μ L. This sample mixture was flowed through the device at a constant rate using a syringe pump (KDS100, KD Scientific, MA, USA) and a 250 μ L syringe (#100, Hamilton, NV, USA). Flow rates in the range of 1-9 μ L/min were evaluated. A short length of ETFE (ethylene tetrafluoroethylene) tubing (#1516, Upchurch Scientific, WA, USA) was used between the syringe and the microfluidic device to minimize reagent losses between the syringe and the microdevice.

The presence of the DNA and the dye in the channel outflow was analyzed using a commercial qPCR/HRMA instrument (Lightscanner 32/LS32, BioFire Diagnostics, UT, USA). The effect of flow rate, channel dimensions, and operating temperature on adhesion was examined.

3.3 Results and Discussion

3.3.1 Identifying and Exploring Reagent Depletion

When less than 30 μ L of the solution are flowed (at a nominal 2 μ L/min) through a 1 mm wide channel with any of the silanes or silicone coatings, images of the channel showed no fluorescence. After exiting the channel, this sample was melted on the LS32, which confirmed the lack of fluorescence. The constituents of the original reaction mixture were then added individually into the microchannel eluent and re-melted on the

LS32. It was found that after adding another 10 % volume concentration of the DNA dye to the flowed sample, its fluorescent melting profile matched that of the original mixture. This indicates that the DNA remained in solution, while the intercalating DNA dye had adhered to the treated microchannel walls.

However, if the flow continued for more than 30uL of solution, at some point (~100 uL for the DDMS-coated channel; different for other coatings), fluorescence began to be observable at the upstream end of the camera's field of view. As seen in Figure 3-4, the spreading of the fluorescence downstream occurred slowly but sharply. Rather than a gradual brightening of the entire channel, there was a distinct interface between the brightly fluorescent and the non-fluorescent regions. This interface moved steadily downstream, giving the appearance of a "fluorescence front" traveling down the channel at a slower velocity than that of the fluid itself. In addition to having a nearly constant velocity, this leading edge of fluorescence also possessed a consistent profile as it progressed along the channel.

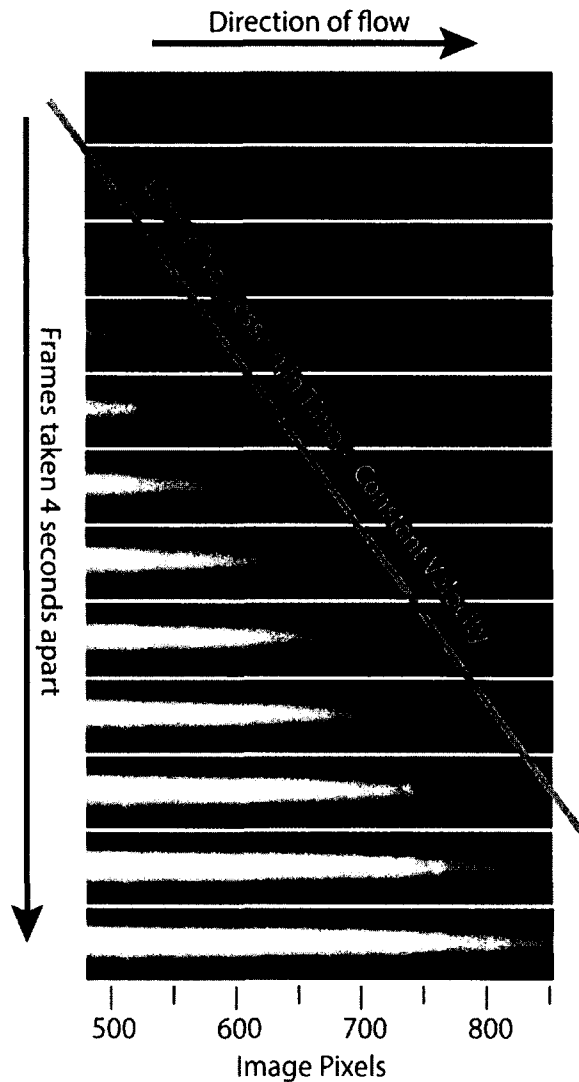


Figure 3-4: A sequence of fluorescence images of one microfluidic channel during sample flow. Initially, no fluorescence is observed. A fluorescence front appears after some time and moves in the direction of the sample flow at a steady rate. The specific experimental conditions for this series of images is provided in Table 3-2 (experiment G).

The sharp profile of the fluorescence front is distinctly different from that of the laminar velocity flow profile (Reynold's Number = 0.023) generated by this microfluidic channel geometry, which is known to have a flat leading edge. The shape of the fluorescence profile, which remains unchanged for a given channel geometry, is attributed to the lateral diffusion of the dye out from the center of the flow stream to the

edges where little dye arrives from upstream. The uniformity of the upstream fluorescence, the constant velocity of the fluorescence front, and the sharpness of that bright-dark interface suggests that:

- A. The dye has a strong affinity to the surfaces that are treated with these bio-passivation coatings.
- B. There is some saturation limit at which no additional dye adheres to the surface.
- C. Upstream of the fluorescence front, the dye remains in solution, at the original concentration.
- D. Downstream of the fluorescent front, no dye is present in the solution.

Therefore, it is hypothesized that the dye is pulled out of solution to attach to the surface only in the near vicinity to the fluorescent front; not upstream because those surfaces are already dye-saturated; not downstream because there is no dye remaining in the downstream solution; it all adheres at the fluorescent front. As the bright-dark interface saturates, the fluorescence front shifts further down the channel. The rate at which this front moves is simply a function of the saturation limit of the channel walls and the rate at which new dye molecules are introduced down the channel.

3.3.2 Derivation of Dye Saturation Model

A mathematical model was developed to explain the observed dye saturation behavior. Consider a microchannel with a rectangular cross-section, having a width much greater than its height, such that it can be approximated as two parallel walls, as shown in Figure 3-5.

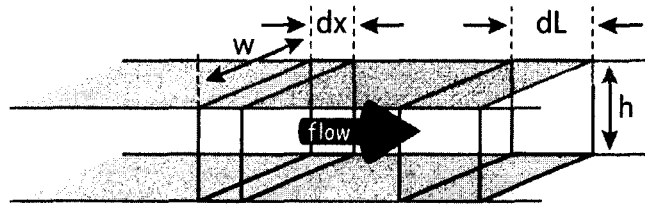


Figure 3-5: Diagram representing the movement of the fluorescence front and the movement of the liquid down a high-aspect-ratio microchannel. Edge effects are ignored, such that the channel can be treated as two parallel walls.

During an infinitesimal time, dt , the liquid moves a distance of dL down the length of the channel, while the fluorescence front moves a smaller distance, dx . Thus, the average liquid velocity (v_{liq}) and the fluorescence saturation velocity (v_{sat}) are, respectively:

$$v_{liq} = \frac{dL}{dt} \quad \text{Eq. 3-1}$$

$$v_{sat} = \frac{dx}{dt} \quad \text{Eq. 3-2}$$

The surface area (A_{sat}) that is saturated over the time dt is:

$$A_{sat} = 2 \cdot w \cdot dx \quad \text{Eq. 3-3}$$

where w is the width of the microchannel. Assuming that dx is smaller than dL , the volume of liquid that passes over this newly saturated area is:

$$V_{liq} = h \cdot w \cdot dx \quad \text{Eq. 3-4}$$

where h is the height of the microchannel. Assuming that only and all the dye originally within this volume was what completely saturated that surface area, then that amount of dye (D_{sat}) is simply:

$$D_{sat} = V_{liq} \cdot C_{dye} \quad \text{Eq. 3-5}$$

where (C_{dye}) is the concentration of the dye in the original liquid mixture. The ratio (N_{sat}) between this saturating amount of dye and the saturated surface area can be defined as a property of the surface:

$$N_{sat} = \frac{D_{sat}}{A_{sat}}. \quad \text{Eq. 3-6}$$

By combining Equations 3-3, 3-5, and 3-6:

$$N_{sat} = \frac{V_{liq} \cdot C_{dye}}{2 \cdot w \cdot dx} \quad \text{Eq. 3-7}$$

and then substituting in Equation 3-4 and simplifying:

$$N_{sat} = \frac{h \cdot dL \cdot C_{dye}}{2 \cdot dx} \quad \text{Eq. 3-8}$$

and finally by using Equations 3-1 and 3-2 to eliminate dL and dx from Equation 3-8, and simplifying:

$$N_{sat} = \frac{1}{2} h \cdot C_{dye} \cdot \left(\frac{v_{liq}}{v_{sat}} \right). \quad \text{Eq. 3-9a}$$

Rather than assuming parallel walls, the microchannel could alternatively be modeled as a cylinder with a circular cross-section of constant radius (R). Following the same derivation process, the surface saturation property would be nearly identical:

$$N_{sat} = \frac{1}{2} R \cdot C_{dye} \cdot \left(\frac{v_{liq}}{v_{sat}} \right). \quad \text{Eq. 3-9b}$$

Repeating this derivation for a microchannel with an arbitrary cross-section yields:

$$N_{sat} = \frac{1}{4} D_h \cdot C_{dye} \cdot \left(\frac{v_{sat}}{v_{sat}} \right) \quad \text{Eq. 3-9c}$$

where D_h is the hydraulic diameter of the microchannel.

Therefore, with any known, wetted cross-sectional geometry, the dye saturation limit of any surface coating can be established experimentally by measuring the velocity of the fluorescent front under known – but essentially arbitrary – operational parameters. Once determined, this N_{sat} value can be used to “dye passivate” any device used under any experimental conditions by using the following equation:

$$D_{px} = N_{sat} \cdot A_{surf} \quad \text{Eq. 3-10}$$

where D_{px} is the amount of dye that should be passed through the microchannel prior to any experiment requiring fluorescence imaging, and A_{surf} is the total interior surface area of the microchannel.

The following sections present the empirical calculation of the N_{sat} values for the four coatings previously described, as well as experimental results that support the validity of Equation 3-9 and Equation 3-10.

3.3.3 Effect of Passivation Coating on Dye Depletion

The position of the visible fluorescence was tracked over time as dye/buffer solution was flowed through channels treated with different coatings. Multiple devices passivated with each silane or silicone ($N = 5$ for DDMS and the fluorosilane, $N = 3$ for Aquaphobe CM and Aquaphobe CF) were evaluated under identical experimental conditions. Fluorescence images such as those shown in Figure 3-3 were collected, and analyzed in MATLAB (Mathworks, MA, USA). The spatial distribution of the fluorescence within these images was calculated as function of time and position, as shown in Figure 3-6.

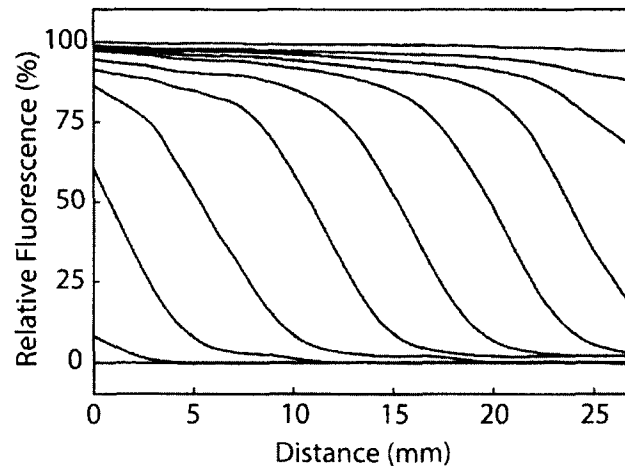


Figure 3-6: Representative curves indicating the fluorescence along the length of the microfluidic channel at time intervals of 12 seconds. Images such as those shown in Figure 3-4 were used to generate these curves (Image analysis algorithm follows that presented in [48]).

For all images, the channel position and time at which the fluorescence reached 30% of its maximum value was calculated. Figure 3-7 shows representative results for: a 1 mm x 100 μ m x 50 mm straight channel, flow rate of 1.5 μ L/min, at room temperature. Fluorescence signal progression was analyzed over a 20 mm section of the channel, where the excitation source most evenly illuminated the channels. The slope of these lines is the velocity of the fluorescent front (v_{sat}). These velocities are different for each surface treatment, indicating that each will have a unique N_{sat} value. The corresponding N_{sat} values for each coating are calculated based on the average saturation velocities and the specific experimental and geometric parameters, and provided in Table 3-1.

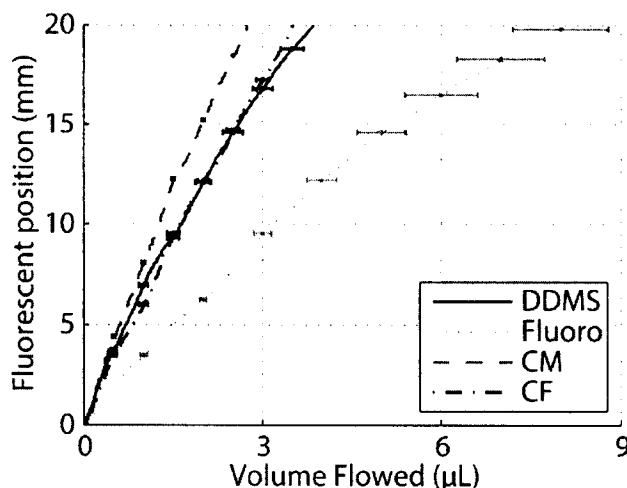


Figure 3-7: Position of fluorescence front as a function of solution volume flowed and glass coating protocol. These curves show the average fluorescent signal progression over multiple trials ($N = 5$ for DDMS and Fluoro, $N = 3$ for CM and CF) in multiple microchannels. The standard deviation between trials was calculated for all 400+ pixels analyzed in the images; to aid in visualization, though, only a select number of these deviations are shown on this graph.

Table 3-1: Empirical values of N_{sat} calculated for each of the four coatings.

Coating	N_{sat} (in X/ mm^2)
DDMS	0.155 ± 0.04
Fluorosilane	0.306 ± 0.06
CM	0.104 ± 0.004
CF	0.149 ± 0.01

The silicone coatings, Aquaphobe CM and CF, have a lower N_{sat} than the silanes, indicating that less dye is required to passivate these channels. The N_{sat} value for DDMS is only slightly greater than that of CF. Between the two silanes tested, DDMS adsorbed less dye than the fluorosilane. Possible trends relating coating type and fluorescent dye interaction can be further explored based on these results. Here, silicones interact with the dye to a lesser extent than the silanes tested. Furthermore, it is notable that both the

fluorinated silane and the fluorinated silicone interact with the dye more than their methyl-terminated counterparts. This suggests that the electro-negative fluoro-terminated surfaces bind more strongly to the dye than the methyl-terminated surfaces. This is analogous to the charge interaction of the dye molecule with the negatively charged backbone of the DNA helix. It is also interesting to observe that there is no correlation between dye adsorption and the molecule length (DDMS has functional groups one carbon atom long while the fluorosilane and silicones range from 8-30 carbon atoms long).

3.3.4 Effect of Experimental Parameters on N_{sat}

The dependence of the N_{sat} values on a variety of test conditions was investigated. The effect of channel width, height, temperature, sample flow velocity, and dye concentration were evaluated independently. Data such as that shown in Figure 3-7 was collected, and the respective fluorescent velocities were calculated and compared against those predicted by Eq. 3-9a. Dependence on surface treatment was described in the previous section; thus, this additional parametric study was performed using a single coating chemistry for all tested channels - DDMS.

The analytical solution indicates that N_{sat} is a property of the coating, and therefore is independent of all arbitrary experimental conditions as well as the microchannel geometry. If N_{sat} is truly a constant, then the saturation velocity v_{sat} is the only dependent variable in Equation 3-9. Baseline experiments ($n = 4$) were performed with the following parameters: temperature = $\sim 25^{\circ}\text{C}$; coating = DDMS; width = 1 mm; average height = 93 μm ; length = 50 mm, straight; $C_{dye} = 1\text{X}/\mu\text{L}$; average $v_{liq} = 0.27$ mm/s. The average and standard deviation of v_{sat} were calculated under these conditions.

Single tests ($n = 1$) were conducted in which one or more of these parameters were changed.

Since Equation 3-9a does not include the variables of channel temperature and width, changes in those variables should leave the ratio of v_{liq} to v_{sat} unchanged. This was confirmed by conducting tests from room temperature ($\sim 25^\circ\text{C}$) to 75°C , and with channel widths from 0.5 mm to 1.5 mm; the fluid velocity (v_{liq}) for each test was controlled by setting the volumetric flow rate.

Equation 3-9a predicts that v_{sat} is directly proportional to channel height, dye concentration, and fluid velocity. The height dependency was examined in the 100 μm and the 320 μm deep channels described above. Dependence on dye concentration was investigated by increasing C_{dye} from 1 X/ μL to 2 X/ μL . The effect of fluid velocity was tested by evaluating v_{sat} for fluid velocities between 50 % and 600 % of the baseline (0.27 mm/s).

The results of these experiments are summarized graphically in Figure 3-8. The average v_{sat} for the baseline tests is shown (A), as well as error bars indicating one standard deviation above and below this average. For (B) through (H), the N_{sat} value for DDMS (see Table 3-1) was used along with the independent experimental parameters (shown in Table 3-2) to predict the v_{sat} values for each scenario. One standard deviation of each predicted value is indicated by a rounded rectangle; the actual measured v_{sat} for each experimental case is shown by a circle. For each parametric test, the measured v_{sat} is within one standard deviation of the value predicted by Equation 3-9a, with the exception of the test using the fastest flow velocity. This test resulted in the fluorescence front moving at a faster velocity than predicted. However, this is reasonable behavior. At high

flow rates, it is expected that the dye does not diffuse to the surface within the distance dx (see Figure 3-4), but is carried further downstream in solution. Dye saturation of the surface, then, does not occur instantaneously in this case, which is assumed in the Eq. 3-9 derivation. Therefore, the data point (E) in Figure 3-8 is not a true measure of the saturation velocity, but rather just a track of the combined fluorescence of the dye on the surface and the dye in solution. Although this highlights a “diffusion limit” that would interfere with the empirical calculation of N_{sat} at high fluid velocities, the application of Eq. 3-10 is not similarly tied to a specific velocity range.

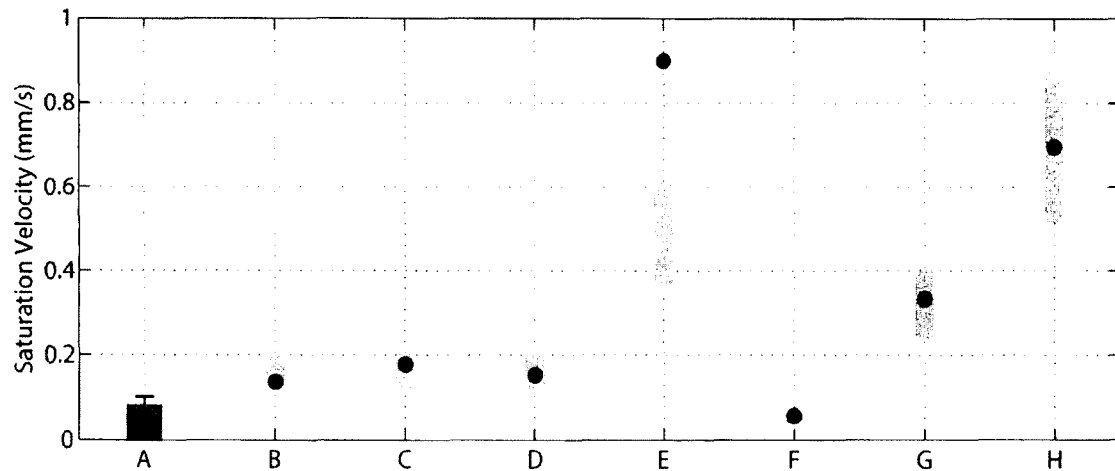


Figure 3-8: The effect of various experimental conditions on the fluorescence saturation rate (v_{sat}) were investigated by tracking signal velocities in DDMS coated microfluidic channels. The parameters used in the baseline experiments (A) as well as the subsequent tests (B-H) are provided in Table 3-2. The rounded rectangles indicate the range of predicted values based on Table 3-1 and Eq. 3-9a.

Table 3-2: Specific experimental conditions used for parametric tests. A-H correspond to experiments described in Figure 3-8. Tests (A-G) were conducted in channels fabricated with 100 μm thick tape and test (H) was conducted in a channel fabricated with a 320 μm thick tape-PDMS layer.

	Flow velocity (mm/s)	Width (mm)	Height (μm)	Temperature ($^{\circ}\text{C}$)	Dye Conc. (X)
A	0.27	1	93	25	1
B	0.54	0.5	92	25	1
C	0.61	1.5	82	25	1
D	0.60	1	83	75	1
E	1.7	1	87	25	1
F	0.16	1	103	25	1
G	0.55	1	91	25	2
H	0.70	1	323	25	1

The functional limit of Eq. 3-9 is the scenario under which v_{liq} and v_{sat} are the same. Under this condition, dye saturation of the surface happens simultaneously as the fluid front passes. Eq. 3-9 indicates that for a DDMS coating ($N_{sat} = 0.155 \pm 0.04 \text{ X/mm}^2$) and a dye concentration of 1 $\text{X}/\mu\text{L}$, this will occur at a channel height of $310 \pm 80 \mu\text{m}$. This was confirmed experimentally as condition (H) of Figure 3-8. The automated algorithm as well as visual inspection of the images confirmed that the fluid flow front and the fluorescence front were in fact superimposed under such conditions. Therefore, both analytical and experimental results agree that Eq. 3-9 can be used to empirically measure N_{sat} for any given surface coating or material.

3.3.5 Pretreatment

To demonstrate the functionality of Eq. 3-10, microfluidic devices were fabricated containing a serpentine channel in the geometry shown in Figure 3-2, all “DNA-passivated” with DDMS. Being 11 cm long x 1 mm wide, the microchannel contained

220 mm² of exposed glass. Table 3-1 with Equation 10 predicts that 34.1 X of LC Green Plus will “dye-passivate” this amount of DDMS-treated surface. Therefore, a mixture was prepared which contained a buffered solution of 1 X/ μ L (10 % v/v) dye. Some of the devices were pre-treated with 35 μ L of this mixture, flowed at 0.5 mm/s (3 μ L/min) and room temperature. DNA melting analysis was performed on these devices (DNA-passivated and dye-passivated) as well as those that were not pre-treated (i.e. DNA-passivated only), using a technique previously described [48]. In short, the microdevice was placed in a heating fixture that would maintain one long edge at a high temperature while cooling the other long edge. In this way, fluid passing through the channel would experience a cyclic temperature gradient between 65°C and 95°C. The DNA/dye solution was then flowed into the microchannel via a syringe pump at 2 μ L/min (0.33 mm/s). Spatial MCA was performed using an in-house image analysis software [48] and was compared to a control experiment in the LightScanner32 system (which ramps temperature in time rather than position). Figure 3-9 shows identical sections of an (A) untreated and (B) treated microchannel after 8 μ L of DNA sample flow entered the imaged section of channel. The fluorescent signal of the DNA sample is only able to be detected in the treated device. Only after an additional 25 minutes (50 μ L) of continuous sample flow did the untreated microchannel begin to fluoresce to the point where spatial MCA was marginally possible. Spatial MCA results in the pretreated channel (Figure 3-9C) were compared to temporal MCA results from the LightScanner32 system (Figure 3-9D). Matching shape and position features of both curves confirm the compatibility between the treated microchannel and the DNA/dye solution.

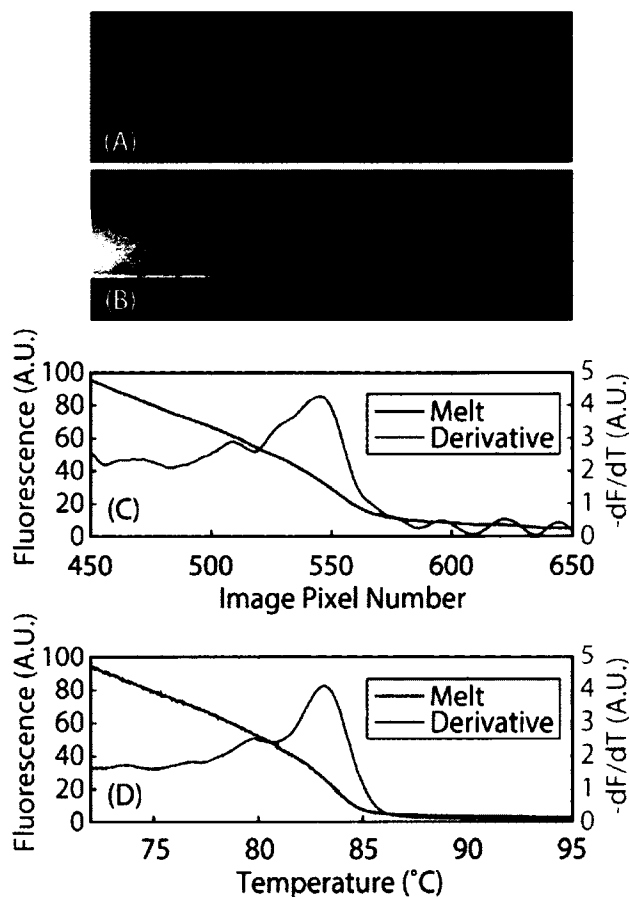


Figure 3-9: A temperature gradient was established along a microchannel silanized with DDMS. Continuous-flow DNA melting was performed (A) without dye pre-treatment, and (B) with dye pre-treatment. The melt curve and derivative plot for (B) is shown in (C). A control sample was also melted in the LightScanner32 system (D) for comparison.

A pretreatment mixture was prepared to passivate the interior of the channel with fluorescent dye, preventing leaching from the sample. The LC Green Plus and MgCl-Tris buffer solution was flowed over a temperature gradient to investigate performance of this technique at a range of higher temperatures. The increase of fluorescent signal due to flow of the pretreatment solution was monitored over time. The dye adhesion to the walls of the device, as measured by the rate of fluorescent intensity increase, was seen to decrease over time (i.e. slowed increase of intensity means less adhesion). As seen in

Figure 3-10, fluorescence increases as more volume is flowed, with lower temperature regions increasing sooner and to higher intensities. The intensity is higher at lower

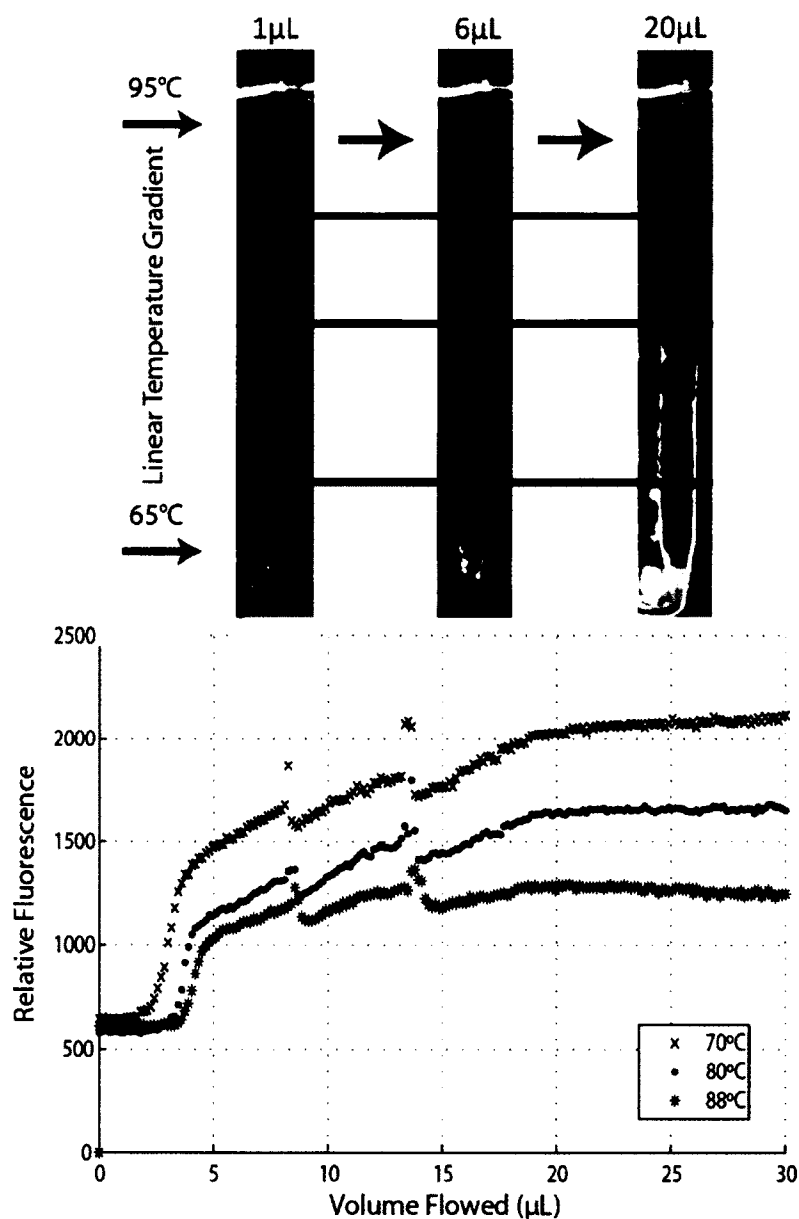


Figure 3-10: Analysis of pretreatment flow in a microfluidic channel on a temperature gradient. Images of a channel flowed with pretreatment solution can be seen on left to show visibly increased fluorescence over time. The channel was analyzed at the three indicated channel positions (three different temperatures) and the resulting fluorescence profiles as functions of volume flowed are color coded.

temperatures and lower intensity at higher temperatures primarily because fluorescent dyes emit less photons at higher operating temperatures [58], but also likely because adhesion will occur less at elevated temperatures.

The channel was analyzed at three different positions, corresponding to temperatures 70, 80, and 88°C. These temperatures fall within a common range used in PCR and MCA, protein denaturation, and cell lysis. It was observed that the signal is lower at higher temperatures (due to the inherent behavior of the dye) and that saturation occurs faster when compared to lower temperatures. Initial rise in intensity happens at 500 arbitrary fluorescence units per microliter flowed (A.U./ μL) for all temperatures. After 3 μL or less of flow, the increase of fluorescence slowed to about 16-33 A.U./ μL , varying with temperature. After 20 μL of sample flow for lower temperatures and only 12 μL at higher temperatures, the fluorescence curves begin to level off, with increase less than 10 A.U./ μL . This indicates the surface is becoming saturated with the dye. Sufficient saturation occurs at higher temperatures after approximately 12 μL and at lower temperatures after approximately 20 μL of pretreatment. After approximately 20 μL of flow, there is a slight decline in intensity of the highest temperature (88°C) curve; it is believed to be due to photo-bleaching of the comparably lower quantity of adhered dye. This effect may be occurring at lower temperatures as well but a decline in intensity isn't seen because there is a higher quantity of immobilized dye at lower temperatures and also because most fluorescent dyes emit less photons at higher operating temperatures.

Bubbles were formed in the channels of the microfluidic device after 10 μL and 15 μL of dye solution was introduced. The disturbances in the curves are due to these air bubbles flowing through the channel. Though these are brief there is some lasting

influence; a small decrease in fluorescent intensity appears immediately after the bubble and takes approximately 2 or 3 μL of flow to recover to the previous increasing fluorescence trend.

3.3.6 Conclusions

The interaction between a third-generation intercalating DNA dye and passivating coatings was explored. A solution has been formulated to solve the problem of dye loss that was observed in fluorescence based assays. The affinity of the dye to attach to the walls of microfluidic devices was characterized by analyzing fluorescent images collected during sample flow. Numerous device conditions were considered and the saturation limit for different coatings was found to constant and independent from flow rate, temperature, dye concentration, and channel dimensions. Upon quantifying the amount of dye that would saturate each surface, a pretreatment method was proposed and verified. By pre-treating the surface with a calculated amount of dye, it becomes saturated, such that no more dye is lost from the microfluidic samples, ensuring fast efficient detection. This technique can be used by other researchers to improve microfluidic fluorescence assays and expand knowledge in the area of passivation/dye interactions.

CHAPTER 4

MICROFLUIDIC HELICASE-DEPENDENT AMPLIFICATION FOR μ TAS APPLICATION

4.1 Introduction

Helicase-dependent amplification (HDA) is a nucleic acid amplification technique of interest for microfluidic application. Where traditional PCR requires cycling between multiple temperatures, HDA requires incubation at a single temperature, lowering thermal control and fluid handling requirements in μ TAS applications. On-chip HDA has been performed [29] but on-chip amplification and sequence specific detection has yet to be achieved. A device is proposed which will accomplish the following:

- 1) On-chip HDA
- 2) On-chip amplification detection
- 3) On-chip melting curve analysis.

In order to approach these goals on a chip based system, HDA protocols were developed in a laboratory setting.

4.2 Isothermal DNA Amplification

4.2.1 Helicase-Dependent Amplification

Helicase dependent amplification is an isothermal nucleic acid amplification technique, utilized here for its robust performance and design adaptability. A HDA kit from BioHelix Corp (IsoAmp III tHDA kit, MA, USA) was used and adapted to facilitate

on-chip amplification. The reaction was optimized to amplify a 110 base pair target on the well-studied Phi X 174 bacteriophage plasmid [67]. The complete sequence for the Phi X 174 template can be found in Appendix A and the 110bp target sequence and primers can be found in Appendix B. Before moving the reaction to a chip based device, the reaction was optimized on a commercial qPCR/HRMA instrument (LightScanner 32/LS32, BioFire Defense, UT, USA). This device was also later used for comparison and positive control tests. Quantitative HDA and melting analysis were performed, using the third generation intercalating DNA dye, LC Green Plus+ (BioFire Diagnostics, UT, USA), to detect amplification and melting of DNA products.

Initial tests using the HDA kit were performed by incubating the reaction mixture in a thin walled plastic centrifuge tube submersed in a water bath heated via hotplate (VWR, Radnor, PA, USA), monitoring the bath temperature near the tube via thermocouple. The reaction mixture contained Phi X 174 template (Integrated DNA Technologies, Coralville, IA, USA) at 20 pg/ μ L, primers (Integrated DNA Technologies) at 75 μ M for each forward and reverse, deoxynucleotide (dNTP) mix (BioHelix), enzyme mixture (BioHelix), buffer mixture (BioHelix). The IsoAmpIII Enzyme Mix contains a proprietary mixture of helicase, polymerase, and single stranded DNA binding protein, optimized for specific amplification of short targets with reduced non-specific products. After incubation in a water bath, the intercalating DNA dye LC Green Plus+ was added to the amplified HDA mixture and Melting Curve Analysis was performed on the LightScanner32 system. The amplified product from the HDA reaction was compared to known melting curves for this sequence, showing matching melt signatures – the negative derivative of the melt curve shows a single peak at 81.5°C (data not shown).

For further developing protocols, moving the incubation step onto the LightScanner32 platform was crucial. The LS32 is capable of amplifying and melting 32 samples in individual glass capillaries, holding 5-20 μL samples in each (a greatly reduced sample volume compared to a water bath incubation method). This allows for observation during amplification (quantitative or real-time HDA) and the comparison of samples with different component ratios. One obstacle was observed and overcome when performing HDA on the LS32: the HDA reaction is inhibited by LC Green. Initial tests performing HDA on the LS32 yielded no detectable product. This is believed to happen because, as described in the previous section concerning LC Green concentration effecting DNA melting temperature, LC Green stabilizes the dsDNA structure. This may in turn make it more difficult or require more energy input for the helicase to unwind and separate the strands, similar to DNA melting requiring more energy, i.e. higher temperature. To test the hypothesis of LC Green inhibiting the reaction, mixtures were incubated with and without added dye, and dye was added to the dye-free sample after incubation. They were then melted, and relative concentrations of amplified target DNA could be determined. Each sample contained 10 μL of the above described HDA mixture and 1 μL of LC Green was added to one sample, yielding a 0.91 X LC Green concentration. This lowered the concentration of the other reagents by approximately 9 %, but this is within a reasonable range for successful amplification. The samples were incubated for 90 min at 65°C. One microliter of dye was added to the dye-free sample, yielding the same concentration. Figure 4-1 shows MCA results for the two samples.

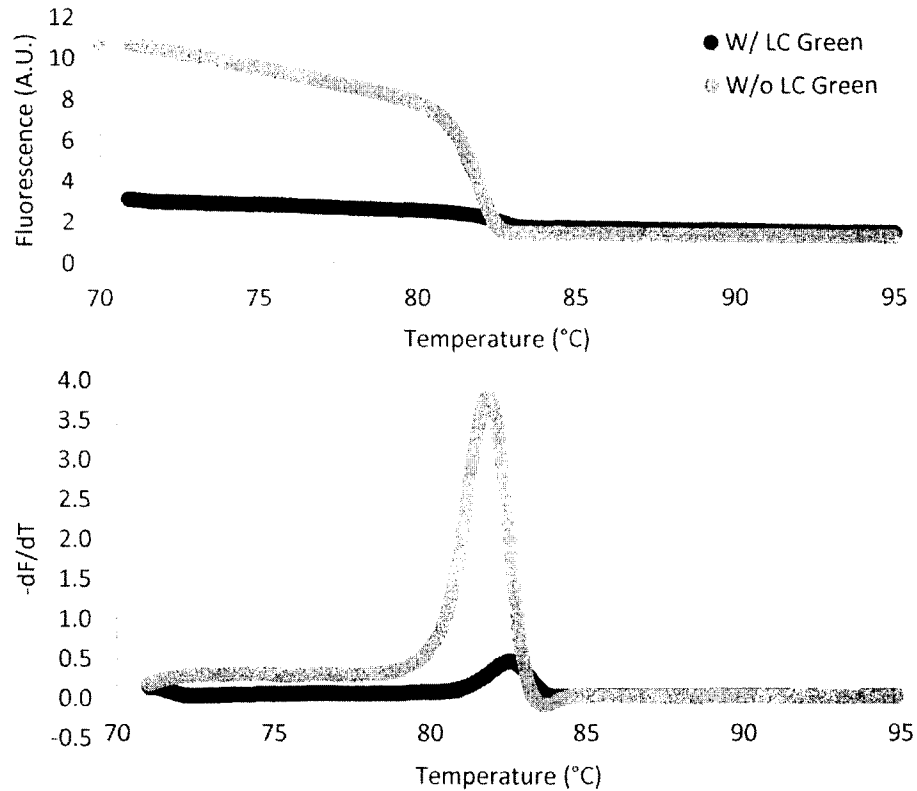


Figure 4-1: The effect of LC Green Plus+ on helicase-dependent amplification. Melting curve analysis results of products amplified in the presence and absence of 1 X concentration LC Green Plus.

The amplified product of the HDA reaction in the presence of LC Green had a much lower fluorescent signal and MCA peak height compared to the amplified product of the HDA reaction in absence of LC Green (3.5 times lower signal intensity between 70°C and 79°C, the temperature region in which the DNA is double stranded and has not yet denatured). This indicates a much lower concentration of nucleic acid was produced due to inhibition of the HDA reaction. The peak in the $-dF/dT$ curve for the dye containing sample is so low that much of the defining features specific to this sequence are lost or distorted, such as accurate melting temperature, peak shape, and peak shoulder (visible in the dye free sample $-dF/dT$ curve at 83°C). When these characteristics are lost,

it becomes difficult to positively identify a product based on MCA results; therefore such low intensity samples are not desirable and this inhibition must be overcome.

It was hypothesized that, increasing enzyme mix concentration (helicase, polymerase, and ssDNA binding protein) would overcome HDA inhibition by LC Green. Samples containing 1 X and 2 X concentration enzyme mix, both with 1 X concentration LC Green, were incubated and melted as in the above experiment. In addition to melting curve analysis, real-time HDA was performed by monitoring the fluorescence of the samples every 2 minutes, yielding 45 acquisitions over the 90 min incubation. Amplification and melting curves can be found in Figure 4-2. Amplification curves show lift-off into the exponential phase after 25 min. After 50 min, another increase in fluorescence occurs, indicating production of a secondary product. Melting analysis showed similar results to the previous experiment, with the standard enzyme concentration sample yielding no detectable amplified DNA and the increased enzyme concentration sample yielding a melting curve of identical shape and similar melting temperature (shifted 1.5°C lower). There is a low intensity peak (~25 times less intense compared to the product) with a T_m of approximately 87°C, likely caused by non-specific product produced later in the HDA incubation. Where primer dimer product formations, due to extension of secondary structures formed by primers annealing to themselves, typically have lower melting temperatures. This high T_m product is likely due to extension of longer sections of the template, occurring after the primary amplification and resulting in a much lower concentration (as indicated by the difference in peak height in MCA). The T_m shift of the primary product was likely due to an unintended interaction between the increased concentration of enzymes and the dye molecules.

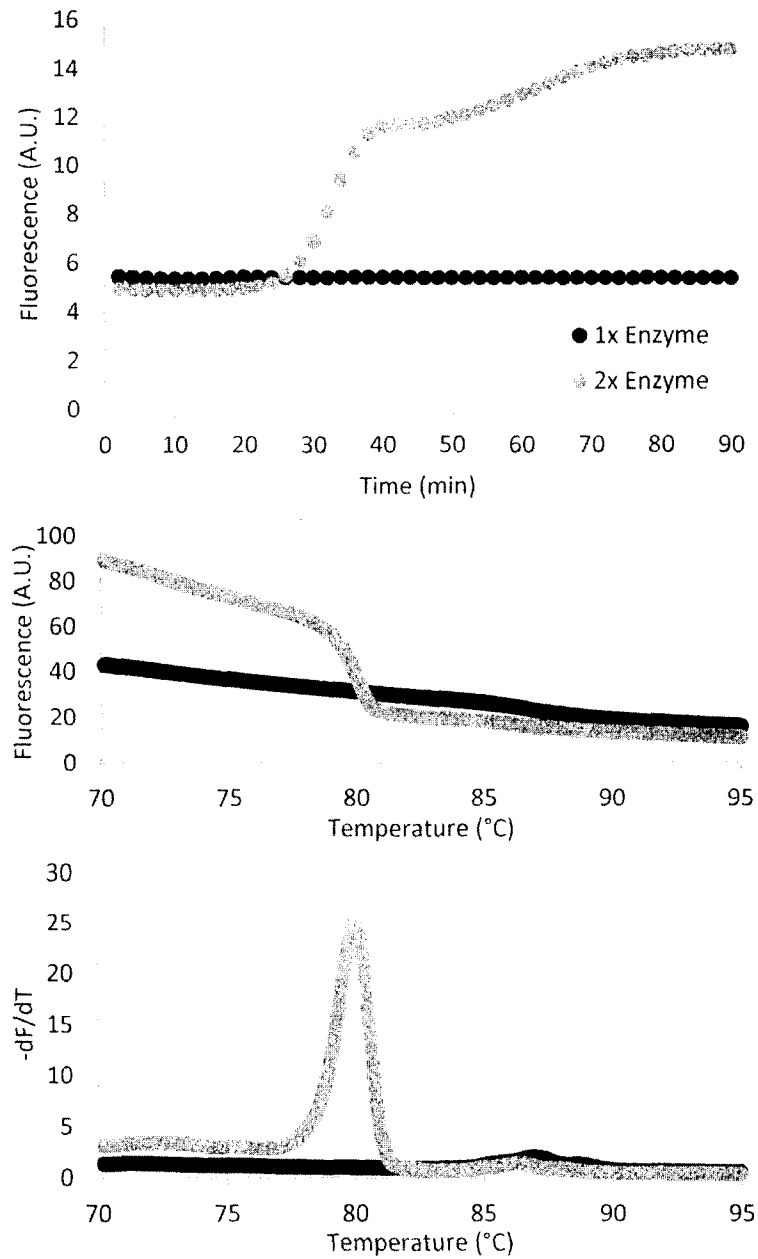


Figure 4-2: Increased enzyme concentration overcomes HDA inhibition by LC Green Plus. Real-time HDA (top) and MCA (middle and bottom) were performed on samples containing 1 X LC Green and either 1 X or 2 X HDA enzyme mix.

4.2.2 Reduction of Incubation Time

With inhibition overcome by increasing enzyme concentration, reduction of the overall reaction time was explored. The bulk of the overall micro-device performance time was projected to be the HDA reaction incubation time (1.5 hours), with the estimated sample preparation and loading time (~10 min) and analysis time (~10 min) being much shorter. Tests were conducted to lower the incubation time by increasing the concentration of the enzyme mixture component of the HDA reaction. It was noted as an unpublished observation that increasing the concentration of this mixture can yield rapid amplification. Using reagent composition similar to the previous tests, four samples were prepared with 1 X concentration LC Green and increasing amounts of enzyme mix: 2 X, 3 X, 4 X, and 5 X concentrations. These samples were incubated for 30 min, rather than 90 min, and then melted. The resulting MCA can be seen in Figure 4-3.

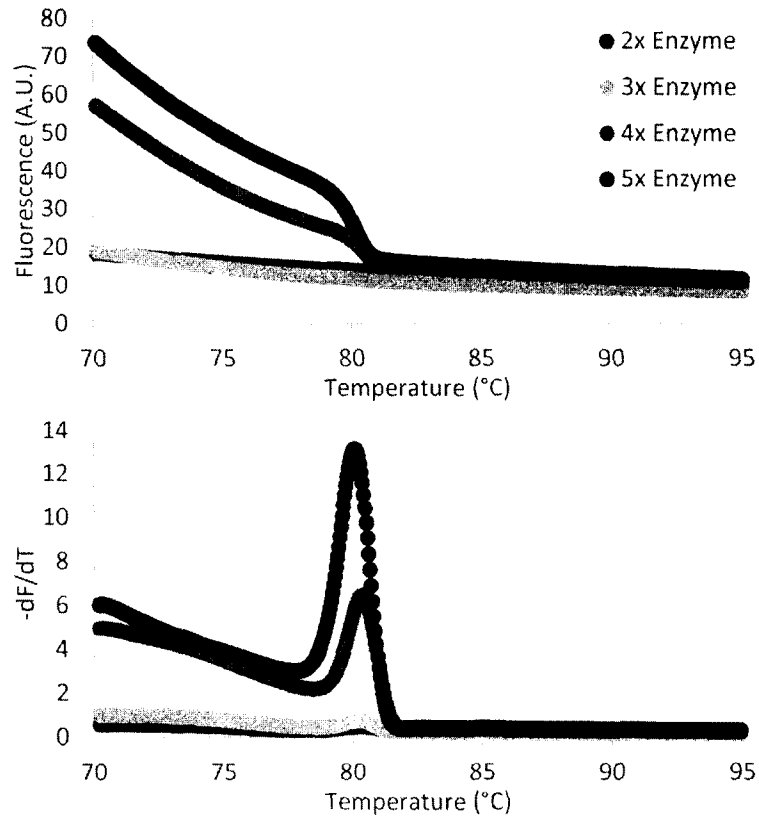


Figure 4-3: Increased enzyme concentration allows for decreased HDA incubation time. HDA mixtures containing enzyme concentrations of 2 X to 5 X were incubated for 30 min and MCA was performed.

At 30 min incubation time, samples containing 2 X and 3 X enzyme were not produce products concentrated enough to identify, but 4 X and 5 X enzyme concentrations were much more identifiable. At lower temperatures, fluorescent intensities were 3.9 times higher when 5 X enzyme was used, and 3 times higher when 4 X enzyme was used, indicating much higher concentrated product.

A helicase-dependent amplification assay was explored and optimized, with the intent to develop as μ TAS DNA analysis device. Real time amplification and melting curve analysis, both utilizing an intercalating DNA dye, were the primary techniques

used. Reaction inhibition was overcome and the incubation time was shortened from 1.5 hr to a potential 30 min.

4.2.3 Asymmetric Helicase-Dependent Amplification

Probe based detection mechanisms rely on attaching a short ssDNA probe to a single stranded or denatured double stranded DNA product. Where PCR and isothermal variants such as HDA produce double stranded DNA products, asymmetric variants produce double-stranded and single-stranded products. The greater quantity of single stranded product can be utilized for probe based detection mechanisms.

With the possibility for probe based detection in mind, asymmetric Helicase-dependent Amplification was explored. The optimal primer ratio for asymmetric amplification was determined by considering quantity and specificity of double stranded product as well as assessing the presence of amplified single stranded product. This was done using amplification curves, MCA results, and gel electrophoresis results. The previously described HDA reaction was modified for asymmetric amplification by changing the ratios of the Phi X 174 primers. Beginning with 75 μM of each, forward and reverse primer concentrations were individually increased to 2 to 1 ratio (150 μM to 75 μM) and 3 to 1 ratio (225 μM to 75 μM). Table 4-1 outlines sample compositions.

Table 4-1: Sample compositions for asymmetric HDA.

Abbreviation	Forward primer Conc. (μM)	Reverse primer conc. (μM)
Control	75	75
F2:1	150	75
F3:1	225	75
R2:1	75	150
R3:1	75	225

These samples were incubated for 90 min in the LS32, under real time monitoring, and then melted. Amplification and melting curves can be seen in Figure 4-4. Four copies of each sample mixture were prepared and tested ($N = 4$), though one F2:1 outlier was ignored due to low sample volume and low fluorescent signal ($N = 3$).

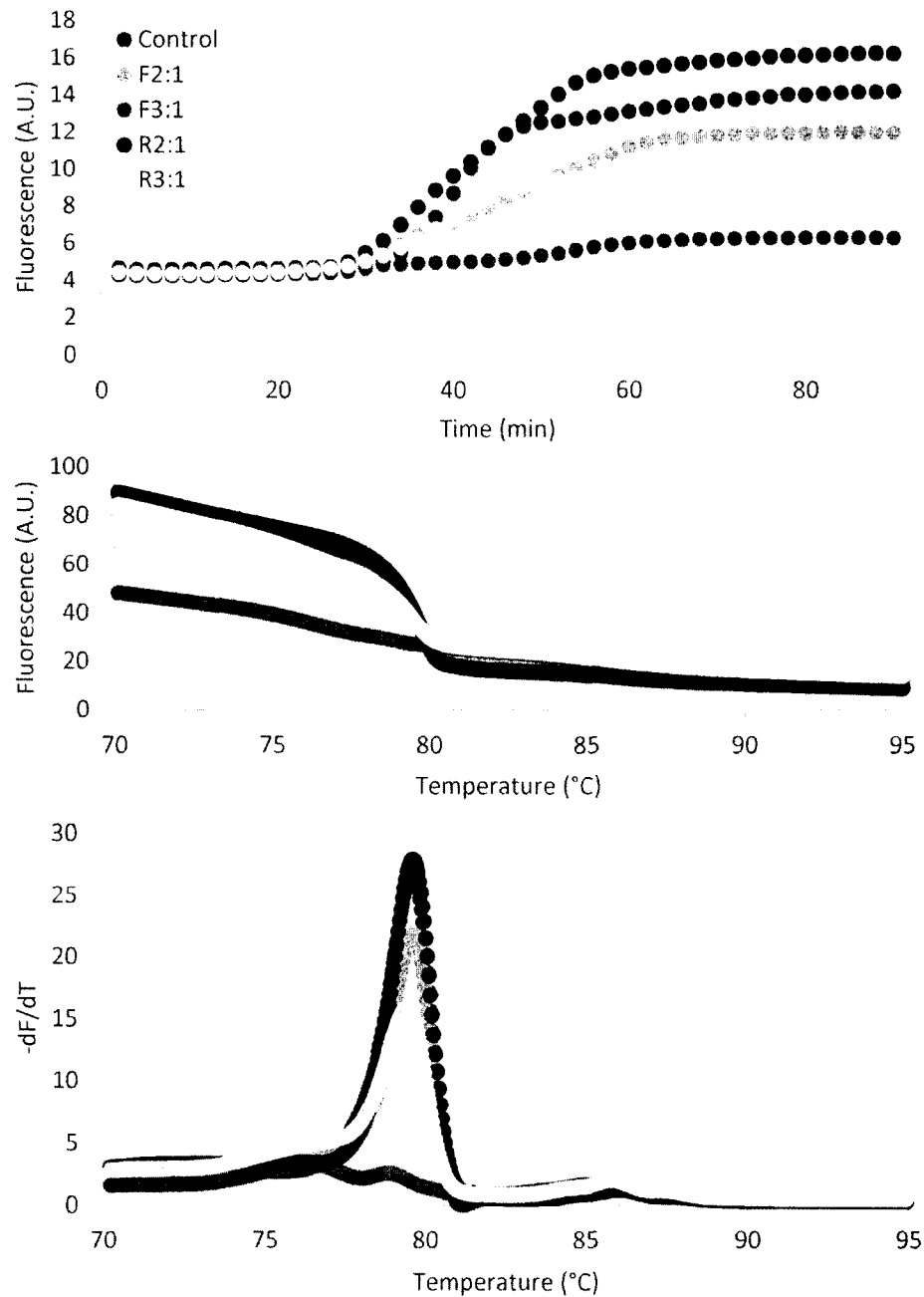


Figure 4-4: Asymmetric HDA amplification (top) and melting curves (middle and bottom) for multiple primer ratios. Each curve was an average of multiple trials ($N = 4$ for each sample type, except F2:1 where $N = 3$).

While it would be expected that the control samples would amplify first or most efficiently (crossing point, C_p , of 29.0 ± 0.90 min), other asymmetric samples amplified just as quickly, though with more variation between duplicates:

F2:1 - $C_p = 29.5 \pm 2.6$ min; R2:1 - $C_p = 27.1 \pm 4.0$ min; R3:1 - $C_p = 28.1 \pm 4.2$ min. The only sample that did not produce detectable fluorescent signal during incubation was the F3:1 sample.

The plateau heights differ mostly predictably, with the R2:1 samples being the highest, followed by the controls, F2:1 samples, R3:1 samples, and lastly the non-detectable F3:1 samples. While the variation of the C_p values is small, the variation in plateau height is more revealing. These heights indicate the quantity of dsDNA and the efficiency of the overall reaction.

The presence and relative quantity of ssDNA was assessed by gel electrophoresis (Galileo Bioscience Inc., Cambridge, MA, USA). One each of the above HDA samples were run in a 5 % agarose gel, at 60 V and 100 mA for 80 min, and imaged with a UVP GelDoc-It system (Upland, CA, USA). Figure 4-5 shows an image of the asymmetric HDA gel, where the channels are as follows – channel 1 is a PCR Marker or gel ladder (New England BioLabs Inc., Ipswich, MA, USA), channel 2 is empty (in order to avoid migration of the ladder into a sample channel), channel 3 is control, channel 4 is F2:1, channel 5 is F3:1, channel 6 is R2:1, and channel 7 is R3:1.

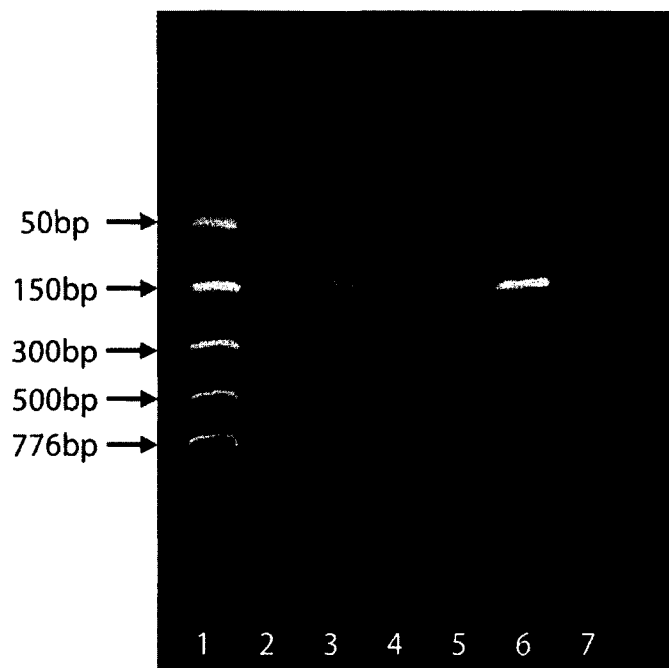


Figure 4-5: Gel electrophoresis imaging for asymmetric HDA. PCR marker (lane 1) is used to compare lengths of samples in lanes 3 through 7.

The position of the sample bands, in relation to the ladder, show the correct size of the target, 110bp. There is some curvature across the bands due to heating of the gel during the run, though the fragment lengths are easily discernable by comparing the control sample band (lane 3) to the ladder, showing product size < 150bp. The band in lane 5 is not visible, indicating no dsDNA was produced in the F3:1 HDA reaction; this is in agreement with the amplification curve and the MCA results. A secondary band is visible with all samples, except the control lane. It is believed that this weak optical signal indicates the presence of ssDNA. While the ethidium bromide stain used in gel electrophoresis is typically intended to stain dsDNA, it is known that ssDNA can form secondary coiled structures that can be stained by ethidium bromide [68].

Symmetric and asymmetric HDA produced dsDNA, detectable by both MCA and gel electrophoresis. In addition to gel electrophoresis, MCA was also used to assess the relative concentration of ssDNA. It was hypothesized that additional primers added after amplification could act as a probe, showing a secondary melting signature, separate from that of the target sequence. Because the previous experiment showed the strongest amplification in the R2:1 sample, that ratio of primers was used in this experiment. After incubation of a symmetric HDA control mixture and asymmetric HDA sample (N = 2 for each), 75 μ M of the forward primer was added to the amplified sample. The forward primer is complementary to the 3 prime end of the resulting ssDNA and anneals at this location, and can then be melted and detected. Figure 4-6 shows MCA results for symmetric and asymmetric HDA products with added forward primers.

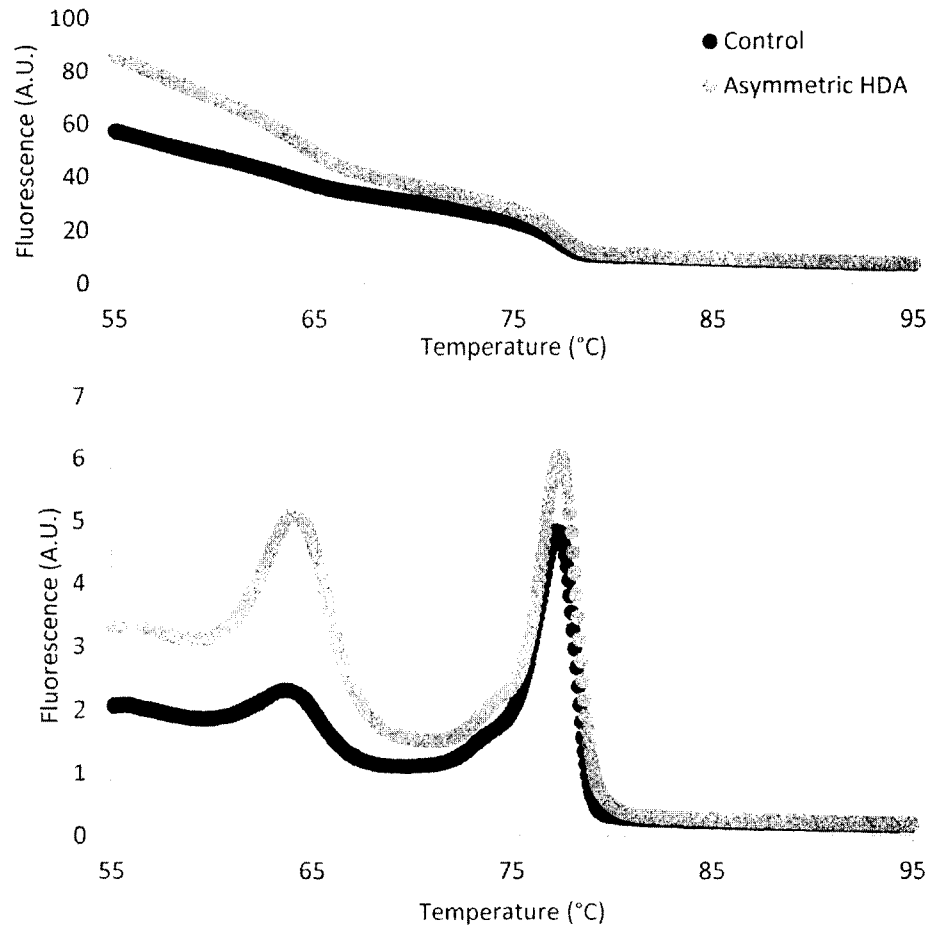


Figure 4-6: Melting curve analysis used to detect ssDNA product of asymmetric helicase-dependent amplification. A primer based probe was added to the symmetric HDA control and asymmetric HDA amplicon, resulting in increased probe-to-target signal ratio in the asymmetric sample.

The added primer probe produced a peak at $T_m = 64^\circ\text{C}$ in both the symmetric HDA control as well as the asymmetric HDA sample. This can be expected because the primer probe is complementary not only to a section of the excess ssDNA produced in the asymmetric reaction, but also to the dsDNA in the symmetric control if the strands are denatured and the primer probe can anneal. The temperature profile of the MCA protocol includes a rapid denature step, ramping to 95°C and cooling to 40°C , followed by the MCA temperature ramp where fluorescent signal was acquired, in this case, from 55°C to

95°C. The denature step allowed the probes to anneal to the amplified ds- and ssDNA. The difference in fluorescent signal at 64°C shows the presence of ssDNA in the asymmetric HDA sample. The ratio of target MCA peak height to probe MCA peak height changed from 2.1:1 in the control to 1.2:1 in the asymmetric sample, indicating a 77% increase in signal from the control to the asymmetric sample at the probe location.

A simple probe based detection mechanism was explored as a potential inclusion into a μ TAS DNA analysis device, utilizing asymmetric HDA and MCA. An asymmetric HDA reaction was optimized on a commercial laboratory based thermocycler, and ssDNA was detected via gel electrophoresis and a probe based MCA technique. This method of nucleic acid amplification and probe based detection is an option for future development of μ TAS based assays.

CHAPTER 5

DESIGN OF A PORTABLE DNA ANALYZER

5.1 Introduction

A lab-on-a-chip device is proposed that accomplishes the following goals:

- 1) On-chip HDA
- 2) On-chip amplification detection
- 3) On-chip melting curve analysis.

These three goals are accomplished by adopting the previously described biology into a glass/polymer composite device, interfaced with heating and fluorescence acquisition systems. All of these components are completely USB powered and controlled, allowing for a portable system, that requires only a laptop. A representative diagram of the overall system is provided in Figure 5-1.

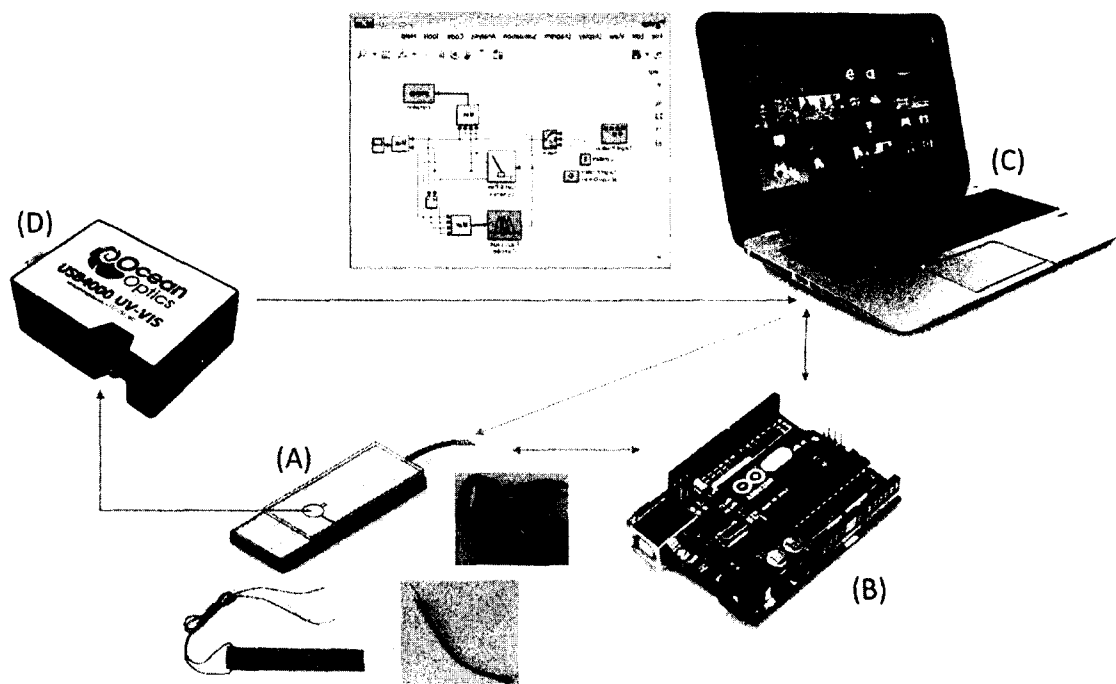


Figure 5-1: Diagram of the DNA analysis lab-on-a-chip system. The glass/polymer microfluidic device (A) is heated via USB power and interfaces via Arduino (B) with a laptop (C). Fluorescent signal is acquired with a USB spectrometer (D). Thermal and optical control and processing are managed simultaneously.

5.2 Fabrication

At the core of the portable DNA analysis system is a glass/polymer microfluidic chip. A molded layer of polydimethylsiloxane (PDMS) (Sylgard 184, Dow Corning, Midland, MI, USA) is bonded with a microscope glass slide (Fischer, Hampton, NH, USA) to form microfluidic reservoirs and channels. These materials were chosen for their specific properties; the glass microscope slide for its moderate thermal conductivity ($K = 0.8 \text{ W/m K}$) and optical transparency and PDMS for its elasticity (360-870 KPa, dependent on base-to-crosslinker ratio) and optical transparency. Heat is applied to the reservoirs through the glass side of the device. The elasticity of the PDMS top of the

device allows for hand controlled pumping, pulling in a liquid sample and moving it between reservoirs without the need of any external pumps or actuation hardware.

5.2.1 Composite Device Fabrication

Channel and reservoir features are produced by molding PDMS around a patterned tape layer. A 100 μm thick polyimide double-adhesive tape (PPTDE 1, Kaptontape.com, CA, USA) is patterned using a knife plotter (CE 6000, Graphtec, USA) and attached to the bottom of a plastic disposable petri dish. The pattern cut into the polyimide tape is shown in Figure 5-2. The outer area was removed, leaving the negative pattern - the thin 0.3 mm wide channels, 6 mm diameter circles, and the 1.5 mm by 2.5 mm channel openings attached to each circle. Additional circular tape layers were cut and layered over the pattern in the petri dish, creating areas of 100 μm thickness (channels) and 500 μm thickness (reservoirs). PDMS pre-polymer was mixed as 90 % v/v base to 10 % v/v crosslinker, producing polymer of moderate elasticity (with reference to the above stated range). The pre-polymer mix was poured into the petri dish, over the patterned tape mold, to a liquid depth of approximately 4 mm. The liquid was degassed in a desiccator chamber, under moderate vacuum (~ 200 mTorr), for 30 min or until all visible air bubbles were removed. The dish was cured at 80°C for 1 hour, with care not to exceed this temperature, which would cause warping of the dish and sample. The sample was left to cool and later the 1 inch by approximately 2.5 inch patterned PDMS area was cut out and removed. The patterned tape mold was removed from the PDMS with tweezers. The resulting features are 300 μm wide, 100 μm deep channels; 6 mm diameter, 300 μm deep reservoirs; 1.5 mm wide, 100 μm deep channel opening between reservoirs.

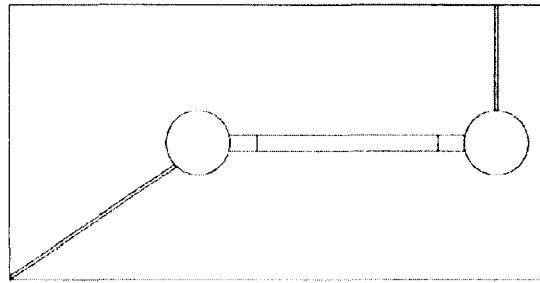


Figure 5-2: Pattern of microfluidic channels and reservoirs. A 100 μm thick polyimide double-adhesive tape was cut via xurography and used to mold a PDMS layer.

Before bonding the molded PDMS and glass microscope slide to form the enclosed channels, a secondary channel type was prepared. A flat, valve channel was formed between the two reservoirs (connecting the two 1.5 mm wide channel openings) by masking the unmolded PDMS with a 2 mm wide strip of patterned polyimide tape. This masked, molded PDMS piece and glass microscope slide were bonded by chemically activating both surfaces via plasma cleaner (PDC-001, Harrick Plasma, Ithaca, NY, USA). The materials were exposed to an oxygen plasma produced by an ambient air in-line for 2 min, then removed, the PDMS was un-masked, and the surfaces were evenly contacted. This produces a permanent covalent bond between the activated surfaces, but not the masked region of the PDMS. This region, while not molded, is also not bonded to the glass and can serve as a valve channel, able to be opened with flow pressure. The fabrication workflow is summarized in Figure 5-3.

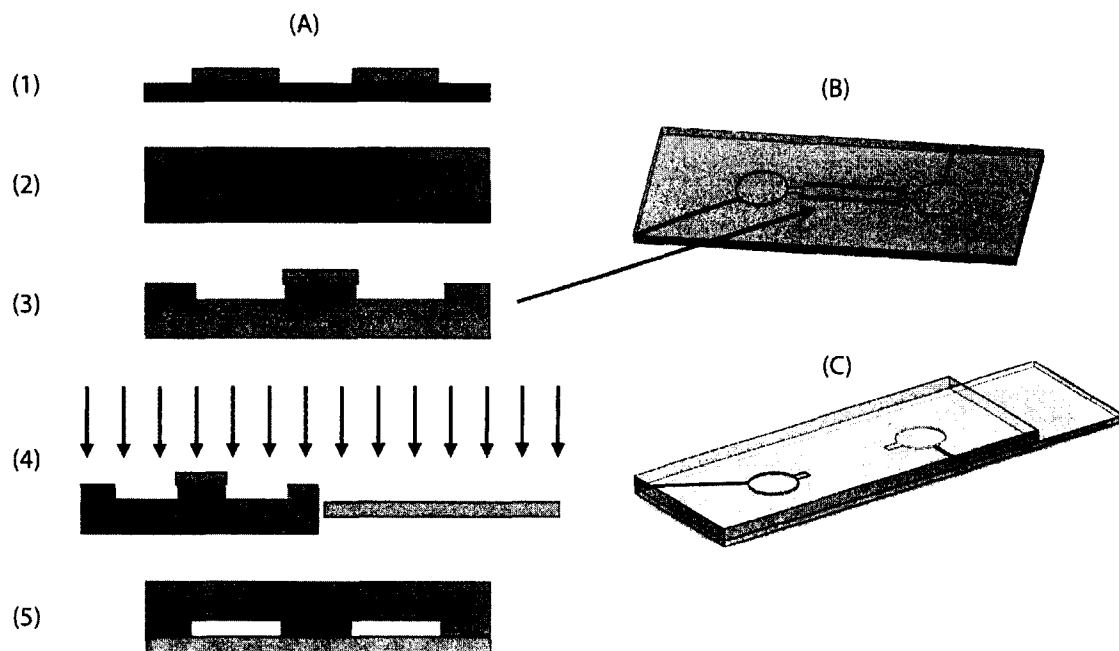


Figure 5-3: Fabrication workflow (A) for microfluidic HDA chip - (1) Pattern tape via xurography (2) Cure PDMS over mold (3) Remove patterned tape and mask molded PDMS (4) Exposed PDMS and glass slide to oxygen plasma (5) Remove mask and bond PDMS to glass. Molded PDMS (B) is masked to form a flat valve channel. The finished chip (C).

The device can be passivated for biological application, prior to or after fabrication, using different methods. Case 1: The glass slide is treated with DDMS, or other silanes/silicones, and the reservoir area is protected with a polyimide tape mask during plasma surface activation. The mask is removed and the surfaces are bonded. Case 2: Neither surface is passivated before bonding, but a flow through passivation technique is used after plasma treatment and bonding. Passivation flow through treatments must use solvents compatible with PDMS, to avoid swelling and damage to the structure [69]. One passivation treatment of interest for Case 2 is Pico-Glide 1 (Dolomite Microfluidics, Charlestown, MA, USA), which is dissolved in a fluorinated oil (compatible with PDMS). Both pretreatment options, DDMS and Pico-Glide 1, were explored, and this

research moved forward with Case 1. Fluorescence passivation techniques described in Chapter 3 were employed, introducing fluorescent dye (~15 μm of 1 X LC Green Plus+ pretreatment solution) into the device before use for biological assays.

Hand pumping and valve channel actuation is accomplished by thumb depression of the 6 mm diameter reservoirs. Depressing the empty chamber, contacting the end of the inlet channel (which is positioned at the bottom corner for ease of access) to a liquid sample, and releasing the depressed reservoir, allows the PDMS to reform pull in the sample. The chamber is then sealed, either by manual clamping or by fast set epoxy; UV cure epoxies (Loctite 3105 and 3106, Henkel Corporation, Westlake, OH, USA) (shielding loaded sample from UV) and fast-setting, two-part epoxies (MinuteWeld, J-B Weld, Sulphur Springs, TX, USA) have both been shown to contain samples up to 80°C, but leak at higher temperatures. When used to seal the device, the sample is not in contact with the sealant, which is separated by a 4.5 cm long (100 μm tall by 400 μm wide) channel.

5.2.2 Fabrication Consistency Testing

5.2.2.1 Thickness Measurement

Multiple PDMS/glass composite devices were fabricated, to test the consistency of the described technique, related to this technique and resulting functionality: 1) device thickness and membrane thickness (potential effect on thumb push function), 2) sample uptake volume.

The devices are being created in an identical manner, according to the above described protocol. Patterned tape is applied in 100 mm diameter by 15 mm height petri dishes, capable of holding two patterns. Petri dishes 145 mm in diameter, capable of

holding eight repeated patterns, were also tested, changing only the volume of PDMS pre-polymer required to achieve a PDMS height of 4 mm. The molded PDMS was bonded to the glass slides, creating a total of ten devices.

Thickness measurements were taken on the ten devices, at seven different locations. A hand micrometer (PK-0505, Mitutoyo Corporation, Kawasaki, Japan) was used, avoiding deformation of the PDMS and particularly avoiding depression of the reservoirs while measurements were taken. The average of three measurements was taken for each location on each chip. Figure 5-4 shows the locations of measurement on a sample device. The height measurements were compared in two different ways. First, measurements at each location were averaged, to yield a single average thickness for each device. These average height measurements are shown in Figure 5-5.

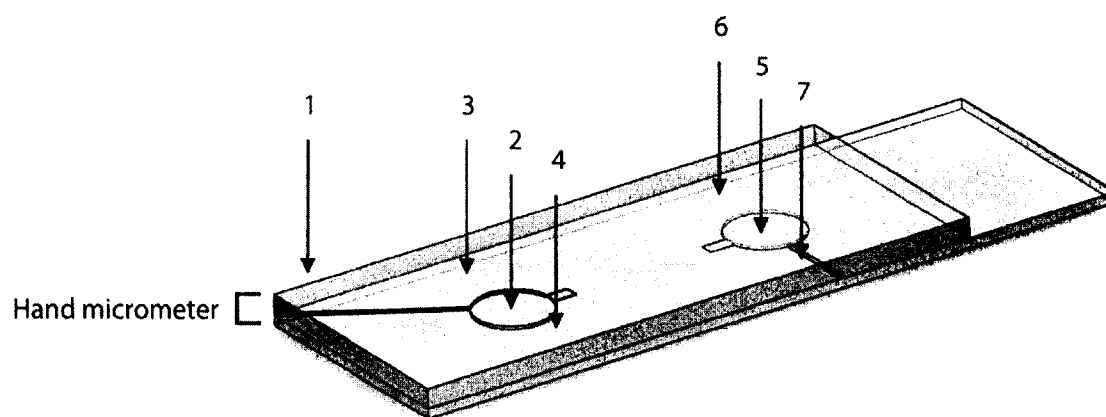


Figure 5-4: The thicknesses of ten identically fabricated PDMS/glass composite devices were measured at points 1-7. The measurements include both PDMS and glass layers.

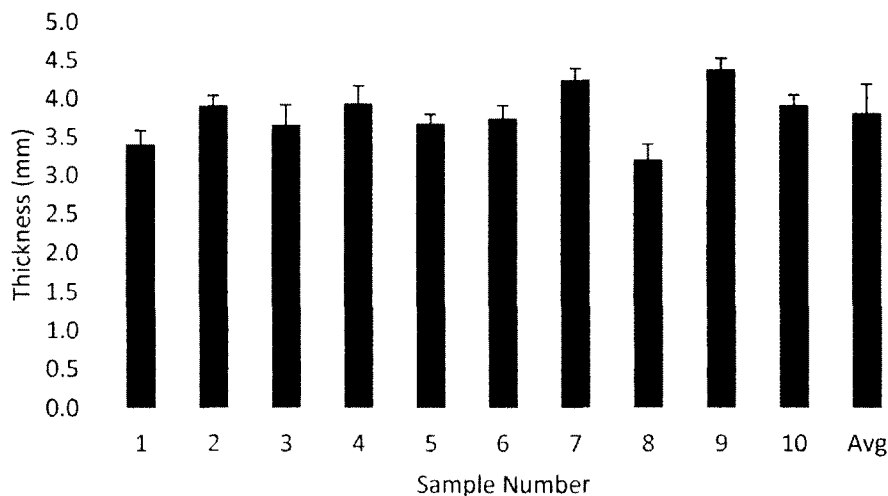


Figure 5-5: Device thickness across ten similarly fabricated PDMS/glass composite microfluidic devices.

The overall average thickness is 3.82 ± 0.37 mm, or $3.82 \text{ mm} \pm 9.8 \%$. The maximum thickness for a single device was 4.39 ± 0.15 mm and the minimum thickness was 3.21 ± 0.20 mm. These values include both layers, PDMS and glass. Reducing the average thickness by the thickness of the microscope slide (1 mm) and by the depth of the reservoir ($500 \mu\text{m}$), the average thickness of the deflecting PDMS over the reservoir is 2.32 ± 0.37 mm (or varying by 15.9 %).

Another analysis method used was to find an average thickness at each measurement location, 1-7, across all chips. This provides insight into the variation across the features in a single device. Figure 5-6 shows height measurements at each location, normalized for variation between each devices average height.

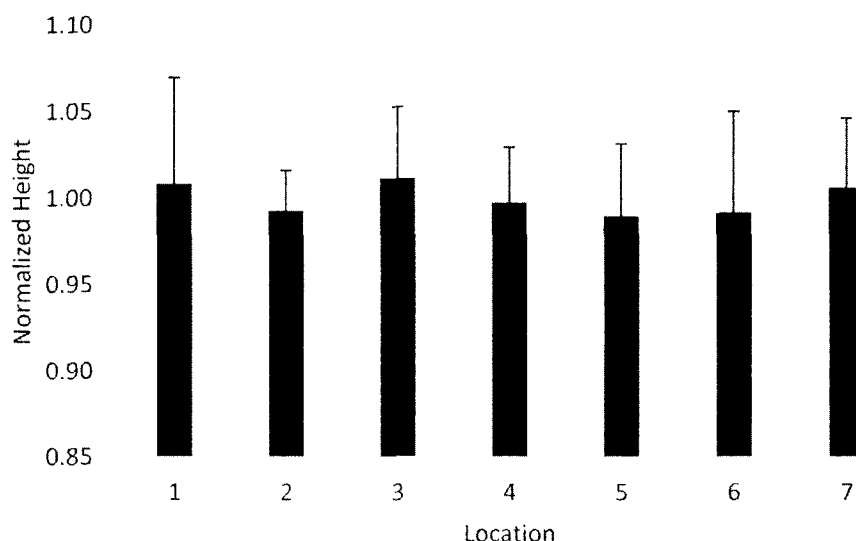


Figure 5-6: Height measurements at each location (shown in Figure 5-5), normalized for average height of each device.

Each location number corresponds to a different area or feature on the devices, as seen previously in Figure 5-4. Location 1 is the thickness at the inlet channel, Location 2 and 5 are reservoirs, and Locations 3 and 4 and Locations 6 and 7 are on either side of the reservoirs (2 and 5 respectively). Most locations vary less than 5 % of the average thickness for that device, with Location 1 varying the most at 6.1 %. There does not appear to be a correlation between average thickness and distance down the chip, either lengthwise or widthwise. While measurements at the reservoirs, Locations 2 and 5, yield some of the lowest thicknesses, they are not significantly lower than average (within 1 %) and have lower than average standard deviation.

5.2.2.2 Sample Volume Uptake

Because the thickness of the PDMS membrane above the reservoirs was found to vary by up to 15.9 %, it is important to investigate the consistency of the pumping action of devices fabricated using this technique. Sample volume uptake was measured for the

ten devices, using thumb actuated pumping action. Four measurements were taken for each device by pipetting 50 μL of DI water on paraffin film, hand pumping the fluid into the device, then with a pipettor measuring the fluid volume remaining on the paraffin film. Figure 5-7 shows the average sample volume measurements for each of 10 devices.

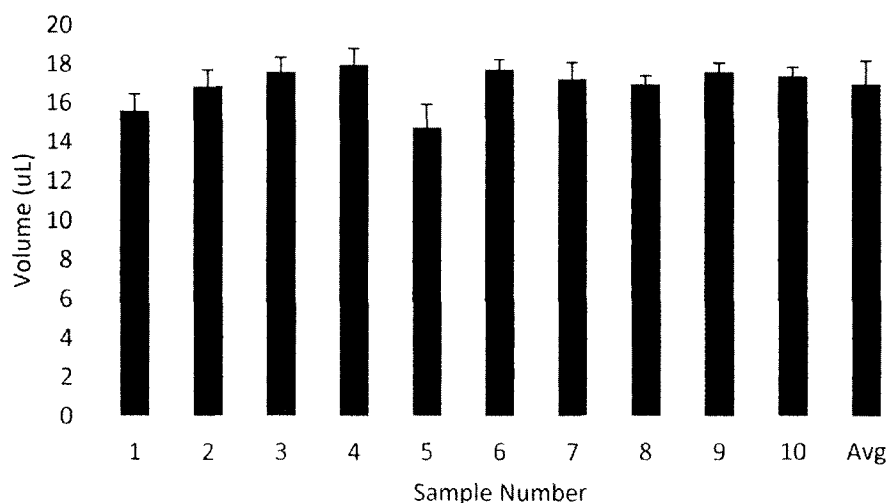


Figure 5-7: Sample uptake volume using thumb actuated pumping in PDMS/glass composite microfluidic chips.

These tests show an average sample uptake of $17.0 \pm 1.2 \mu\text{L}$ (variation of 7.1 %). Device 5 is somewhat of an outlier, with the lowest average sample uptake ($14.75 \mu\text{L}$, 13.2 % lower than average) and the highest variation between subsequent measurements (standard deviation of $1.2 \mu\text{L}$, 40 % higher than the average standard deviation). While special care was taken to fully evacuate each chamber after each measurement, Device 5 showed a decrease in volume uptake after the first sample, indicating some liquid remained inside between measurements. Removing Sample 5 results in an average sample uptake of $17.2 \pm 0.9 \mu\text{L}$ (variation of 5.2 %, which is considerably less than the variation thickness).

5.3 Thermal Management

5.3.1 Heating Element Design

To perform Helicase-dependent amplification, the liquid sample must be incubated at 65°C for 30 to 90 min (incubation time optimized dependent on reaction mixture components, as discussed in Chapter 4). Glass was chosen as one of the microfluidic device materials, for its thermal conductivity, as well as optical properties and surface passivation options. The bottom glass slide acts as route through which heat is applied to the device and to the sample. To create a portable analysis device, heating power and control are managed by laptop USB.

Initial on-chip HDA tests were done by placing the microfluidic chip on an in house heater block (also referenced in Chapter 3). The aluminum blocks, containing PID controlled cartridge heaters, contacted the bottom edge of the microfluidic device, save a 1 cm gap down the length of the device. The heaters were each set to 68°C, maintaining a device temperature of 65°C, monitored via IR Camera.

This heating method was replaced by incorporating a polyimide thin film heater that is USB powered and controlled. A 55 mm by 6 mm, 6 Ω (measured 5.3 Ω) thin film heater (Minco, Minneapolis, MN, USA) was attached to the underside of the glass/PDMS device via innate acrylic adhesive. A laptop computer USB 3.0 port supplied 5 V to the heater. Because of power requirements, a USB 3.0 port must be used over a USB 2.0, because it is capable of supplying 900 mA to 1.5 A, up from USB 2.0's 500 mA limit. When 5 V is applied to this heater, the current draw is just under 1.5 A, also producing temperatures well above our intended range of 65 to 95°C. A feedback control loop is implemented by putting the heater and 5 V source in series with a solid state relay, which

is controlled via Arduino microcontroller (Arduino Uno, Arduino, New York, NY, USA) and thermistor temperature sensing.

A 10 K Ω negative temperature coefficient thermistor (U.S. Sensor Corp., Orange, CA, USA) was attached to the surface of the thin film heater via epoxy (Loctite E-05CL, Henkel Corporation, Westlake, OH, USA). The device was insulated with melamine foam (McMaster-Carr, Douglasville, GA, USA), which has a conductivity as low as 0.045 W/m K, to mitigate heat losses. The heater/thermistor assembly is able to be removed and attached to a new microfluidic chip after each biological test. This exchange prevents any cross contamination, but requires further analysis of thermal behavior should the application of the heater vary. A model of the device can be seen in Figure 5-8.

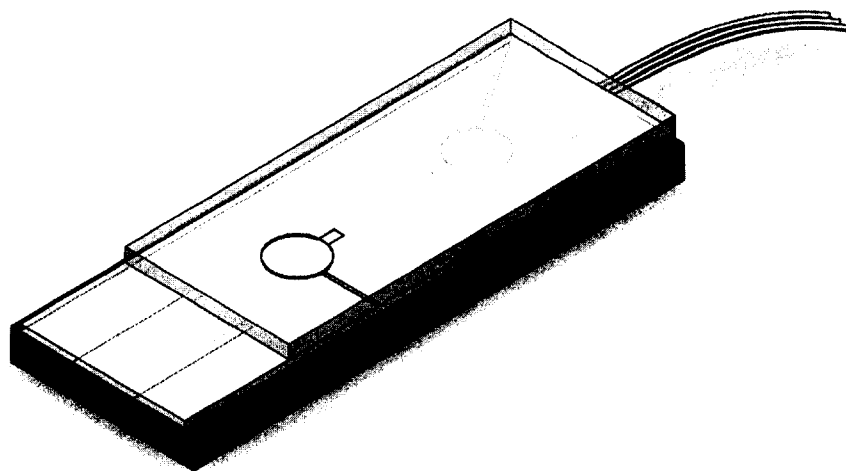


Figure 5-8: The glass/PDMS composite device with mounted thin film heater, thermistor, and insulating foam.

The thermistor's resistance versus temperature profile was measured using a simple voltage divider circuit and by controlling the thin film heater with a PID controller

(CN79000, Omega, Norwalk, CT, USA) and DC power. The temperature value measured by the thermistor is provided by:

$$T_{val} = \frac{B_{val}}{\log\left(\frac{R_{val}}{R_{cal} \cdot e^{\left(\frac{-B_{val}}{T_{cal}}\right)}}\right)} \quad \text{Eq. 5-1}$$

where T_{val} is the temperature (K) measured, B_{val} is the calibration constant specific to the thermistor, T_{cal} is the temperature at which the thermistor was calibrated, R_{cal} is the resistance of the thermistor at the calibration temperature, and R_{val} is the resistance of the thermistor at the measured temperature. B_{val} , T_{cal} , and R_{cal} are all provided by the manufacturer, and used to convert measurements take with the thermistor. The R_{val} resistance (Ω) is measured using a simple voltage divider circuit. This circuit is interfaced with the Arduino microcontroller and the signal is communicated to a Matlab interface (MathWorks, Natick, MA, USA) for signal processing and control.

A Matlab based fuzzy logic controller is used to control the temperature of the sample chamber, maintaining the 65°C target. The voltage signal from the thermistor-voltage divider is converted to a temperature using the relationship in Eq. 5-1 and input to the fuzzy logic controller; the output is a voltage value. The membership functions (and thus the output voltage) were tuned based on temperature measurements of the system at thermal equilibrium for different applied heater voltages, ranging from 3 to 4 V. The output from the fuzzy controller is converted to a number between 5 and 100, used to control the percent of the time that the heater is exposed to the USB 5 V source, and thus approximating voltages in the required 3 to 4 V range. This converted time value is communicated back to the Arduino, which pulses the heater to maintain temperature.

Using the Mamdani fuzzy inference mechanism, different sets of membership functions

have been defined in order to achieve specific temperatures on the microfluidic device. These settings were able to be changed, depending on requirements established by thermal modeling. The circuit layout for the heating and control systems is in Appendix D.

5.3.2 Thermal Modeling

Thermal model simulations were performed to investigate the functionality of this design, primarily concerned with a few parameters: 1) target temperature in the reaction reservoir, 2) the impact of thermal contact resistance associated with the heater/glass contact, and 3) response time of the heating of the system. An investigation of these topics was performed using Solidworks Simulation (Dassault Systemes SOLIDWORKS Corp., Waltham, MA, USA), both steady state and transient models.

The target temperature for the isothermal amplification reaction was defined as $65 \pm 2^\circ\text{C}$. Although the incubation time has been optimized to be lower (30-45 min), the original duration of 1-1.5 hrs was considered. A simplified model of the device was created for use in thermal studies, as seen in Figure 5-9. The thermistor and connection wires to the heater were removed, and the heater was treated as a 0.5 mm thick polyimide rectangle on the bottom side of the glass slide, with the same area as the thin film heater (55 mm by 6 mm). The features of the channels and reservoirs were maintained, and treated to contain water. Material properties were specified for glass and water using material libraries available in Solidworks, while other literature sources were used for PDMS [70], polyimide (Dupont, Wilmington, DE, USA), and melamine foam (BASF Corporation, St. Laurent, Quebec, Canada).

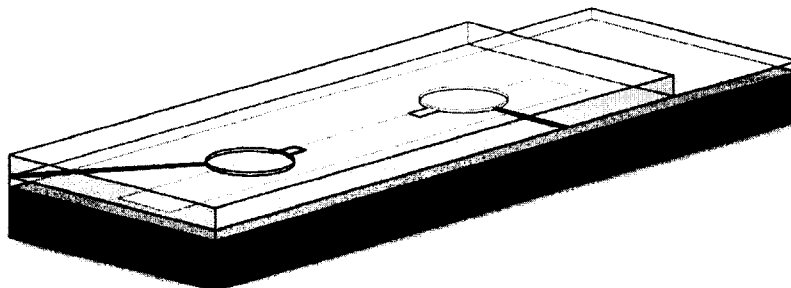


Figure 5-9: Simplified model of glass/PDMS microfluidic device, used for thermal modeling.

First a steady state model was used to assess the heat distribution in the device. The top surface of the heater was treated to be a set temperature source of 67°C; this is 2°C higher than the target temperature to compensate for heat loss through the 1 mm thick glass slide. A thermal resistance between the heater and the glass slide was assumed, and two cases were modeled: a best case, in which 10 % of the surface area is occupied by 10 μm thick air voids, and a worst case, in which 90 % of the surface area is occupied by 40 μm thick air voids. Distributed resistance values were calculated for these two cases and applied to the model: $9.05 \times 10^{-5} \text{ m}^2\text{K/W}$ and $1.16 \times 10^{-3} \text{ m}^2\text{K/W}$ respectively. Ambient conditions of 25°C and a convection coefficient, h , of 10 W/m²K were used. Temperatures were probed through the thickness of the device, at the center of the reservoir area, while at equilibrium state. Figure 5-10 shows temperature as a function of distance through the device thickness, for each defined contact resistance scenario.

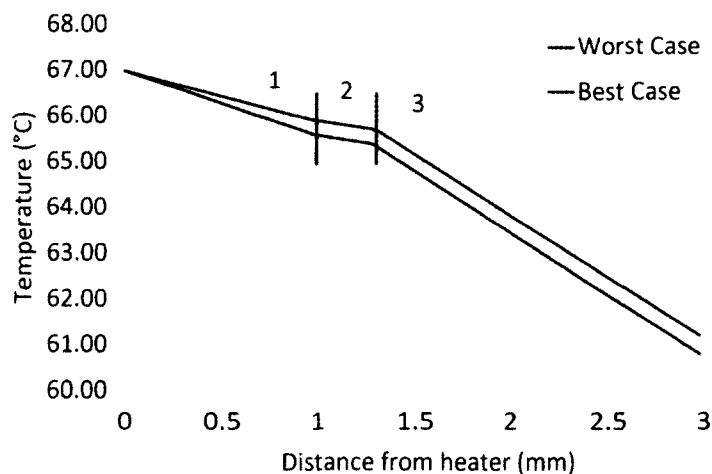


Figure 5-10: Modelled effect of heater contact resistance on the device temperature. Based on the best case and worst case scenarios described above, the temperature due to a 67°C heat source can be seen in the three zones: 1) the glass slide, 2) the reservoir, 3) the PDMS.

These results verify the reservoir temperature and explore the role of contact resistance on sample temperature during incubation. Using a heat source of 67°C was shown to produce temperatures between 65 and 66°C in the sample reservoir, within the defined target range. Changing the contact resistance between these two cases yielded a change $< 0.5^{\circ}\text{C}$ in the sample reservoir.

A series of transient studies were performed in order to assess the temperature difference between the temperature sensor used in the feedback control system and the sample reservoir. This is especially important when the temperature is system is changing, such as during melting curve analysis or when ramping to the incubation temperature. The temperature difference, or thermal lag, between the thermistor sensor and sample is due to heat dissipated into the 1 mm of glass, the surrounding insulating material, and the ambient environment.

A transient model of the heating of the device was used to investigate the response time. A step size of 5 sec was used for all transient models. Initially a power source (rather than temperature source) was applied to the heater/glass interface. A 2.67 W power source was used to simulate the power draw from a 4 V potential applied to the 6 Ω heater. This yields an uninhibited temperature increase, where in reality the controller limits the voltage when the target temperature is reached. To more accurately model the response, the temperature profile of the heater in response to a 2.67 W load of was recorded and then input as a time dependent temperature source. From 0 to 35 sec the temperature response due to the power source was input, and after reaching the target temperature at 40 seconds, a value of 67°C was used. This resulted in a piecewise function temperature input, which, while not completely realistic, can be used to approximate a critically damped version of an actual response from a closed loop controlled heater. The temperature response at the center of the reservoir was modeled in response to this input heater temperature profile, as shown in Figure 5-11.

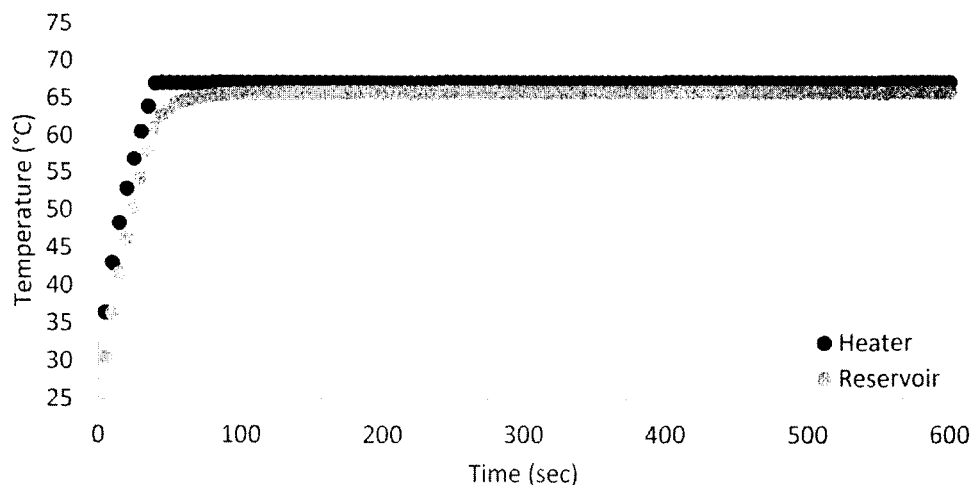


Figure 5-11: Modelled time response of reservoir temperature to an input time-variable heater temperature.

The heater is set to 67°C and the final temperature of the reservoir is 65.69°C. The time constant describing the response of the system was found. The temperature at which 63.2 % of the total temperature change, ΔT (40.69°C), had occurred is 50.7°C. This is reached after 25 sec. This shows that the system heats up very fast but does not realistically represent damping effects. When 4 V (2.67 W) is used, the system will heat up to the set temperature very quickly, but is not guaranteed to equilibrate this quickly. As the device temperature approaches the set temperature, the voltage is reduced, extending this time somewhat.

Despite the response time model, the actual device heat up time was much higher (time constant of about 75 sec). Two methods were taken to reconcile this in the models: by increasing the ambient convective heat transfer away from the device or by decreasing the effective power to the heaters. The first method, changing the convection coefficient from 10 W/m²K to 25 or 50 W/m²K, resulted in an increase in time coefficient (approximately 35 and 45 sec respectively), but more notably caused a drop in equilibrium temperature (reaching only 64.2°C and 62.3°C, compared to the previous equilibrium temperatures of 65.7°C). A decrease in effective power to the heaters (by ¼ and by ½) did not decrease the equilibrium temperatures but did decrease time constants (to about 40 sec and 60 sec, respectively). It is theorized that some combination of increased losses and/or reduced power to the device is responsible for the lower experimental time constant, but this heat up time is manageable (and expected in experimental practice) and does not negatively affect device performance.

One last concern is the temperature lag prior to reaching equilibrium. This is a greater problem when conducting melting curve analysis, where the change in fluorescent signal is a function of temperature, and changes in fluorescence at specific temperatures are unique to the DNA samples. The convection coefficient was varied between 10 and 20 W/m²K and additional heat losses in the form of conductive heat flux away from the system from all sides, with values of 10, 100, and 200 W/m². These were all applied to a low power system, 2 W supplied to the heater, with the intent of creating a wide range of scenarios of heat loss. For each of these cases the difference between the heater and reservoir temperatures was monitored and the average across all scenarios was found to be $6.0 \pm 0.2^\circ\text{C}$. Because the results were comparable for every case, a correction of 6°C was used when calibrating MCA on this device.

5.4 Optical System

Fluorescent detection of the HDA reaction and sample is made possible by incorporating a spectrometer and LED excitation source. The intercalating DNA dye in the sample is excited via specific wavelengths from the filtered LED, emission from the dye is filtered and passed through the cable, and the spectrometer detects the signal. The signal is digitally filtered and plotted versus time to detect intensity changes associated with DNA amplification or melting. The LED and spectrometer are USB powered, furthering the portability of the system. The system is operated in a dark room environment (ignoring laptop monitor light), but can also be used in ambient lighting if properly covered with an opaque material. Further testing on thermal effects of such an enclosure are required.

An Ocean Optics USB 4000 spectrometer is coupled with a 0.2 m long, 1 mm core fiber optic cable (ThorLabs Inc., Newton, NJ, USA) and then filtered with a band-pass optical filter, allowing transmission through a 40nm band centered on 500 nm or approximately 480-520 nm (ThorLabs Inc.). The cable is attached to the spectrometer via SMA and to a SMA-to-one-inch adaptor that is coupled with a 1/3 inch long, one inch diameter optics tube. The optics tube houses the band-pass optical filter and a protective glass insert. The excitation source is a blue 447.5 nm peak wavelength LED (Luxeon Star LEDs, Brantford, ON, CA) mounted to an one inch diameter optics tube cap that serves as a heat sink and attaches to a 1/2 inch long optics tube that houses another band-pass optical filter, allowing transmission through a 50 nm band centered around 450 nm or approximately 425-475 nm (ThorLabs Inc.). It is important to note that the filtered light band into the spectrometer and the filtered light band out of the LED do not overlap, ensuring that no light from the LED is detected by the spectrometer. In addition to being equipped with a filter, this LED is also equipped with a 3 mm by 15 mm slit. The LED fixture is positioned perpendicular to the 1 inch side of the glass/polymer device, illuminating the sample reservoir through $< \frac{1}{2}$ inch of glass and PDMS. The fiber optic cable with filter is positioned directly in front of the microfluidic chip, centered on the sample well. The microfluidic device, spectrometer cable, and LED are secured in a foam cutout during development testing, in order to stabilize and standardize their orientations. The orientation of the optical, thermal, and biological systems are shown in Figure 5-12.

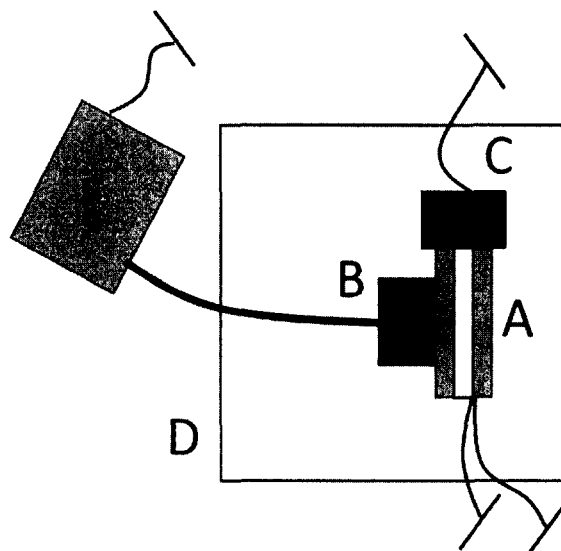


Figure 5-12: Experimental setup for on-chip DNA analysis testing. Microfluidic chip with heating element (A), filtered fiber optic cable (B), and filtered LED excitation source (C) are mounted in a cutout foam block (D). Spectrometer (E), heating, and illumination are all USB powered and controlled.

The spectrometer detects light emission from the DNA dye, ranging from 470 nm to 520 nm, which corresponds to the light allowed through the spectrometer band-pass filter. A sample spectra is shown in Figure 5-13. The intensity values over the peak emission region, taken to be 500-510 nm, were smoothed over wavelength using a Savitzky-Golay digital filter. An average value was calculated from the smoothed values over this wavelength range for each sample time and these average values were also smoothed using a Savitzky-Golay filter. The resulting curves, intensity as a function of time, are used to generate amplification and melting analysis curves, depending on biological and heating profile conditions.

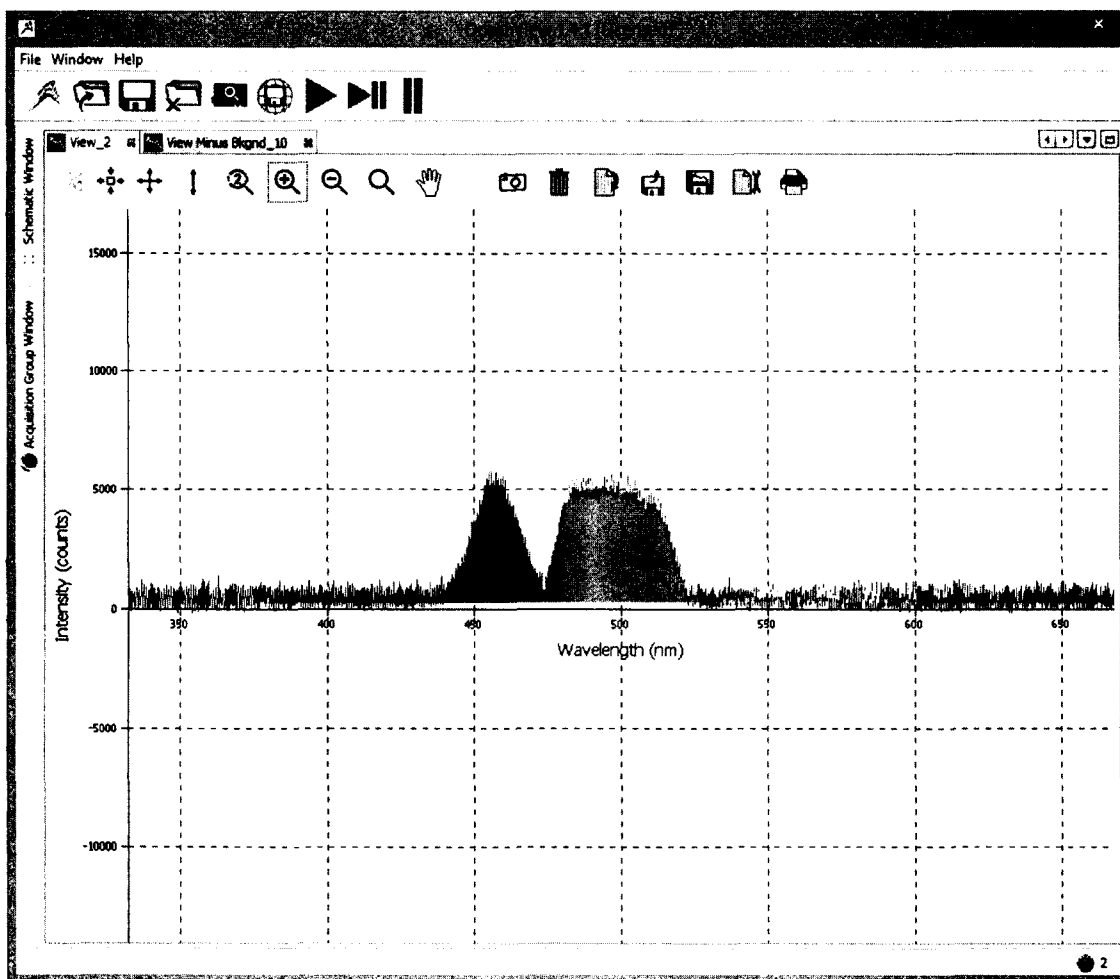


Figure 5-13: Sample spectra resultant of the described optics configuration, shown in the OceanOptics spectrometer interface, OceanView. The filtered LED excitation source is detected and seen as the shorter wavelength peak (~445-470 nm) and the sample's fluorescent emission signal is detected and seen as the longer wavelength peak (~445-520 nm). The intensity of the sample fluorescent signal is tracked over time during both incubation and melting.

5.5 On-Chip Testing

5.5.1 On-Chip Amplification

On-chip Helicase-dependent amplification was initially performed without the integrated fluorescence detection system, but was verified by removing the amplified sample and performing melting curve analysis on a separate commercially available

device (LightScanner32). The previously described HDA mixture was used: Biohelix IsoAmpIII kit with Phi X 174 110bp target, 2 X enzyme mix, and 1 X LC Green Plus+. The on-chip product was compared to amplicon from positive and negative control (reaction mixture with no template) reactions performed on the commercial device. MCA results are shown in Figure 5-14.

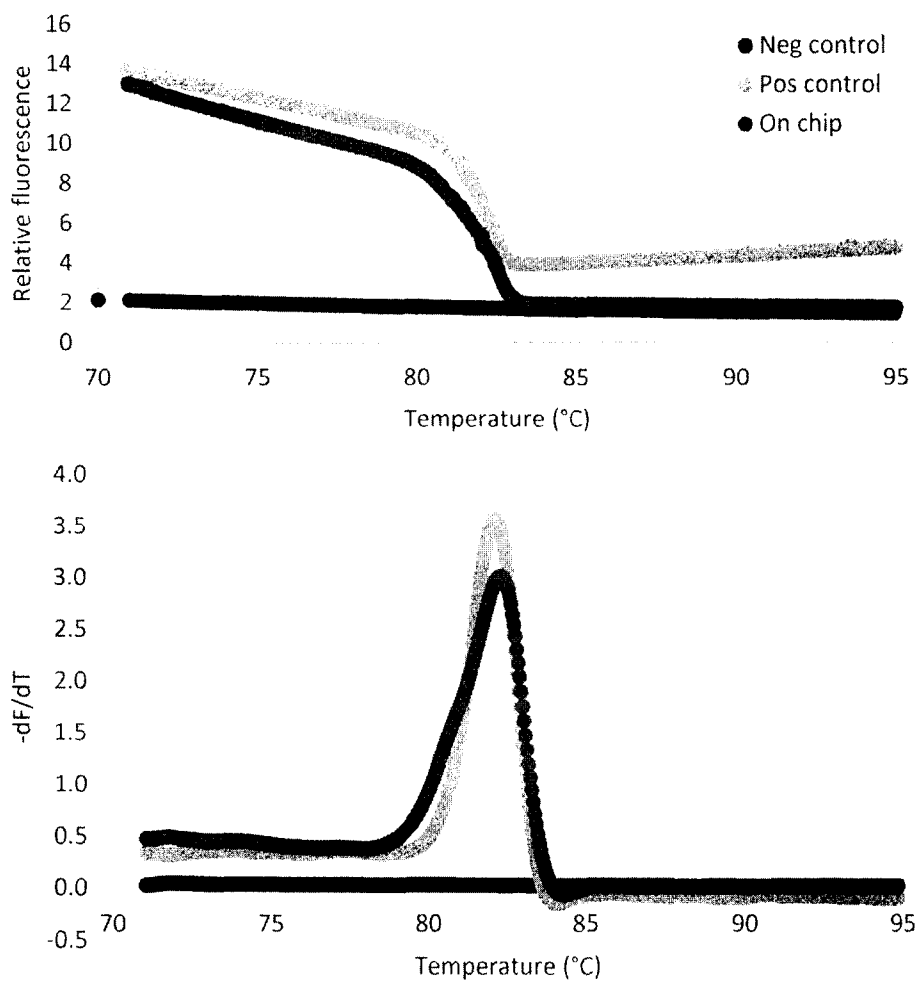


Figure 5-14: Melting curve analysis was used to compare products from on-chip helicase dependent amplification and a control reaction performed on a commercially available device.

Specific amplification of the target sequence was achieved on the glass/PDMS device, verified by matching melting temperature ($T_m = 82^\circ\text{C}$), and comparable concentration (84 % peak height signal compared to the control).

The glass/PDMS device proved capable of HDA, containing the sample mixture at the incubation temperature of 65°C . As previously noted, sample containment became difficult at temperatures in excess of 80°C , causing sample to evaporate and pressurize the chamber. The epoxy sealant and clamping methods did not completely prevent sample loss through the device inlet. To circumvent this issue, a secondary microfluidic device design was used for melting curve analysis. A glass/polyimide composite device was fabricated via xurography as detailed in Chapter 3. This device possesses many of the same qualities as the glass/PDMS device: the same reservoir and sample size ($15\ \mu\text{L}$), identical interchangeable heating system, optics orientation (LED position, fluorescent signal detected through 1 mm glass rather than 1.3 mm of PDMS). As with the glass/PDMS device, melamine foam is used to insulate the bottom glass side of the device, but melamine is also used to insulate the top surface, avoiding the reservoirs and signal acquisition area. This device differs in sample insertion; rather than thumb actuated pumping, a syringe is used to insert the sample via microfluidic tubing into the reservoir through mounted PDMS ports. The glass microscope slides were passivated with DDMS prior to assembly, and the device was fluorescence passivated as discussed in Chapter 3.

On-chip HDA and MCA were performed on this device, interfaced with the USB powered/controlled heating and optics systems. To obtain amplification curves, fluorescent signal was acquired via spectrometer in a 200 ms window every 30 seconds,

over a 45 min incubation period. The signal was smoothed with respect to wavelength using a Savitzky-Golay filter, averaged over a 10 nm wavelength range, and smoothed, again using Savitzky-Golay filtering, with respect to time. Baseline signal measurements were taken by heating and monitoring a negative control sample, comprised of only a buffered dye solution. These baseline measurements were subtracted from the HDA incubation signal, to produce an amplification curve, shown in Figure 5-15 with an amplification curve obtained on the commercial device.

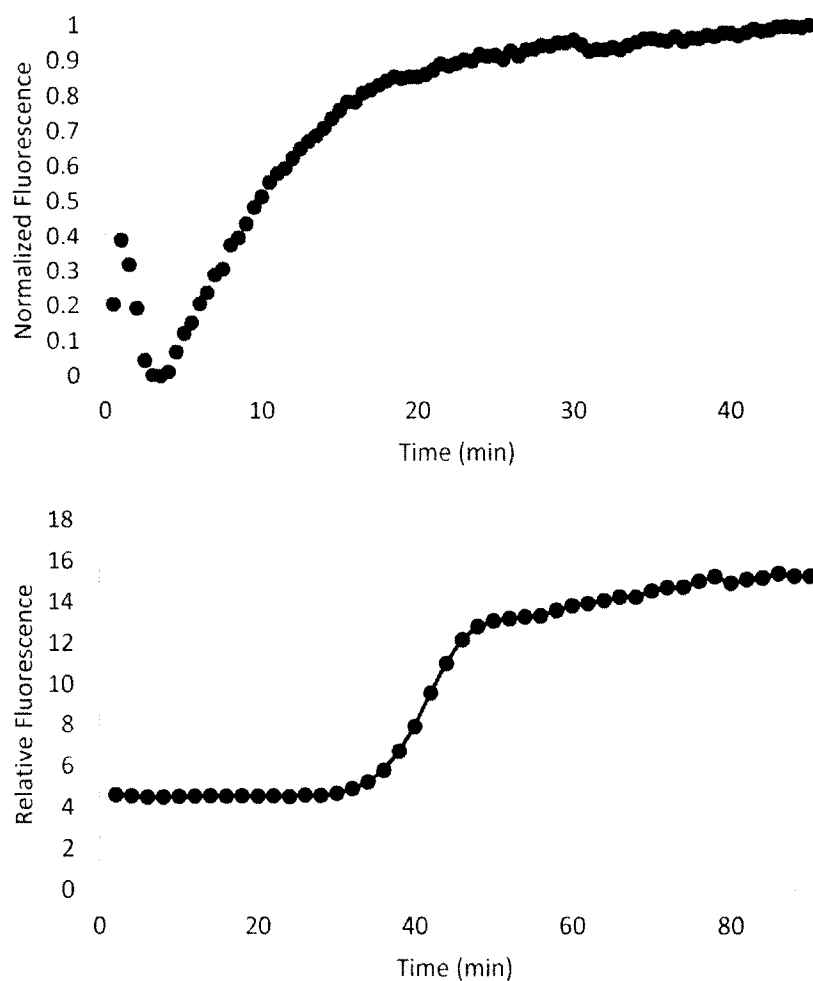


Figure 5-15: Amplification curves from HDA reactions carried out in the portable device (top) and commercial system (bottom).

Heating began at time 0 min, reaching the incubation temperature, 3 min into the 45 min incubation time. Most notably, the on-chip sample showed signal increase as early as 5 min. A crossing point of 5 or 6 min of incubation is not possible when compared to amplification in the commercial system yielding a crossing point of 37 min. This is due to the sample mixture being held at room temperature during extended preparation time. While the sample was not jeopardized, quantitative analysis during the incubation phase was not possible with current workflow for this system. Improved sample handling and process time are required.

Melting curve analysis was performed on-chip, by measuring the fluorescent signal in 200 ms windows every 5 sec as temperature was increased to upwards of 90°C. Two synthetic DNA melting duplexes were measured: a 50bp high temperature melting sequence $T_m = 81.9^\circ\text{C}$ and a 50bp low temperature melting sequence $T_m = 58^\circ\text{C}$. The 50bp sequence was injected into a glass/polymide device, and the fluorescence signal was monitored as the temperature was ramped from 45°C to 90°C. Because the temperature does not vary linearly with time, time stamp information was collected in the heater controller as well as the spectrometer measurements. These were matched, producing a fluorescence versus temperature curve. Background measurements were taken for this heating protocol, measuring the fluorescence versus temperature profile for a buffered dye, negative control. Employing Savitzky-Golay smoothing, the background signal was normalized with respect to and was subtracted from the DNA fluorescent signal, resulting in a melting curve for this sequence, seen in Figure 5-16.

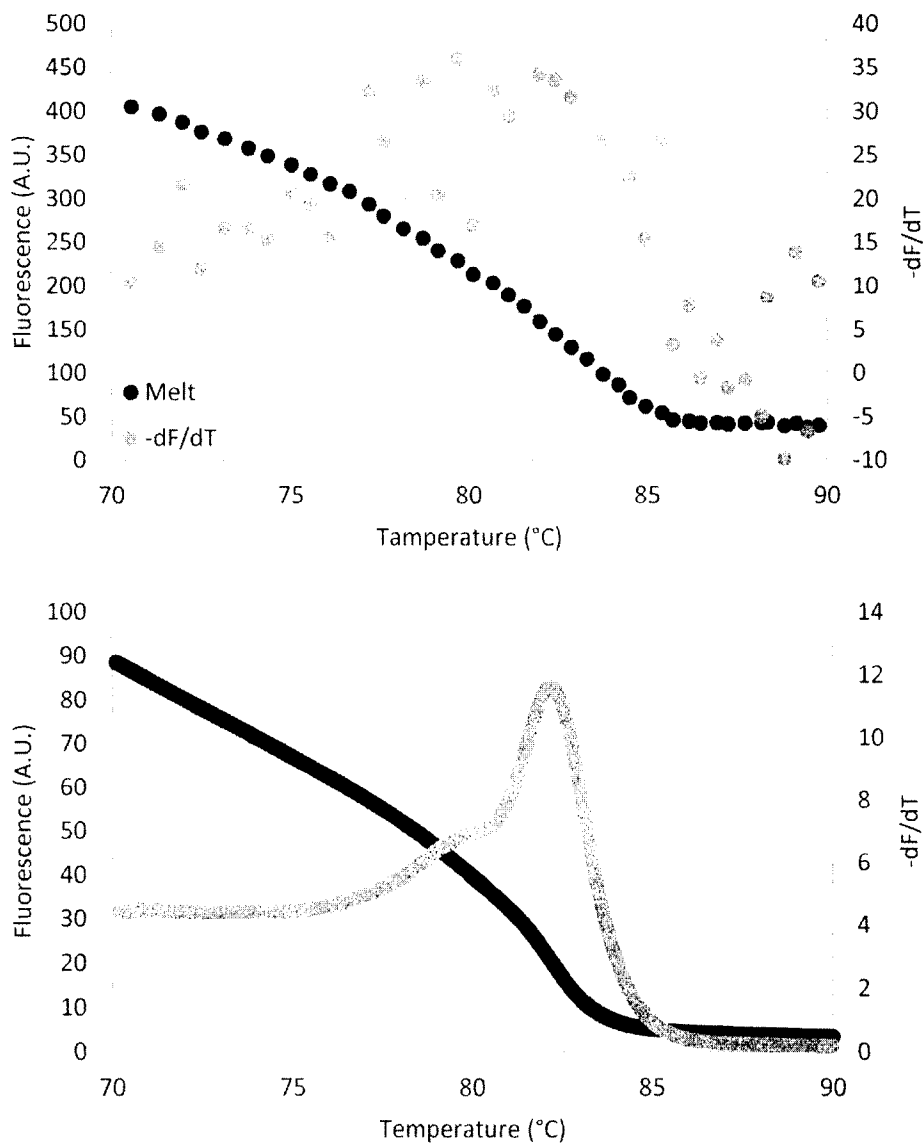


Figure 5-16: On-chip melting curve analysis (top) results for a synthetic 50bp DNA melting duplex ($T_m = 81.9^\circ\text{C}$), compared to control MCA performed on a commercial thermocycler (bottom).

The resulting melt curve produced by the on-chip analysis is very close to the control melt, decreasing nearly linearly while heating from 70°C to 78°C , then decreasing more rapidly during melting between 78°C to 85°C . The produced melting temperature is easily estimated from the melting curve, but detailed curve features are not clearly discernable from the negative first derivative.

MCA was also conducted, melting two sequences simultaneously, the high and low temperature melting duplexes. This technique of including two distinct melting temperatures, i.e. two known signals, the thermal profile of this device and other devices can be calibrated. An additional processing technique was explored; the fluorescent profile was smoothed with a small window Savitzky-Golay filter (with special care not to obscure any signal curvature details) and a high order polynomial was fit to the curve using a designated curve fitting software (Curve Expert, CurveExpert.net, Madison, AL, USA). The resulting melt curves are seen in Figure 5-17.

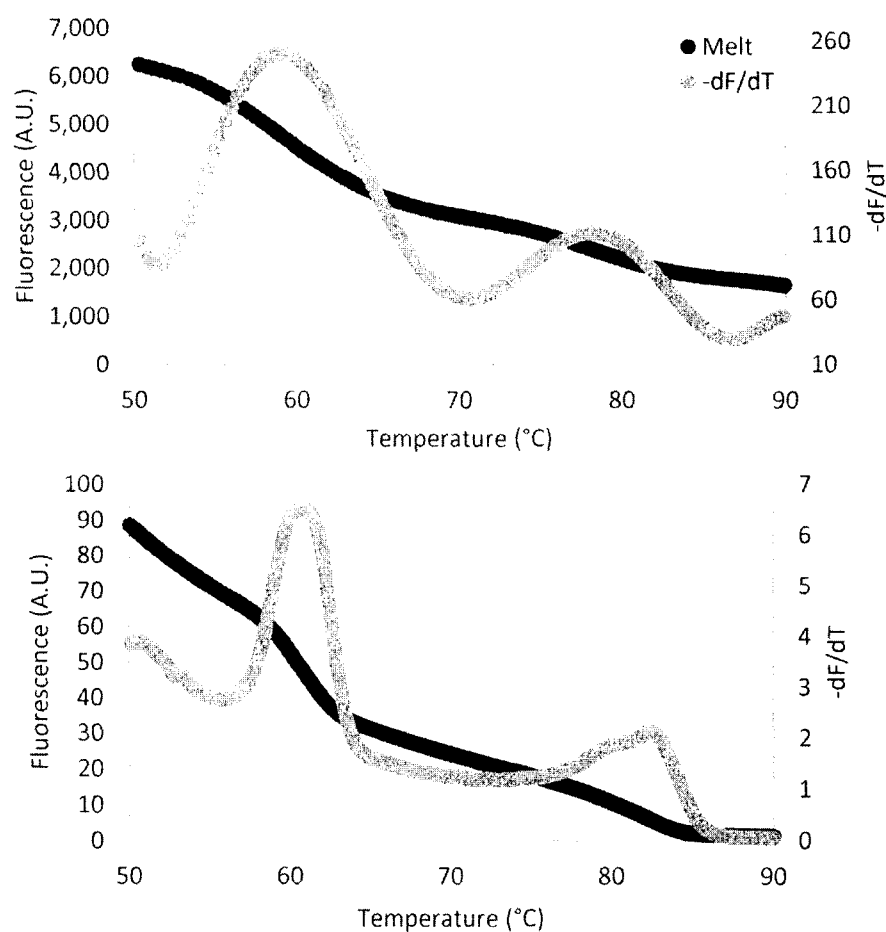


Figure 5-17: On-chip melting curve analysis (top) for two synthetic DNA sequences, compared to control MCA performed on a commercial thermocycler (bottom). Curve fitting was employed in addition to signal filtering.

Comparing results from the two processing methods, the second method of polynomial fitting yields a much clearer result, but upon close inspection, a downward shift in T_m of the higher sample can be detected. Smoothing methods, are potentially the cause of this 2-3°C shift, though other factors, such as thermal disturbances, could contribute. The difference in peak height between high and low melting sequence can be expected due to the thermal behavior of intercalating DNA dyes; this is seen in on-chip melting and in the control.

5.6 Summary

A portable μ TAS DNA analyzer was designed and developed. Thermal and optical subsystems were powered and controlled via USB, lending to portability of the system. Helicase dependent amplification was illustrated on-chip, as well as amplification detection and melting analysis capabilities.

CHAPTER 6

CONCLUSIONS AND FUTURE WORK

6.1 Conclusions

6.1.1 Accomplishments

Microfluidic DNA analysis systems were improved in two ways: 1) a technique was established to passivate glass microfluidic devices for fluorescence based assays, and 2) a portable DNA analysis device that incorporates helicase-dependent amplification and on-chip fluorescent detection was designed.

6.1.2 Impact

Improvements and innovations have been made to the field of bio-microfluidics. Passivation of fluorescent-based, glass microfluidics had not been sufficiently investigated prior to this work.

The interaction between a third-generation intercalating dye and common passivating coatings was investigated for use in glass based microfluidic devices. It was observed that these coatings left the glass benign to DNA, but not to the dye. The adsorption of dye to passivated surfaces was compared for different coatings and was characterized by analyzing fluorescent images collected during sample flow. The saturation limit for each coating was demonstrated to be a stable material property, independent of experimental conditions. Upon quantifying the amount of dye that would saturate each surface, a pretreatment method was proposed and verified. By pre-treating

the surface with a calculated amount of dye, it becomes “dye-passivated”, such that following fluorescent samples are immediately visible.

It is beyond the scope of this work to provide a full study of the chemical and physical mechanisms that contribute to a material’s N_{sat} property. Rather, this work serves to establish a method with which to quantify the dye-surface interaction, and to suggest an experimental procedure to negate the initial dye adsorption loss of fluorescent signal. Use of these techniques and knowledge of dye/coating interaction can benefit future fluorescence-based microfluidic assays and devices, allowing for improved signal-to-noise ratio and consistent, repeatable signal acquisition.

While portable systems do exist, there is much room for advancement in handling, operation, and cost of DNA analysis systems. A portable, USB powered device was illustrated, combining microfluidic helicase-dependent amplification and paired with on-chip detection. Isothermal amplification techniques, such as HDA, become crucial to miniaturizing analysis systems required to tackle global issues in epidemiology, healthcare, and food safety, among others.

6.2 Future Work

As mentioned, because of the wide range of surface chemistry modifications in microfluidic, for passivation and tailor-made applications, other passivation/dye interactions can be explored. The methodology for preparation of surfaces for fluorescent-based assays can be applied and a database of surface/dye interactions can be made available to researchers.

The portable DNA analysis device combined many aspects, some of which require more development. The thumb activated sample intake proved reliable, but

handling issues related to this design prevented sample retention at temperatures over 80°C. Modified sealing methods or reorientation of microfluidic geometry is required to fully combine this type of sample handling with melting curve analysis. At this stage in development, data analysis and post processing is cumbersome. After physical parameters, such as modified microfluidic geometry and sealing, are modified, the thermal behavior will be even more predictable, eliminating the need for any additional temperature-sensitive background fluorescence measurements. These assays can be streamlined by developing automated corrections for each heating or fluorescence measurement protocol.

Fully integrated μ TAS devices require not only sound operation and design, but special attention to the development of sample preparation and processing. This device only illustrated biological tests from isolated DNA, where in realistic applications, field tests with such portable systems encounter cellular, tissue, and blood samples. Ideally integrated sample processing, such as cell lysis, chemical washes, or nucleic acid capture can be incorporated into the glass/polymer composite devices presented here. The simple fabrication techniques and low cost polymer materials employed here lend themselves to rapid innovation and customization.

APPENDIX A

**NUCLEIC ACID SEQUENCES FOR DNA ANALYSIS DEVICE
DEVELOPMENT**

A.1 Phi X 174 Sequence

A.1.1 Phi X 174 Template Sequence

1 gagttttatc gcttccatga cgcagaagtt aacactttcg gatatttctg atgagtcgaa
61 aaattatctt gataaagcag gaattactac tgcttggtta cgaattaaat cgaagtggac
121 tgctggcgga aatgagaaa attcgaccta tccttgcgca gctcgagaag ctcttacttt
181 gcgaccttc gccatcaact aacgattctg tcaaaaactg acgcggttga tgaggagaag
241 tggcttaata tgcttggcac gttcgtcaag gactgggtta gatatgagtc acattttgtt
301 catgtagag attctcttgt tgacatttta aaagagcgtg gattactatc tgagtccgat
361 gctgttcaac cactaatagg taagaaatca tgagtcaagt tactgaacaa tccgtacgtt
421 tcagaccgc tttggcctct attaagctca tcaggettc tgccgtttg gatttaaccg
481 aagatgattt cgattttctg acgagtaaca aagtttggat tgctactgac cgctctcgtg
541 ctgctcgtg cgttgaggct tgcgtttatg gtacgctgga ctttgggga taccctcgt
601 ttctgctcc tgttgagttt attgctgccg tcattgctta ttatgttcat cccgtcaaca
661 tcaaacggc ctgtctcacc atggaaggcg ctgaatttac ggaaaacatt attaatggcg
721 tcgagcgtcc ggttaaagcc getgaattgt tcgcgtttac cttgcgtgta cgcgcaggaa
781 aactgacgt tcttactgac gcagaagaaa acgtgcgtca aaaattacgt gcggaaggag
841 tgatgtaatg tctaaagga aaaaacgttc tggcgctcgc cctggctcgc cgcagccgtt

901 gcgaggctact aaaggcaagc gtaaaggcgc tcgtctttgg tatgtaggtg gtcaacaatt
961 ttaattgcag gggcttcggc cccttacttg aggataaatt atgtctaata ttcaaactgg
1021 cgccgagcgt atgccgcatg acctttcca tcttggttc cttgctggtc agattggctg
1081 tcttattacc attcaacta ctccggttat cgctggcgac tccttcgaga tggacgccgt
1141 tggcgctctc cgtctttctc cattgctcg tggccttgc attgactcta ctgtagacat
1201 tttactttt tatgtccctc atcgtcacgt ttatggtgaa cagtggatta agttcatgaa
1261 ggatggtgtt aatgccactc ctctcccgac tgtaaacact actggttata ttgaccatgc
1321 cgcttttctt ggcacgatta acctgatac caataaaac cctaagcatt tgttcaggg
1381 ttattgaa atctataaca actatttaa agcggcgtgg atgcctgacc gtaccgaggc
1441 taaccctaat gagcttaac aagatgatgc tcgttatggt tccggttgc gccatctcaa
1501 aacatttgg actgctccgc ttctctga gactgagctt tctcggcaaa tgacgacttc
1561 taccacatct attgacatta tgggtctgca agctgcttat gctaattgc atactgacca
1621 agaacgtgat tactcatgc agcgttacca tgatgttatt tcttcattg gaggtaaaac
1681 ctcttatgac gctgacaacc gtccttact tgctatgcgc tetaatctct gggcatctgg
1741 ctatgatgtt gatggaactg accaaacgac gttaggccag tttctggtc gtgtcaaca
1801 gacctataaa cattctgtgc cgcgtttctt tgttctgag catggcacta tgttactct
1861 tgcgcttgtt cgtttccgc ctactcgac taaagagatt cagtacctta acgctaaagg
1921 tgccttgact tataccgata ttgctggcga cctgtttg tatggcaact tgcgcccgcg
1981 tgaaattct atgaaggatg tttccgttc tgggtattcg tctaagaagt ttaagattgc
2041 tgagggtcag tggatcgtt atgcgccttc gtatgttct cctgcttacc accttctga
2101 aggcttcca tcattcagg aaccgccttc tggtgattg caagaacgag tacttattcg
2161 ccaccatgat tatgaccagt gttccagtc cgttcagttg ttgcagtga atagtcaggt
2221 taaattaat gtgaccgtt atcgcaatct gccgaccact cgcgattcaa tcatgacttc

2281 gtgataaaag atfgagtgtg aggtataac gccgaagcgg taaaatttt aattttgcc
2341 gctgaggggt tgaccaagcg aagcgcggtg ggtttctgc ttaggagttt aatcatgttt
2401 cagacttta tttctcgcca taattcaaac tttttctg ataagctggt tctcactct
2461 gttactccag cttctcgcc acctgttta cagacaccta aagctacac gtcaacgtta
2521 tattttgata gtttgacggt taatgctggt aatggtggtt ttctcattg cattcagatg
2581 gatacatctg tcaacgccgc taatcagggt gtttctgtg gtgctgatat tgctttgat
2641 gccgaccta aatttttgc ctgttggtt cgcttgagt cttctcggt tccgactacc
2701 ctcccactg cctatgatgt ttatccttg aatggtgcc atgatggtgg ttattatacc
2761 gtcaaggact gtgtgactat tgacgcctt ccccgtagc cgggcaataa cgtttatgtt
2821 ggttcatgg ttggctctaa cttaccgct actaaatgcc gcggattggt ttcgctgaat
2881 caggttatta aagagattat ttgtccag ccacttaagt gaggtgattt atgttggtg
2941 ctattgctgg cggattgct tctgctctg ctggtggcgc catgtctaaa ttgttggag
3001 gcggtcaaaa agccgcctcc ggtggcattc aaggtgatgt gcttctacc gataacaata
3061 ctgtaggcat gggatgct ggtattaaat ctgccattca aggtctaat gttcctaacc
3121 ctgatgaggc cccccctagt tttgttctg gtgctatggc taaagctggt aaaggacttc
3181 ttgaaggtag gttgcaggct ggcactctg ccgttctga taagtgcctt gatttggtg
3241 gacttggtgg caagtctgcc gctgataaag gaaaggatac tctgattat cttgctgctg
3301 catttctga gcttaatgct tgggagcgtg ctggtgctga tgcctctct gctggtatgg
3361 ttgacgccgg atttgagaat caaaaagagc ttactaaaat gcaactggac aatcagaaaag
3421 agattgccga gatgcaaat gagactcaaa aagagattgc tggcattcag tccgagactt
3481 cacgccagaa tacgaaagac caggtatatg cacaaaatga gatgcttct tatcaacaga
3541 aggagtctac tgctcgcgtt gcgtctatta tggaaaacac caatcttcc aagcaacagc
3601 aggttccga gattatgcgc caaatgctta ctcaagctca aacggctggt cagtatttta

3661 ccaatgacca aatcaaagaa atgactcgca aggttagtgc tgaggttgac ttagtcatc
3721 agcaaacgca gaatcagcgg tatggctctt ctcatttgg cgctactgca aaggatatt
3781 ctaatgtcgt cactgatgct gcttctggg tggtgatat tttcatggt atgataaag
3841 ctgttgccga tacttggaac aattctgga aagacggtaa agctgatggt attggctcta
3901 atttgtctag gaaataaccg tcaggattga caccctccca attgtatgtt tcatgcctc
3961 caaatcttgg aggcttttt atggttcgtt cttattacc ttctgaatgt cacgctgatt
4021 atttgactt tgagcgtatc gaggctctta aacctgctat tgaggcttgt ggcatttcta
4081 ctctttctca atcccaatg cttggcttcc ataagcagat ggataaccgc atcaagctct
4141 tggaagagat tctgtcttt cgtatgcagg gcgttgagtt cgataatggt gatatgatg
4201 ttgacggcca taaggctgct tctgacgttc gtgatgagtt tgtatctgtt actgagaagt
4261 taatggatga attggcacia tgctacaatg tgctcccca acttgatatt aataacacta
4321 tagaccaccg ccccgagggg gacgaaaaat ggttttaga gaacgagaag acggttacgc
4381 agtttgccg caagctggct gctgaacgcc ctcttaagga tattcgcgat gagtataatt
4441 acccaaaaa gaaaggtatt aaggatgagt gttcaagatt gctggaggcc tccactatga
4501 aatcgcgtag aggctttgct atcagcgtt tgatgaatgc aatcgacag gctcatgctg
4561 atggttggtt tategtttt gacactctca cgttggtga cgaccgatta gaggcgttt
4621 atgataatcc caatgcttg cgtgactatt ttcgtgatat tggcgtatg gttcttgctg
4681 ccgagggtcg caaggctaat gattcacacg ccgactgcta tcagtatttt tgtgtgcctg
4741 agtatggtac agctaatgac cgtcttcatt tccatgcggg gcactttatg cggacacttc
4801 ctacaggtag cgttgacct aatttggtc gtcgggtacg caatcgccgc cagttaaata
4861 gcttgcaaaa tacgtggcct tatggttaca gtatgcccac cgcagttcgc tacacgcagg
4921 acgcttttc acgttctggt tggttgtggc ctgtgatgc taaaggtgag ccgcttaaag
4981 ctaccagttat tatggctggt ggttctatg tggctaaata cgtaacaaa aagtcagata

5041 tggacctgc tgctaaaggt ctaggagcta aagaatggaa caactcacta aaaaccaagc
 5101 tgtegetact tcccaagaag ctgttcagaa tcagaatgag cgcgaacttc gggatgaaaa
 5161 tgctcacaat gacaaatctg tccacggagt gcttaatcca acttaccag ctgggttacg
 5221 acgcgacgcc gttcaaccag atattgaagc agaacgcaa aagagagatg agattgaggc
 5281 tgggaaaagt tactgtagcc gacgttttg cggcgcaacc tgtgacgaca aatctgctca
 5341 aatttatgcg cgcttcgata aaaatgattg gcgatccaa cctgca

A.1.2 Phi X 174 110bp Target Sequence

1 cgttcgtcaa ggactgggtt agatatgagt cacattttgt tcatggtaga gattctcttg
 61 ttgacattt aaaagagcgt ggattactat ctgagtcga tgctgttcaa

A.1.3 Phi X 174 110bp Primer Sequences

Forward

5'- GGT TCG TCA AGG ACT GGT TT -3'

Reverse

5'- TTG AAC AGC ATC GGA CTC AG -3'

A.2 Synthetic Melting Duplex Sequences

A.2.1 Low T_m Sequence (58°C)

Forward

5'-TTA AAT TAT AAA ATA TTT ATA ATA TTA ATT ATA TAT ATA TAA
 ATA TAA TA/3ddC/

A.2.2 High T_m Sequence (81.9°C)

Forward

5'-GAG CGA CCT GTA ATG ACA TTT GAC GGC CGA GCG ACT GAT
 GGA GGT GCT TA/3ddC/

APPENDIX B

μTAS HDA SYSTEM CONTROL DOCUMENTS

B.1 Circuit Diagram for Heating Control and LED Illumination Systems

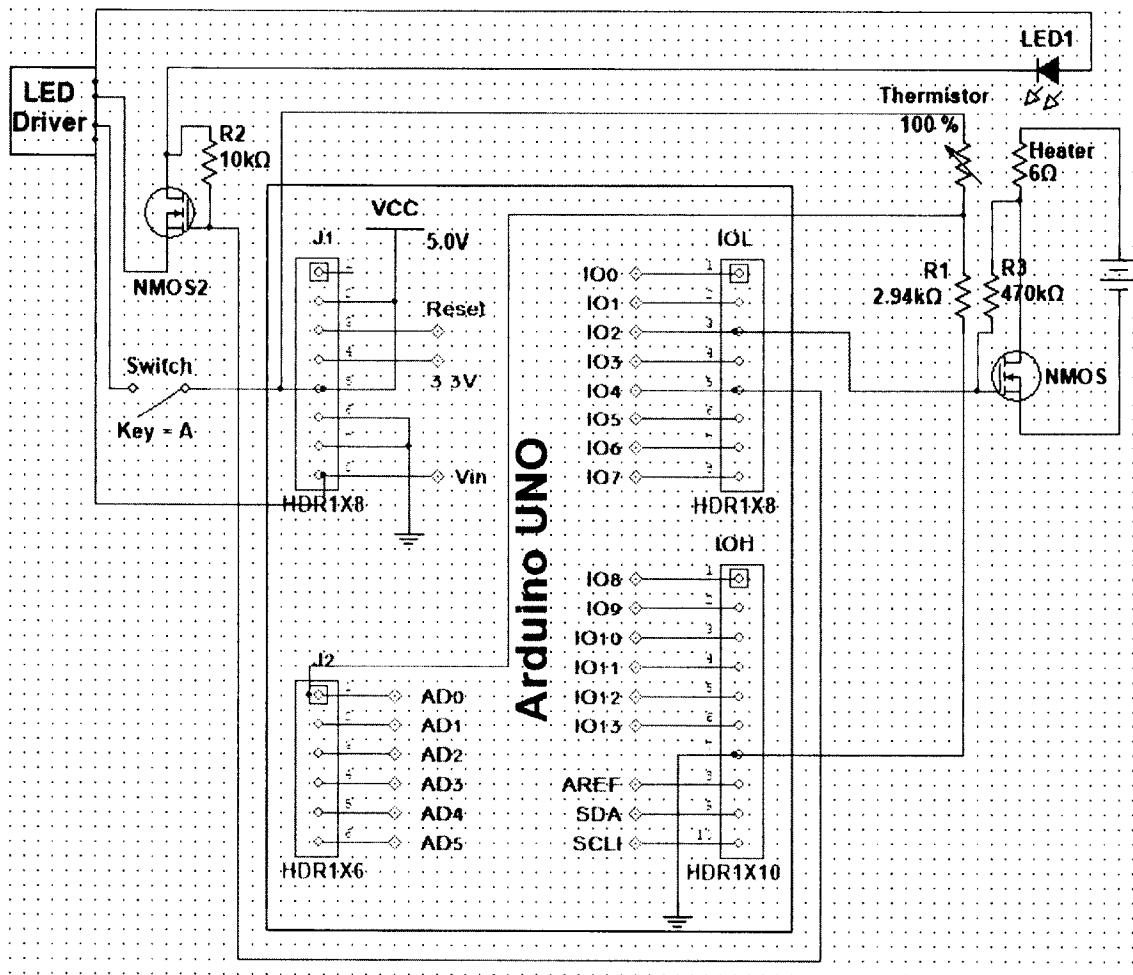


Figure B-1: Circuit Diagram for Heating Control and LED Illumination Systems

B.2 μ TAS Control Codes

B.2.1 Matlab Heater Control Code

```

s1 = serial('COM3');           % define serial port
s1.BaudRate=115200;           % define baud rate

try
    fopen(s1);                 % open serial port
catch
    allPorts=instrfind;
    if isempty(allPorts)==0
        fclose(allPorts);
    end

    fopen(s1);
end

for i=1:5                      % You can kind of ignore these lines for now
    onePt=fscanf(s1);          % They are just used to flush the junk characters
end                             % out of the serial port that the Arduino prints
                                % when it first starts up.

fis=readfis('heater67');
% fis=readfis('heater90');
goVal=1;
i=1;
% goVal=get(onOff_toggle,'Value');

refV=5;                         % reference voltage
R_top=2930;                      % resistance of other resistor in Ohms
V_in=5;                          % input voltage (from the Arduino)
B_val=3470;                      % calibration value of the thermistor
R_cal=10000;                    % resistance of thermistor at the calibration value
T_cal=273+25;

c1=clock; % exp start time
tic
while goVal==1                  % Using this syntax, the variable 'i' will
                                % start at one, then increase by 1 each time
                                % time through the loop until it get to 1000.

    onePt=fscanf(s1,'%u');      % read one line of characters from s1.
                                % The '%u' is the syntax that indicates
                                % that the characters should be read as

```

```

                                % unsigned integers.

if size(onePt)==0                % check for a value for val from arduino
    onePt=512;                   % just in case it hangs up
end

Vval= refV-refV*onePt/1024;
%Vval=onePt;
Rval=(R_top*Vval)/(V_in-Vval);
Tval=B_val/log(Rval/(R_cal*exp(-B_val/T_cal)))-273;

if Tval>100
    error('Too hot!')
end

Rfis=refV-Vval;
fizout(i)=evalfis(Rfis, fis);   % perform fuzzy operation on V across thermistor

%   u=(fizout(i)-2.6)*100/(1.3); % convert the value out of the controller
                                % to a usec val, 3.9 is Vmax, 2.6 is min,
                                % 1.3 is the difference between
                                % for 67 in foam block
    u=(fizout(i)-1.9)*100/(2);   % better for 67
%   u=(fizout(i)-.8)*100/(3.1); % for 95 control, peak fuzzy output is 4V
%   u=(fizout(i)-0)*100/(4);    % make 5millisec the min
    if u<5
        u=5;
    end

    fwrite(s1, u,'int8');        % u is the output from the fuzzy logic

%   c2=clock;
%   if c2(6)<=3
%       y=300;
%       fwrite(s1, y,'int8');    % y is a value that will be read by arduino to
                                % trigger the LED
%   else
%       y=400;
%       fwrite(s1, y,'int8');
%   end

timeList(i)=toc;
tempList(i)=Tval;
if length(tempList)<101
    plot(timeList,tempList,'g.-')
else
    plot(timeList(end-100:end),tempList(end-100:end),'g.-')
end

```

```

end
xlabel('Time(s)')
ylabel('Temperature (\circC)')
% xlim([0 pts2get/10])
ylim([15 100])
grid on
drawnow
i=i+1;
end

fclose(s1); % close the serial port!

```

B.2.2 Matlab Fuzzy Logic Toolbox Code

B.2.2.1 For 67°C Setting

```

[System]
Name='test2'
Type='mamdani'
Version=2.0
NumInputs=1
NumOutputs=1
NumRules=3
AndMethod='min'
OrMethod='max'
ImpMethod='min'
AggMethod='max'
DefuzzMethod='centroid'

[Input1]
Name='input1'
Range=[1.95 3.82]
NumMFs=3
MF1='mf1':'trimf',[1.40283068783069 2.15283068783069 2.61583068783069]
MF2='mf2':'trimf',[2.62527777777778 2.68 2.75]
MF3='mf3':'trimf',[2.74 3.90162698412698 4.23]

[Output1]
Name='output1'
Range=[2.3 4.5]
NumMFs=3
MF1='mf1':'trimf',[1.57368253968254 2.45368253968254 3.17668253968254]
MF2='mf2':'trimf',[3.19 3.25 3.33888888888889]
MF3='mf3':'trimf',[3.244 3.973 4.474]

```

```
[Rules]
1, 3 (1) : 1
2, 2 (1) : 1
3, 1 (1) : 1
```

B.2.2.2 For MCA Protocol

```
[System]
Name='collin'
Type='mamdani'
Version=2.0
NumInputs=1
NumOutputs=1
NumRules=3
AndMethod='min'
OrMethod='max'
ImpMethod='min'
AggMethod='max'
DefuzzMethod='centroid'
```

```
[Input1]
Name='input1'
Range=[1.36 1.57]
NumMFs=3
MF1='mf1': 'trimf',[1.276 1.36 1.444]
MF2='mf2': 'trimf',[1.426 1.491 1.535]
MF3='mf3': 'trimf',[1.486 1.57 1.654]
```

```
[Output1]
Name='output1'
Range=[3.65 4]
NumMFs=3
MF1='mf1': 'trimf',[3.65 3.65 3.774]
MF2='mf2': 'trimf',[3.76 3.8875 3.96]
MF3='mf3': 'trimf',[3.853 4 4.14]
```

```
[Rules]
1, 1 (1) : 1
2, 2 (1) : 1
3, 3 (1) : 1
```

B.2.3 Arduino Heater and LED Control Code

```
//
```

```
// This program gathers input from a sensor,  
// records the time at which the measurement was taken,  
// and passes both through the serial connection  
//  
int val;          // the variable named "val" will be an integer  
unsigned long time; // the variable "time" will be an unsigned long integer  
int val2;        // the incoming serial value from fuzzy  
int ledState = LOW;  
unsigned long previousMillis = 0;  
const long interval = 12*1000;  
const long interval2 = 18*1000;  
  
void setup() {  
  Serial.begin(115200); // setup serial display  
  pinMode(2,OUTPUT);    // establish pin out for heater transistor control  
  pinMode(4,OUTPUT);    // establish pin out for LED transistor control  
  
  delay(100);  
}  
  
void loop() {  
  // send signal from thermistor/voltage divider to Matlab  
  val = analogRead(0); // read the input pin
```

```
Serial.println(val); // print value to serial monitor

//begin LED control

  unsigned long currentMillis = millis();

  if (currentMillis >= previousMillis + interval2) {

    if ( ledState == HIGH){

      previousMillis = currentMillis;

      ledState = LOW;

      digitalWrite(4, ledState);

    }

    if (currentMillis - previousMillis >= interval) {

      if (ledState == LOW) {

        previousMillis = currentMillis;

        ledState = HIGH;

        digitalWrite(4, ledState);

      }

      //delay(100); //only use if heater control is commented out

    }

  }

//end LED control

//check for value from Matlab and use it to control heater

if (Serial.available() > 0){

  val2 = Serial.read(); // read val from fuzzy
```

```
digitalWrite(2, HIGH); // write value from fuzzy logic to heater transistor
delay(val2);          // use fuzzy val to control time heater is on
digitalWrite(2, LOW); // the heater is turned off
delay(100-val2); }   // and kept off for the remainder of a 100ms interval

else{
delay(100);}          // if there is no fuzzy signal to read it will just wait 100ms
}
```

BIBLIOGRAPHY

- [1] D. Micklos, J. Witkowski, S. Chan, B. Terrill, C.-h. Yang, D. Farraye, *et al.*, "DNA Interactive," ed: Dolan DNA Learning Center, Cold Spring Harbor Laboratory, 2003.
- [2] P. Domachuk, K. Tsioris, F. G. Omenetto, and D. L. Kaplan, "Bio-microfluidics: Biomaterials and Biomimetic Designs," *Advanced Materials*, vol. 22, pp. 249-260, 2010.
- [3] H. A. Stone, A. D. Stroock, and A. Ajdari, "Engineering flows in small devices: microfluidics toward a lab-on-a-chip," *Annu. Rev. Fluid Mech.*, vol. 36, pp. 381-411, 2004.
- [4] T. M. Squires and S. R. Quake, "Microfluidics: Fluid physics at the nanoliter scale," *Reviews of Modern Physics*, vol. 77, p. 977, 2005.
- [5] G. M. Whitesides, "The origins and the future of microfluidics," *Nature*, vol. 442, pp. 368-373, 2006.
- [6] L. Kricka and P. Wilding, "Microchip pcr," *Analytical and Bioanalytical Chemistry*, vol. 377, pp. 820-825, 2003.
- [7] P. Kainz, "The PCR plateau phase—towards an understanding of its limitations," *Biochimica et Biophysica Acta (BBA)-Gene Structure and Expression*, vol. 1494, pp. 23-27, 2000.
- [8] C. R. Newton and A. Graham, *PCR*: Bios Scientific Publishers Ltd, 1997.
- [9] M. Kubista, J. M. Andrade, M. Bengtsson, A. Forootan, J. Jonák, K. Lind, *et al.*, "The real-time polymerase chain reaction," *Molecular Aspects of Medicine*, vol. 27, pp. 95-125, 2006.
- [10] J. Wilhelm and A. Pingoud, "Real-time polymerase chain reaction," *ChemBiochem*, vol. 4, pp. 1120-1128, 2003.
- [11] C. T. Wittwer, G. H. Reed, C. N. Gundry, J. G. Vandersteen, and R. J. Pryor, "High-resolution genotyping by amplicon melting analysis using LCGreen," *Clinical Chemistry*, vol. 49, pp. 853-860, 2003.

- [12] A. C. Tsiatis, A. Norris-Kirby, R. G. Rich, M. J. Hafez, C. D. Gocke, J. R. Eshleman, *et al.*, "Comparison of Sanger sequencing, pyrosequencing, and melting curve analysis for the detection of KRAS mutations: diagnostic and clinical implications," *The Journal of Molecular Diagnostics*, vol. 12, pp. 425-432, 2010.
- [13] I. Pjescic and N. Crews, "Genotyping from saliva with a one-step microdevice," *Lab on a Chip*, vol. 12, pp. 2514-2519, 2012.
- [14] N. Crews, C. T. Wittwer, J. Montgomery, R. Pryor, and B. Gale, "Spatial DNA melting analysis for genotyping and variant scanning," *Analytical Chemistry*, vol. 81, pp. 2053-2058, 2009.
- [15] G. H. Reed, J. O. Kent, and C. T. Wittwer, "High-resolution DNA melting analysis for simple and efficient molecular diagnostics," *Pharmacogenomics*, vol. 8, pp. 597-608, 2007.
- [16] O. Popanda, T. Schattenberg, C. T. Phong, D. Butkiewicz, A. Risch, L. Edler, *et al.*, "Specific combinations of DNA repair gene variants and increased risk for non-small cell lung cancer," *Carcinogenesis*, vol. 25, pp. 2433-2441, 2004.
- [17] C. T. Wittwer, "High-resolution DNA melting analysis: advancements and limitations," *Human Mutation*, vol. 30, pp. 857-859, 2009.
- [18] G. H. Reed and C. T. Wittwer, "Sensitivity and specificity of single-nucleotide polymorphism scanning by high-resolution melting analysis," *Clinical Chemistry*, vol. 50, pp. 1748-1754, 2004.
- [19] H. Gudnason, M. Dufva, D. D. Bang, and A. Wolff, "Comparison of multiple DNA dyes for real-time PCR: effects of dye concentration and sequence composition on DNA amplification and melting temperature," *Nucleic Acids Research*, vol. 35, p. e127, 2007.
- [20] P. Gill and A. Ghaemi, "Nucleic acid isothermal amplification technologies—a review," *Nucleosides, Nucleotides, and Nucleic Acids*, vol. 27, pp. 224-243, 2008.
- [21] M. Vincent, Y. Xu, and H. Kong, "Helicase-dependent isothermal DNA amplification," *EMBO Reports*, vol. 5, pp. 795-800, 2004.
- [22] T. Notomi, H. Okayama, H. Masubuchi, T. Yonekawa, K. Watanabe, N. Amino, *et al.*, "Loop-mediated isothermal amplification of DNA," *Nucleic Acids Research*, vol. 28, pp. e63-e63, 2000.
- [23] S. W. Lee, "LED illumination lamp," ed: Google Patents, 2007.

- [24] K. Kébé, O. Ndiaye, H. D. Ndiaye, P. M. Mengue, P. Guindo, S. Diallo, *et al.*, "RNA versus DNA (NucliSENS EasyQ HIV-1 v1. 2 versus Amplicor HIV-1 DNA test v1. 5) for early diagnosis of HIV-1 infection in infants in Senegal," *Journal of Clinical Microbiology*, vol. 49, pp. 2590-2593, 2011.
- [25] R. Lilian, K. Bhowan, and G. Sherman, "Early diagnosis of human immunodeficiency virus-1 infection in infants with the NucliSens EasyQ assay on dried blood spots," *Journal of Clinical Virology*, vol. 48, pp. 40-43, 2010.
- [26] P. Halfon, D. Benmoura, A. Agostini, H. Khiri, A. Martineau, G. Penaranda, *et al.*, "Relevance of HPV mRNA detection in a population of ASCUS plus women using the NucliSENS EasyQ® HPV assay," *Journal of Clinical Virology*, vol. 47, pp. 177-181, 2010.
- [27] W. Tang, W. H. A. Chow, L. Ying, H. Kong, Y.-W. Tang, and B. Lemieux, "Nucleic acid assay system for tier II laboratories and moderately complex clinics to detect HIV in low-resource settings," *Journal of Infectious Diseases*, vol. 201, pp. S46-S51, 2010.
- [28] S. Santiago-Felipe, L. A. Tortajada-Genaro, R. Puchades, and A. Maquieira, "Recombinase polymerase and enzyme-linked immunosorbent assay as a DNA amplification-detection strategy for food analysis," *Analytica Chimica acta*, vol. 811, pp. 81-87, 2014.
- [29] M. Mahalanabis, J. Do, H. ALMuayad, J. Y. Zhang, and C. M. Klapperich, "An integrated disposable device for DNA extraction and helicase dependent amplification," *Biomedical Microdevices*, vol. 12, pp. 353-359, 2010.
- [30] F. Kivlehan, F. Mavré, L. Talini, B. Limoges, and D. Marchal, "Real-time electrochemical monitoring of isothermal helicase-dependent amplification of nucleic acids," *Analyst*, vol. 136, pp. 3635-3642, 2011.
- [31] N. Nagatani, K. Yamanaka, M. Saito, R. Koketsu, T. Sasaki, K. Ikuta, *et al.*, "Semi-real time electrochemical monitoring for influenza virus RNA by reverse transcription loop-mediated isothermal amplification using a USB powered portable potentiostat," *Analyst*, vol. 136, pp. 5143-5150, 2011.
- [32] T. Jiang, J. Liu, Y.-Q. Deng, J.-L. Su, L.-J. Xu, Z.-H. Liu, *et al.*, "Development of RT-LAMP and real-time RT-PCR assays for the rapid detection of the new duck Tembusu-like BYD virus," *Archives of Virology*, vol. 157, pp. 2273-2280, 2012.
- [33] K. Ren, J. Zhou, and H. Wu, "Materials for microfluidic chip fabrication," *Accounts of Chemical Research*, vol. 46, pp. 2396-2406, 2013.

- [34] D. B. Weibel, A. C. Siegel, A. Lee, A. H. George, and G. M. Whitesides, "Pumping fluids in microfluidic systems using the elastic deformation of poly (dimethylsiloxane)," *Lab on a Chip*, vol. 7, pp. 1832-1836, 2007.
- [35] A. K. Au, H. Lai, B. R. Utela, and A. Folch, "Microvalves and micropumps for BioMEMS," *Micromachines*, vol. 2, pp. 179-220, 2011.
- [36] J. Greer, S. O. Sundberg, C. T. Wittwer, and B. K. Gale, "Comparison of glass etching to xurography prototyping of microfluidic channels for DNA melting analysis," *Journal of Micromechanics and Microengineering*, vol. 17, p. 2407, 2007.
- [37] P. P. de Santana, T. P. Segato, E. Carrilho, R. S. Lima, N. Dossi, M. Y. Kamogawa, *et al.*, "Fabrication of glass microchannels by xurography for electrophoresis applications," *Analyst*, vol. 138, pp. 1660-1664, 2013.
- [38] C. N. Lim, K. S. Koh, Y. Ren, J. K. Chin, Y. Shi, and Y. Yan, "Analysis of Liquid-Liquid Droplets Fission and Encapsulation in Single/Two Layer Microfluidic Devices Fabricated by Xurographic Method," *Micromachines*, vol. 8, p. 49, 2017.
- [39] A. Neuville, L. Renaud, T. T. Luu, M. W. Minde, E. Jettestuen, J. L. Vinningland, *et al.*, "Xurography for microfluidics on a reactive solid," *Lab on a Chip*, vol. 17, p. 293-303, 2017.
- [40] D. A. Bartholomeusz, R. W. Boutté, and J. D. Andrade, "Xurography: rapid prototyping of microstructures using a cutting plotter," *Journal of Microelectromechanical Systems*, vol. 14, pp. 1364-1374, 2005.
- [41] K. Tang, E. Liao, W. Ong, J. Wong, A. Agarwal, R. Nagarajan, *et al.*, "Evaluation of bonding between oxygen plasma treated polydimethyl siloxane and passivated silicon," in *Journal of Physics: Conference Series*, 2006, p. 155.
- [42] J. R. Anderson, D. T. Chiu, H. Wu, O. Schueller, and G. M. Whitesides, "Fabrication of microfluidic systems in poly (dimethylsiloxane)," *Electrophoresis*, vol. 21, pp. 27-40, 2000.
- [43] C. Zhang, J. Xu, W. Ma, and W. Zhang, "PCR microfluidic devices for DNA amplification," *Biotechnology Advances*, pp. 243-284, 2006.
- [44] T. B. Christensen, C. M. Pedersen, K. G. Grondahl, T. G. Jensen, A. Sekulovic, D. D. Bang, *et al.*, "PCR biocompatibility of lab-on-a-chip and MEMS materials," *Journal of Micromechanics and Microengineering*, pp. 1527-1532, 2007.

- [45] W. Wang, Z.-X. Li, R. Luo, S.-H. Lu, A.-D. Xu, and Y.-J. Yang, "Droplet-based micro oscillating-flow PCR chip," *Journal of Micromechanics and Microengineering*, pp. 1369-1377, 2005.
- [46] D. S. Gray, J. L. Tan, J. Voldman, and C. S. Chen, "Dielectrophoretic registration of living cells to a microelectrode array," *Biosensors and Bioelectronics*, pp. 1765-1774, 2004.
- [47] C. Zhang and D. Xing, "Miniaturized PCR Chips for Nucleic Acid Amplification and Analysis: Latest Advances and Future Trends," *Nucleic Acids Research*, vol. 35, pp. 4223-4237, 2007.
- [48] I. Pjescic, C. Tranter, P. L. Hindmarsh, and N. D. Crews, "Glass-composite prototyping for flow PCR with *in situ* DNA analysis," *Biomedical Microdevices*, pp. 333-343, 2010.
- [49] D. J. Guckenberger, E. Berthier, E. W. K. Young, and D. J. Beebe, "Fluorescence-based assessment of plasma-induced hydrophilicity in microfluidic devices via Nile Red adsorption and depletion," *Analytical Chemistry*, pp. 7258-7263, 2014.
- [50] I. Schneegass, R. Brautigam, and J. Kholer, "Miniaturized flow-through PCR with different template types in a silicon chip thermocycler," *Lab on a Chip*, pp. 42-49, 2001.
- [51] Y. Matsubara, K. Kerman, M. Kobayashi, S. Yamamura, Y. Morita, and E. Tamiya, "Microchamber array based DNA quantification and specific sequence detection from a single copy via PCR in nanoliter volumes," *Biosensors and Bioelectronics*, pp. 1482-1490, 2005.
- [52] Y.-K. Cho, J. Kim, Y. Lee, Y.-A. Kim, K. Namkoong, H. Lim, *et al.*, "Clinical evaluation of micro-scale chip-based PCR system for rapid detection of hepatitis B virus," *Biosensors and Bioelectronics*, pp. 2161-2169, 2006.
- [53] M. Wu and A. K. Singh, "Single-cell protein analysis," *Current Opinion in Biotechnology*, pp. 1-6, 2011.
- [54] N. Crews, C. T. Wittwer, J. Montgomery, R. Pryor, and B. Gale, "Spatial DNA melting analysis for genotyping and variant scanning," *Analytical Chemistry*, pp. 2053-2058, 2009.
- [55] V. K. Ramanujan, J. A. Jo, G. Cantu, and B. A. Herman, "Spatially resolved fluorescence lifetime mapping of enzyme kinetics in living cells," *Journal of Microscopy*, pp. 329-338, 2008.

- [56] D. H. Lin, C. R. Taylor, W. F. Anderson, A. Scherer, and E. P. Kartalov, "Internally Calibrated Quantification of VEGF in Human Plasma by Fluorescence Immunoassays in Disposable Elastomeric Microfluidic Devices," *J. Chromatogr. B Analyt. Technol. Biomed. Life Sci.*, pp. 258-263, 2010.
- [57] R. Prakash, K. Pabbaraju, S. Wong, A. Wong, R. Tellier, and K. V. I. S. Kaler, "Multiplex, Quantitative, Reverse Transcription PCR Detection of Influenza Viruses Using Droplet Microfluidic Technology," *Micromachines*, vol. 6, pp. 63-79, 2015.
- [58] W.-T. Liu, J.-H. Wu, E. S.-Y. Li, and E. S. Selamat, "Emission characteristics of fluorescent labels with respect to temperature changes and subsequent effects on DNA microchip studies," *Applied and Environmental Microbiology*, vol. 71, pp. 6453-6457, 2005.
- [59] J. Kim, M. Johnson, P. Hill, and B. K. Gale, "Microfluidic sample preparation: cell lysis and nucleic acid purification," *Integrative Biology*, vol. 1, pp. 574-586, 2009.
- [60] M. Mahalanabis, J. Do, H. ALMuayad, J. Y. Zhang, and C. M. Klapperich, "An integrated disposable device for DNA extraction and helicase dependent amplification," *Biomed Microdevices*, vol. 12, pp. 353-359, 2010.
- [61] S. S. Y. Ho, C. Chua, L. Gole, A. Biswas, E. Koay, and M. Choolani, "Same-day prenatal diagnosis of common chromosomal aneuploidis using microfluidics-fluorescence *in situ* hybridization," *Prenatal Diagnosis*, vol. 32, pp. 321-328, 2012.
- [62] K.-J. Kao, C.-H. Tai, W.-H. Chang, T.-S. Yeh, T.-C. Chen, and G.-B. Lee, "A fluorescence *in situ* hybridization (FISH) microfluidic platform for detection of HER2 amplification in cancer cells," *Biosensors and Bioelectronics*, vol. 69, pp. 272-279, 2015.
- [63] C. E. Estrada-Perez, Y. A. Hassan, and S. Tan, "Experimental characterization of temperature sensitive dyes for laser induced fluorescence thermometry," *Review of Scientific Instruments*, 2011.
- [64] D. Matulis, J. K. Kranz, F. R. Salemme, and M. J. Todd, "Thermodynamic Stability of Carbonic Anhydrase: Measurements of Binding Affinity and Stoichiometry Using ThermoFluor," *Biochemistry*, vol. 44, pp. 5258-5266, 2005.
- [65] J. Yu, J. Zhou, A. Sutherland, W. Wei, Y. S. Shin, M. Xue, *et al.*, "Microfluidics-Based Single-Cell Functional Proteomics for Fundamental and Applied Biomedical Applications," *Analytical Chemistry*, vol. 7, pp. 275-295, 2014.

- [66] S. Bhattacharya, A. Datta, J. M. Berg, and S. Gangopadhyay, "Studies on Surface Wettability of Poly(Dimethyl) Siloxane (PDMS) and Glass Under Oxygen-Plasma Treatment and Correlation With Bond Strength," *Journal of Microelectromechanical Systems*, vol. 14, pp. 590-597, 2005.
- [67] D. J. Hall, "Phi X 174," 2013.
- [68] J. Sambrook and D. W. Russell, "Detection of DNA in agarose gels," *Cold Spring Harbor Protocols*, vol. 2006, p. pdb. prot4022, 2006.
- [69] J. N. Lee, C. Park, and G. M. Whitesides, "Solvent compatibility of poly (dimethylsiloxane)-based microfluidic devices," *Analytical Chemistry*, vol. 75, pp. 6544-6554, 2003.
- [70] A. Kuo, "Polymer data handbook," *Polymer Data Handbook*, 1999.